OFFICIAL JOURNAL OF THE SCIENTIFIC SOCIETY OF ANATOMISTS, HISTOLOGISTS, EMBRYOLOGISTS AND TOPOGRAPHIC ANATOMISTS OF UKRAINE

DOI: 10.31393
ISSN 1818-1295
eISSN 2616-6194

ВІСНИК МОРФОЛОГІЇ
REPORTS OF MORPHOLOGY

Vol. 29, №4, 2023

Scientific peer-reviewed journal in the fields of normal and pathological anatomy, histology, cytology and embryology, topographical anatomy and operative surgery, biomedical anthropology, ecology, molecular biology, biology of development

Published since 1993
Periodicity: 4 times a year

Vinnytsya · 2023

ВІСНИК МОРФОЛОГІЇ - REPORTS OF MORPHOLOGY

Founded by the "Scientific Society of Anatomists, Histologists, Embryologists, and Topographic Anatomists of Ukraine" and National Pyrogov Memorial Medical University, Vinnytsya in 1993

Certificate of state registration КВ №9310 from 02.11.2004

Professional scientific publication of Ukraine in the field of medical sciences in specialties 221, 222, 228, 229
According to the list of professional scientific publications of Ukraine, approved by the order of the Ministry of Education and Science of Ukraine No. 1188 of 24.09.2020
Professional scientific publication of Ukraine in the field of biological sciences in specialty 091
According to the list of professional scientific publications of Ukraine, approved by the order of the Ministry of Education and Science of Ukraine No. 1471 of 26.11.2020

Approved by the Academic Council of National Pyrogov Memorial Medical University, Vinnytsya, protocol №5 from 30.11.2023.

Indexation: CrossRef, Index Copernicus, Google Schoolar Metrics, National Library of Ukraine Vernadsky

Address editors and publisher:
Pyrogov Str. 56,
Vinnytsya, Ukraine - 21018
Tel.: +38 (0432) 553959
E-mail: nila@vnmu.edu.ua

Computer page-proofs - Klopotovska L.O.
Translator - Gunas V.I.
Technical support - Levenchuk S.S.
Scientific editing - editorship

The site of the magazine - https://morphology-journal.com

CONTENT

DOI: 10.31393/morphology-journal-2023-29(4)-01 Reports of Morphology, Vol. 29, №4, Pages 5-10

ISSN 1818-1295 eISSN 2616-6194

REPORTS OF MORPHOLOGY

Official Journal of the Scientific Society of Anatomists, Histologists, Embryologists and Topographic Anatomists of Ukraine

journal homepage: https://morphology-journal.com

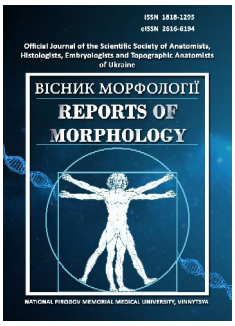

Regression models of the area of the soft palate and tongue in young men and young women with an orthognathic bite without and taking into account the type of face depending on teleroentgenometric indicators of the upper respiratory tract

Kostiuchenko-Faifor O. S., Piliponova V. V., Beliaiev E. V., Ocheretna O. L., Ivanitsa A. O., Vakar T. V., Koliadenko S. V.

National Pirogov Memorial Medical University, Vinnytsia, Ukraine

ARTICLE INFO

Received: 22 August 2023

Accepted: 12 September 2023

UDC: 616.21:616.314.26-053.81-073.75

CORRESPONDING AUTHOR

e-mail: kostyuchenko.olha.91@gmail.com

Kostiuchenko-Faifor O. S.

CONFLICT OF INTEREST

The authors have no conflicts of interest to declare.

FUNDING

Not applicable.

DATA SHARING

Data are available upon reasonable request to corresponding author.

The prevalence of pathologies related to the soft palate and its surrounding structures is a serious challenge for medicine. Sleep apnea and other diseases directly related to this anatomical region pose a threat not only due to the actual cause of deaths, but also complications of concomitant diseases. In this regard, the definition of normative indicators of the upper respiratory tract, in particular the soft palate and its surrounding structures, is a relevant topic for study. The purpose of the work is to build and analyze the regression models of the area of the soft palate and tongue in young men and young women with an orthognathic bite without and taking into account the type of face, depending on the features of teleroentgenometric indicators of the upper respiratory tract. With the help of the licensed medical software OnyxCeph³™, version 3DPro and the diagnostic program "UniqCeph", a cephalometric analysis of lateral teleroentgenograms of 49 young men and 76 young women with an orthognathic bite and the absence of upper respiratory tract pathology was performed (primary teleroentgenograms were obtained from the database of the Research Center and Department of Pediatric Dentistry, National Pirogov Memorial Medical University, Vinnytsia). Face types in young men and young women were determined using the Garson index. Regression models of the area of the soft palate and tongue depending on teleroentgenometric indicators of the upper respiratory tract were built using the license package "Statistica 6.0". In Ukrainian young women with an orthognathic bite, regardless of face type, with very wide and wide face types, all possible models of the area of the soft palate and tongue were built depending on teleroentgenometric indicators of the upper respiratory tract with a coefficient of determination (R^2) greater than 0.5 (R^2= from 0.682 to 0.937, p<0.001), which most often include the thickness of the soft palate and the length of the soft palate (42.9 % each), tongue height and tongue length (30.0% each), the value of the position of the hyoid bone relative to the vertical mandibular plane and the angle of inclination of the soft palate (20.0 % each). In Ukrainian young men with an orthognathic bite without taking into account the type of face and with a wide face type, all possible models of the area of the soft palate and tongue were also built depending on teleroentgenometric indicators of the upper respiratory tract with a coefficient of determination greater than 0.5 (R^2= from 0.562 to 0.925, p<0.001), which most often include the thickness of the soft palate and the length of the soft palate (33.3 % each).

Keywords: *teleradiography, cephalometry, soft palate, tongue, regression models, Ukrainian young men and young women, orthognathic bite, facial types.*

Introduction

Respiratory tracts are generally divided into upper and lower parts, which is due to differences in their functions in the respiratory system as a whole. The upper respiratory tract is responsible for performing various functions, such

as filtering, warming the air, moistening it and, of course, conducting it into the lower respiratory tract.

An important and relevant direction in modern medical anthropology is the study of the dimensions of the upper respiratory tract, because as research results have shown, they are directly related to the risk of occurrence and severity of certain diseases.

One of these diseases is bronchial asthma, which is becoming more and more common among young people. Clinical symptoms of asthma, according to the observations of doctors, have increased among this age group in all corners of the world [1]. Indeed, when examining individuals with bronchial asthma, compared to healthy individuals, they have significantly lower indicators of the total volume of the upper respiratory tract (p=0.01) and the area of the narrowest part of the oropharynx (p=0.007) [2].

Another disease that also has a significant prevalence, but is related to the size of the respiratory tract, is obstructive sleep apnea. In addition, it is necessary to take into account the complications of this disease and the possibility of death. The literature describes the observation of one doctor who described 12 fatal cases that occurred as a result of this pathology in post-operative patients [3]. In persons with obstructive sleep apnea, such accompanying pathologies from the cardiovascular system are observed, such as: hypertension (30-83 %), coronary heart disease (30-58 %), myocardial infarction (43-91 %), atrial fibrillation (25-80 %) [7] and the activation of oxidative stress processes affecting such target organs as the brain and heart [15] is noted.

An interesting fact is that between both diseases (obstructive sleep apnea and bronchial asthma), strong reliable connections were found regarding the severity of the course, [22] which indicates in favor of the existence of a common mechanism in the pathogenesis, one of which is a violation in the size of the respiratory tract. Thus, when performing the advancement of the upper jaw, an increase in the size of the respiratory tract by an average of 2.5 times was noted. In patients before treatment, the apnea/hypopnea index was 46, after treatment - 4 [21]. In general, a review of literary sources indicates that the performance of orthodontic interventions often changes the size of the respiratory tract - it can be both an increase and, conversely, a decrease [11].

Age is a key factor causing changes in most airway parameters. An analysis of the results of computed tomography of 192 children of various ages revealed that the value of 21 parameters of the respiratory tract changes with age. The biggest changes occur in the first 3 years of life. An equally important factor affecting the parameters of the respiratory tract is body weight [16].

One of the questions that still worries researchers is the determination of the influence of craniofacial indicators on the parameters of the respiratory tract. At present, the results of research carried out in this direction are contradictory and do not provide an opportunity to unequivocally assert the existence of such a connection [12]. Also, the study of the influence and relationship of parameters of the soft palate and tongue with indicators of the respiratory tract is practically unexplored.

The purpose of the work is to build and analyze the regression models of the area of the soft palate and tongue in Ukrainian young men and young women with an orthognathic bite without and taking into account the type of face, depending on the features of teleroentgenometric indicators of the upper respiratory tract.

Materials and methods

Primary lateral radiographs of Ukrainian young men (YM) (n=49, age - from 17 to 21 years) and Ukrainian young women (YW) (n=76, age - from 16 to 20 years) with an orthognathic bite and the absence of upper respiratory pathology ways are taken from the database of the Research Center and Department of Pediatric Dentistry National Pirogov Memorial Medical University, Vinnytsya. After applying for dental care, all young men and young women underwent a teleradiographic examination (effective radiation dose up to 0.001 mSv) at the private dental clinic "Vinintermed" using a Veraviewepocs 3D Morita (Japan) dental cone-beam tomograph.

Committee on Bioethics of National Pirogov Memorial Medical University, Vinnytsya (protocol № 8 from 30.09.2021) found that the studies do not contradict the basic bioethical standards of the Declaration of Helsinki, the Council of Europe Convention on Human Rights and Biomedicine (1977), the relevant WHO regulations and laws of Ukraine.

Face types were determined using Garson's

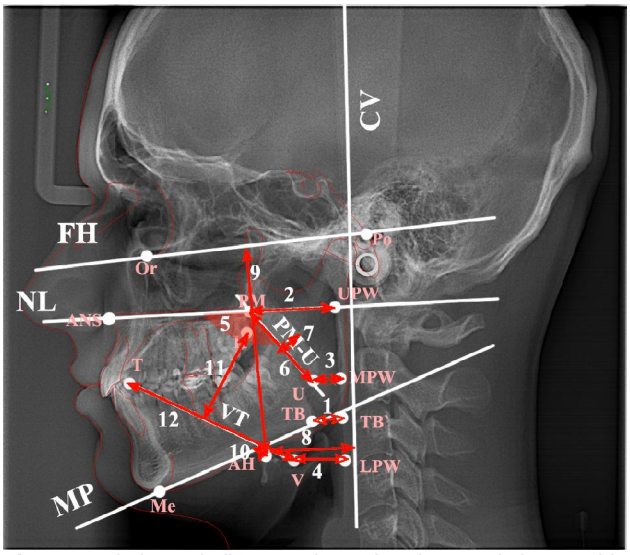

Fig. 1. Cephalometric linear and angular characteristics used in cephalometric examination of the upper respiratory tract. 1 - distance PASmin, 2 - distance PM-UPW, 3 - distance U-MPW, 4 - distance V-LPW, 5 - angle NL/PM-U, 6 - distance PM-U, 7 - distance SPT, 8 - distance AH-CV, 9 - distance AH-FH, 10 - distance AH-MP, 11 - distance H-VT, 12 - distance VT.

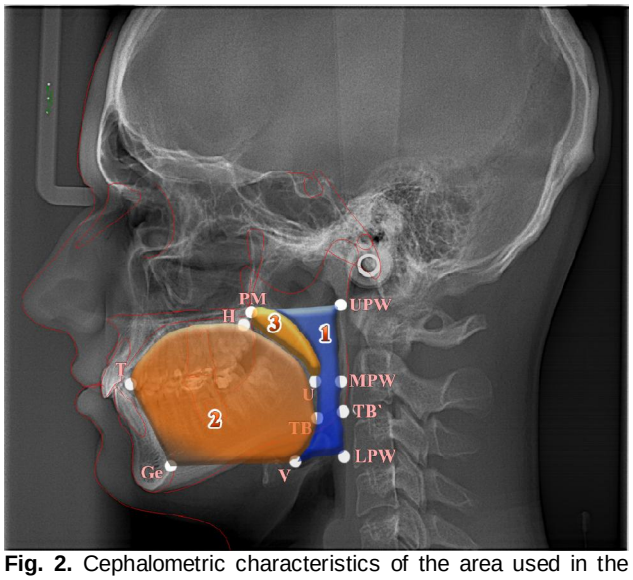

Fig. 2. Cephalometric characteristics of the area used in the cephalometric study of the upper respiratory tract. 1 - area UAA (upper respiratory tract area), 2 - area TA (tongue area), 3 - area SPA (soft palate area).

morphological index [18]. The following distribution was established: in YM - 5 with a very wide face, 22 with a wide face, 11 with an average face and 8 with a narrow face; in YW, 25 with very wide face, 25 with wide face, 10 with average face and 12 with narrow face.

Cephalometric analysis of the soft palate, tongue and upper respiratory tract itself (Fig. 1, 2) was performed using licensed medical software OnyxCeph$^{3™}$, version 3DPro (company Image Instruments GmbH, Germany) and diagnostic program "UniqCeph" (created in National Pirogov Memorial Medical University, Vinnytsya).

Regression models of the area of the soft palate and tongue depending on teleroentgenometric indicators of the upper respiratory tract were built using the license package "Statistica 6.0".

Results

Taking into account the distribution of YM and YW by face types, modeling of soft palate and tongue teleradiographic indicators of the area was carried out in YM without taking into account the face type and with a wide face type, as well as in YW without taking into account the face type and with very wide and wide face types.

Regression models of the area of the soft palate and tongue constructed in Ukrainian young men and young women with an orthognathic bite have the form of the following linear equations:

- *soft palate area (YM regardless of face type)* = -114.6 + 19.95 x SPT + 4.655 x PM-U + 1.648 x V-LPW - 0.019 x TA (R^2=0.888, F(4.44)=87.35, p<0.001),

- *soft palate area (YM with a wide face type)* = -130.5 + 20.47 x SPT + 4.337 x PM-U (R^2=0.925, F(2.19)=116.4, p<0.001),

- *tongue area (YM regardless of face type)* = 278.3 + 18.70 x VT + 44.40 x V-LPW + 16.44 x H-VT - 35.15 x PASmin (R^2=0.562, F(4.44)=14.09, p<0.001),

- *tongue area (YM with a wide face type)* = 8.952 + 23.12 x AH-FH + 19.87 x PM-UPW - 12.55 x AH-CV + 15.91 x PM-U (R^2=0.723, F(4.17)=11.10, p<0.001),

- *soft palate area (YW regardless of face type)* = -121.2 + 19.48 x SPT + 4.146 x PM-U (R^2=0.775, F(2.73)=125.7, p<0.001),

- *soft palate area (YW with a very wide face type)* = -117.1 + 20.56 x SPT + 3.739 x PM-U (R^2=0.937, F(2,22)=163.2, p<0.001),

- *soft palate area (YW with a wide face type)* = -215.5 + 19.51 x SPT + 3.440 x PM-U + 0.052 x TA (R^2=0.682, F(3.21)=15.04, p<0.001),

- *tongue area (YW regardless of face type)* = -1335 + 60.91 x H-VT + 30.03 x VT - 10.30 x AH-MP - 4.920 x NL/PM-U (R^2=0.824, F(4.71)=83.10, p<0.001),

- *tongue area (YW with a very wide face type)* = -1014 + 28.94 x VT + 55.12 x H-VT - 8.250 x NL/PM-U (R^2=0.907, F(3.21)=68.53, p<0.001),

- *tongue area (YW with a wide face type)* = -1788 + 55.57 x H-VT + 36.19 x VT - 18.54 x AH-MP (R^2=0.729, F(3.21)=18.85, p<0.001),

where, the area of the soft palate and tongue - in mm^2; SPT - known as Maximum soft palate thickness (mm); PM-U - known as Soft palate length (mm); V-LPW - known as Hypopharyngeal airway space (mm); TA - known as Tongue area (mm^2); VT - known as Length of the tongue (mm); H-VT - known as Height of the tongue (mm); PASmin - known as Retroglossal oropharyngeal airway space (mm); AH-FH - known as Vertical position of the hyoid with respect to the Frankfort plane (mm); PM-UPW - known as Nasopharyngeal airway space (mm); AH-CV - known as Horizontal position of the hyoid (mm); AH-MP - known as Vertical position of the hyoid with respect to the mandible (mm); NL/PM-U - known as Soft palate inclination angle (°); R^2 - coefficient of determination; F - Fisher's test; p-level - confidence level.

Discussion

Thus, in Ukrainian YM and YW with an orthognathic bite without pathology of the upper respiratory tract, the analysis of regression models of the area of the soft palate and tongue revealed:

soft palate area - in YW, regardless of face type, all reliable models were built with very wide and wide face types (R^2= from 0.682 to 0.937; p<0.001 in all cases), which most often include the thickness of the soft palate and the length of the soft palate (42.9 % of all independent variables); in YM without taking into account the type of face and with a wide face type, all reliable models were built (R^2=0.888 and 0.925; p<0.001 in both cases), which most often include the thickness of the soft palate and the length of the soft palate (33.3 % of all independent variables);

tongue area - in YW, regardless of face type, with very wide and wide face types, all reliable models were built

(R^2= from 0.729 to 0.907; p<0.001 in all cases), which most often include tongue height and tongue length (30.0 % each of all independent variables), as well as the value of the position of the hyoid bone relative to the vertical mandibular plane and the value of the angle of inclination of the soft palate (20.0 % of all independent variables each); in YM without taking into account the type of face and with a wide type of face, all reliable models were built (R^2=0.562 and 0.723; p<0.001 in both cases), which evenly include various teleroentgenometric indicators of the upper respiratory tract.

Determining the characteristics of various anthropometric indicators depending on nationality, region of residence, age, gender and other indicators is justified within the limits of the Ukrainian population. The results of research by Ukrainian anthropologists testify to the heterogeneity of the distribution of different types of craniotypes and face types in different regions of Ukraine, with a predominance of brachycephals with a narrow or very narrow face type [10].

In the study of Marchenko A. V. et al. [17] in Ukrainian young men and young women with an orthognathic bite and different types of faces, regression models of teleroentgenographic parameters according to Schwarz A. M. were built and analyzed, which can be corrected during surgery depending on teleroentgenographic parameters that usually do not change. Built reliable highly informative models provide an individualized approach to the necessary dental intervention.

In foreign publications, there are few studies on the relationship between respiratory tract parameters and craniofacial morphology. Individuals with a brachyfacial face type had greater nasopharyngeal width values than individuals with a mesofacial (p=0.030) or dolichofacial (p=0.034) face type. Together with an increase in the value of Vert, the width of the nasopharynx increased (R^2=26.2 %, p<0.001) [8]. However, in the study of Di Carlo G. et al. [6], any relationship between the parameters of the respiratory tract and the types of skeletal malocclusion was not found.

Indriksone I. and Jakobsone G. [13], analyzing the data of 276 healthy individuals aged 17-27 years, found a small number of weak relationships between craniofacial parameters and parameters of the upper respiratory tract, namely: the volume of the nasopharyngeal respiratory tract is affected by the angle of SNA, gender and the presence of adenoids. Weak correlations were found between SNB angle and OPV (r=0.144, p<0.05) and CSAmin (r=0.182, p<0.01).

Zheng Z. H. and others [25] found a relationship between anterior-posterior craniofacial parameters and the volume and Min-CSA of the pharyngeal airways (p<0.05). In addition, significant (p<0.05) differences in the volume of nasopharyngeal airways were found between representatives with different facial skeletal types.

In general, it is proven that excess weight is associated with an increased risk of respiratory tract collapse, which affects changes in the position of the hyoid bone, which in turn causes changes in the indicators of pharynx length, tongue length, tongue volume and volume upper respiratory tract [9].

Studies of the parameters of the tongue and its influence on the volume of the respiratory tract are more common in the world scientific literature [4, 24]. In particular, it has been proven that patients with apnea have a larger tongue (p=0.001) and an increased amount of fat (p=0.002) compared to healthy individuals, even when adjusting for body mass index, sex, age, and race [14]. The loss of body weight is associated with a decrease in the amount of fat in the tongue. The decrease in fat on the tongue was closely correlated with the decrease in the apnea-hypopnea index (Pearson's rho=0.62, p<0.0001) [23].

Rana S. S. and others [19] found a significant and positive correlation with tongue volume, oral cavity volume, and tongue volume (r=0.65; p=0.009). In addition, the authors found a significant negative correlation between the volume of the tongue, the volume of the oral cavity and the oropharynx (r=-0.51; p=0.04), the volume of the tongue, the volume of the oral cavity and the volume of the respiratory oral cavity pathways (r=-0.74; p=0.002).

After the correction of mandibular prognathism, a significant decrease in the area of the pharynx (p=0.046), a slight decrease in the area of the tongue (p=0.305) and an increase in the speed of air flow in the pharynx (p=0.133) were noted [5]. In another study, after a similar procedure, a significant increase in tongue length (p<0.001), a significant increase in airway parameters (p<0.001) was also found [20].

Conclusion

1. With the help of stepwise regression analysis, highly informative models of the area of the soft palate and tongue were built depending on teleroentgenometric indicators of the upper respiratory tract in Ukrainian YW with an orthognathic bite without taking into account the type of face, with very wide and wide face types (R^2= from 0.682 to 0.937, p<0.001 in all cases) and in Ukrainian YM with an orthognathic bite regardless of face type and with a wide face type (R^2= from 0.562 to 0.925, p<0.001 in both cases).

2. In YW, the models of the area of the soft palate and tongue most often include the thickness of the soft palate and the length of the soft palate (42.9 % each), the height of the tongue and the length of the tongue (30.0 % each), the value of the position of the hyoid bone relative to vertical mandibular plane and the value of the angle of inclination of the soft palate (20.0 % each); in YM - the thickness of the soft palate and the length of the soft palate (33.3 % each).

References

[1] Asher, M. I., Garcia-Marcos, L., Pearce, N. E., & Strachan, D. P. (2020). Trends in worldwide asthma prevalence. *European Respiratory Journal,* 56(6), 2002094. doi: 10.1183/13993003.02094-2020

[2] Bandeira, A. M., Oltramari-Navarro, P. V. P., de Lima Navarro, R., de Castro Ferreira Conti, A. C., de Almeida, M. R., & Fernandes,

K. B. P. (2014). Three-dimensional upper-airway assessment in patients with bronchial asthma. *The Angle Orthodontist,* 84(2), 254-259. doi: 10.2319/030113-176

[3] Benumof, J. L. (2016). Mismanagement of obstructive sleep apnea may result in finding these patients dead in bed. *Canadian Journal of Anesthesia,* 63(1), 3-7. doi: 10.1007/s12630-015-0513-x

[4] Brown, E. C., Cheng, S., McKenzie, D. K., Butler, J. E., Gandevia, S. C., & Bilston, L. E. (2013). Tongue and lateral upper airway movement with mandibular advancement. *Sleep,* 36(3), 397-404. doi: 10.5665/sleep.2458

[5] Chen, C. M., Yu, T. Y., Chou, S. T., Cheng, J. H., Chen, S. C., Pan, C. Y., & Tseng, Y. C. (2021). Changes in tongue area, pharyngeal area, and pharyngeal airway velocity after correction of mandibular prognathism. *Journal of Clinical Medicine,* 10(19), 4560. doi: 10.3390/jcm10194560

[6] Di Carlo, G., Polimeni, A., Melsen, B., & Cattaneo, P. M. (2015). The relationship between upper airways and craniofacial morphology studied in 3 D. A CBCT study. *Orthodontics & craniofacial research,* 18(1), 1-11. doi: 10.1111/ocr.12053

[7] Floras, J. S. (2018). Sleep apnea and cardiovascular disease: an enigmatic risk factor. *Circulation research,* 122(12), 1741-1764. doi: 10.1161/CIRCRESAHA.118.310783

[8] Flores-Blancas, A. P., Carruitero, M. J., & Flores-Mir, C. (2017). Comparison of airway dimensions in skeletal Class I malocclusion subjects with different vertical facial patterns. *Dental press journal of orthodontics,* 22, 35-42. doi: 10.1590/2177-6709.22.6.035-042.oar

[9] Genta, P. R., Schorr, F., Eckert, D. J., Gebrim, E., Kayamori, F., Moriya, H. T., ... & Lorenzi-Filho, G. (2014). Upper airway collapsibility is associated with obesity and hyoid position. *Sleep,* 37(10), 1673-1678. doi: 10.5665/sleep.4078

[10] Gunas, I. V., Shinkaruk-Dykovytska, M. M., Kotsyura, O. O., Orlovskiy, V. O., Dmytrenko, S. V., Shayuk, A. V., & Glushak, A. A. (2017). Differences of craniotype distribution and types of face among apparently healthy men from different regions of Ukraine. *Folia Morphologica,* 76(3), 473-477. doi: 10.5603/FM.a2017.0017

[11] Hu, Z., Yin, X., Liao, J., Zhou, C., Yang, Z., & Zou, S. (2015). The effect of teeth extraction for orthodontic treatment on the upper airway: a systematic review. *Sleep and Breathing,* 19, 441-451. doi: 10.1007/s11325-015-1122-1

[12] Indriksone, I., & Jakobsone, G. (2014). The upper airway dimensions in different sagittal craniofacial patterns: a systematic review. *Stomatologija,* 16(3), 109-117.

[13] Indriksone, I., & Jakobsone, G. (2015). The influence of craniofacial morphology on the upper airway dimensions. *The Angle Orthodontist,* 85(5), 874-880. doi: 10.2319/061014-418.1

[14] Kim, A. M., Keenan, B. T., Jackson, N., Chan, E. L., Staley, B., Poptani, H., ... & Schwab, R. J. (2014). Tongue fat and its relationship to obstructive sleep apnea. *Sleep,* 37(10), 1639-1648. doi: 10.5665/sleep.4072

[15] Lavie, L. (2015). Oxidative stress in obstructive sleep apnea and intermittent hypoxia-revisited-the bad ugly and good: implications to the heart and brain. *Sleep medicine reviews,* 20, 27-45. doi: 10.1016/j.smrv.2014.07.003

[16] Luscan, R., Leboulanger, N., Fayoux, P., Kerner, G., Belhous, K., Couloigner, V., ... & Thierry, B. (2020). Developmental changes of upper airway dimensions in children. *Pediatric Anesthesia,* 30(4), 435-445. doi: 10.1111/pan.13832

[17] Marchenko, A. V., Prokopenko, O. S., Dzevulska, I. V., Zakalata, T. R., & Gunas, I. V. (2021). Mathematical modeling of teleroentgenographic parameters according to the method of Schwarz A.M. depending on the basic cephalometric parameters in Ukrainian young men and young women with different face types. *Wiadomosci lekarskie* (Warsaw, Poland: 1960), 74(6), 1488-1492. PMID: 34159943

[18] Proffit, U. R., Fildz, G. U., & Saver, D. M. (2006). *Современная ортодонтия* (перевод с английского Д. С. Персина) [*Modern orthodontics* (translation from English by D. S. Persina)]. M.: МЕДпресс-информ - M.: MEDpress-inform.

[19] Rana, S. S., Kharbanda, O. P., & Agarwal, B. (2020). Influence of tongue volume, oral cavity volume and their ratio on upper airway: A cone beam computed tomography study. *Journal of Oral Biology and Craniofacial Research,* 10(2), 110-117. doi: 10.1016/j.jobcr.2020.03.006

[20] Sahoo, N. K., Agarwal, S. S., Datana, S., & Bhandari, S. K. (2020). Effect of mandibular advancement surgery on tongue length and height and its correlation with upper airway dimensions. *Journal of Maxillofacial and Oral Surgery,* 19, 624-629. doi: 10.1007/s12663-020-01375-2

[21] Schendel, S. A., Broujerdi, J. A., & Jacobson, R. L. (2014). Three-dimensional upper-airway changes with maxillomandibular advancement for obstructive sleep apnea treatment. *American Journal of Orthodontics and Dentofacial Orthopedics,* 146(3), 385-393. doi: 10.1016/j.ajodo.2014.01.026

[22] Wang, D., Zhou, Y., Chen, R., Zeng, X., Zhang, S., Su, X., ... & Zhang, N. (2023). The relationship between obstructive sleep apnea and asthma severity and vice versa: a systematic review and meta-analysis. *European Journal of Medical Research,* 28(1), 139. doi: 10.1186/s40001-023-01097-4

[23] Wang, S. H., Keenan, B. T., Wiemken, A., Zang, Y., Staley, B., Sarwer, D. B., ... & Schwab, R. J. (2020). Effect of weight loss on upper airway anatomy and the apnea-hypopnea index. *The importance of tongue fat. American journal of respiratory and critical care medicine,* 201(6), 718-727. doi: 10.1164/rccm.201903-0692OC

[24] Zhao, C., Viana, A., Ma, Y., & Capasso, R. (2020). High tongue position is a risk factor for upper airway concentric collapse in obstructive sleep apnea: observation through sleep endoscopy. *Nature and Science of Sleep*, 767-774. doi: 10.2147/NSS.S273129

[25] Zheng, Z. H., Yamaguchi, T., Kurihara, A., Li, H. F., & Maki, K. (2014). Three-dimensional evaluation of upper airway in patients with different anteroposterior skeletal patterns. *Orthodontics & craniofacial research,* 17(1), 38-48. doi: 10.1111/ocr.12029

РЕГРЕСІЙНІ МОДЕЛІ ПЛОЩІ М'ЯКОГО ПІДНЕБІННЯ ТА ЯЗИКА В ЮНАКІВ І ДІВЧАТ ІЗ ОРТОГНАТИЧНИМ ПРИКУСОМ БЕЗ І З УРАХУВАННЯМ ТИПУ ОБЛИЧЧЯ В ЗАЛЕЖНОСТІ ВІД ТЕЛЕРЕНТГЕНОМЕТРИЧНИХ ПОКАЗНИКІВ ВЕРХНІХ ДИХАЛЬНИХ ШЛЯХІВ

Костюченко-Файфор О. С., Піліпонова В. В., Беляєв Е. В., Очеретна О. Л., Іваниця А. О., Вакар Т. В., Коляденко С. В.

Поширеність патологій, пов'язаних з м'яким піднебінням та оточуючими його структурами є серйозним викликом для медицини. Апное сну та інші захворювання напряму пов'язані з даним анатомічним регіоном несуть загрозу не тільки за рахунок власне можливості летальних випадків, але і ускладнення супутніх захворювань. У зв'язку з цим визначення нормативних показників верхніх дихальних шляхів, зокрема м'якого піднебіння і оточуючих його структур є актуальною темою для вивчення. Мета роботи - побудувати та провести аналіз регресійних моделей площі м'якого піднебіння та язика

в українських юнаків і дівчат із ортогнатичним прикусом без і з урахуванням типу обличчя у залежності від особливостей телерентгенометричних показників верхніх дихальних шляхів. За допомогою ліцензованого медичного програмного забезпечення OnyxCeph³™, версії 3DPro та діагностичної програми "UniqCeph" проведено цефалометричний аналіз бокових телерентгенограм 49 українських юнаків і 76 українських дівчат із ортогнатичним прикусом і відсутністю патології верхніх дихальних шляхів (первинні телерентгенограми отримані з бази даних науково-дослідного центру та кафедри стоматології дитячого віку Вінницького національного медичного університету ім. М. І. Пирогова). Типи обличчя в юнаків і дівчат визначали за допомогою індексу Гарсона. Регресійні моделі площі м'якого піднебіння та язика у залежності від телерентгенометричних показників верхніх дихальних шляхів побудовані за допомогою ліцензійного пакету "Statistica 6.0". В українських дівчат із ортогнатичним прикусом без урахування типу обличчя, з дуже широким і широким типами обличчя побудовані усі можливі моделі площі м'якого піднебіння та язика в залежності від телерентгенометричних показників верхніх дихальних шляхів з коефіцієнтом детермінації (R^2) більшим 0,5 (R^2= від 0,682 до 0,937, p<0,001), до яких найчастіше входять товщина м'якого піднебіння та довжина м'якого піднебіння (по 42,9 %), висота язика та довжина язика (по 30,0 %), величина положення під'язикової кістки відносно нижньощелепної площини за вертикаллю та величина кута нахилу м'якого піднебіння (по 20,0 %). В українських юнаків із ортогнатичним прикусом без урахування типу обличчя та з широким типом обличчя також побудовані усі можливі моделі площі м'якого піднебіння та язика в залежності від телерентгенометричних показників верхніх дихальних шляхів з коефіцієнтом детермінації більшим 0,5 (R^2= від 0,562 до 0,925, p<0,001), до яких найчастіше входять товщина м'якого піднебіння та довжина м'якого піднебіння (по 33,3 %).

Ключові слова: *телерентгенографія, цефалометрія, м'яке піднебіння, язик, регресійні моделі, українські юнаки та дівчата, ортогнатичний прикус, типи обличчя.*

Author's contribution

Kostiuchenko-Faifor O. S.: conceptualization, research, review writing and editing, methodology and writing of the original draft, formal analysis and validation.
Piliponova V. V.: project administration.
Beliaiev E. V.: data visualization.
Ocheretna O. L.: resources.
Ivanitsa A. O.: software.
Vakar T. V.: supervision.
Koliadenko S. V.: resources.

DOI: 10.31393/morphology-journal-2023-29(4)-02 Reports of Morphology, Vol. 29, №4, Pages 11-18

ISSN 1818-1295 eISSN 2616-6194

REPORTS OF MORPHOLOGY

Official Journal of the Scientific Society of Anatomists, Histologists, Embryologists and Topographic Anatomists of Ukraine

journal homepage: https://morphology-journal.com

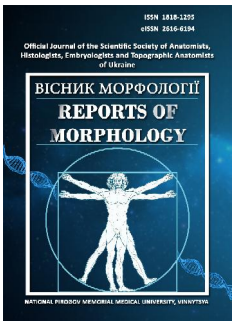

A method of evaluation of the shape of the human cerebellum: MRI study

Kalinichenko M. O.
Kharkiv National Medical University, Kharkiv, Ukraine

ARTICLE INFO
Received: 19 July 2023
Accepted: 15 September 2023

UDC: 611.817.1.088.5:611.91

CORRESPONDING AUTHOR
e-mail: kelend13@gmail.com
Kalinichenko M. O.

CONFLICT OF INTEREST
The authors have no conflicts of interest to declare.

FUNDING
Not applicable.

DATA SHARING
Data are available upon reasonable request to corresponding author.

The variability of shape of an organ is one of the manifestations of its individual anatomical variability. Magnetic resonance imaging and other modern neurovisualization methods allow for in vivo determination of morphological characteristics of organs, considering their natural positioning. The aim of this study is to develop a method of evaluation of the shape of the human cerebellum based on the results of MR imaging morphometry. MR images of the brain were obtained from 30 subjects (15 male and 15 female aged between 20 and 40 years) without apparent brain pathology. MRI was performed using a 1.5 T MRI machine (Siemens Magnetom Symphony, Munich, Germany). The width of the cerebellum was determined in axial (W_{ax}) and coronal (W_{cor}) planes, the length was determined in axial (L_{ax}) and sagittal (L_{sag}) planes, the height was determined in coronal (Hcor) and sagittal (Hsag) planes. It was observed that the width of the cerebellum is determined almost equally in two different planes, the greater disparity is noted in the measurements of length and the maximum difference in values was found in the measurements of height. A moderate and statistically significant linear relationship was discovered between the variables W_{ax} and L_{ax} ($r=0.48$; $p<0.01$), as well as between W_{cor} and H_{cor} ($r=0.39$; $p<0.05$). Variability in the values of paired linear dimensions measured in a single plane and the absence of a functional relationship between them lead to variability in their ratios, or shape factors (W_{ax} / Lax, W_{cor} / H_{cor}, L_{sag} / H_{sag}). These shape factors, in turn, influence the shape of intracerebellar structures, primarily the cerebellar nuclei. To evaluate the overall shape of the cerebellum, the following parameters have been proposed, which describe the relationships between one linear dimension of the cerebellum to the other two: relative width of the cerebellum ($W_r=(W_{ax}xW_{cor}) / (L_{ax}xH_{cor})$), relative length of the cerebellum ($L_r=(L_{ax}xL_{sag}) / (W_{ax}xH_{sag})$), and relative height of the cerebellum ($H_r=(H_{cor}xH_{sag}) / (W_{cor}xL_{sag})$). Further analysis of these parameters defines which of the linear dimensions has a greater influence on the shape of the cerebellum, determining its structural features, such as the shape of its lobules, the course of its fissures, and the three-dimensional organization of its nuclei, among others. In vivo evaluation of cerebellar shape will facilitate improvements in the diagnosis of cerebellar disorders using MRI and will be valuable in conducting neuromorphological research studies.

Keywords: *human, anatomy, cerebellum, MRI, morphometry.*

Introduction

According to previous studies, the functions of the cerebellum are to regulate balance, posture, and muscle coordination; however, it was later found to also include cognitive functions such as memory [15], speech [8], and emotion [1]. The cerebellum was also associated with swallowing function in adults [13]. At the same time, each of the functions of the cerebellum is localized in specific areas of the cerebellum and functions within the limits of the neural network [5, 16, 19]. At present, studies of the morphology of the cerebellum are being conducted to create models of its development and track the periods of modification of individual functions, in particular in newborns and children [24, 26].

Development of the cerebellum begins approximately from the fourth week of pregnancy and continues throughout the first postnatal year [23]. The basic micromorphology of the cerebellum, formed as a result of the proliferation of neurons, processes of migration and differentiation, is

finally established around the 20th week of pregnancy [6]. In the subsequent period up to the 40th week of pregnancy, the cerebellum undergoes a faster increase in volume and surface complexity than other brain structures [3]. As a result, the features of the morphology of the cerebellum at various stages of intrauterine development, such as its linear dimensions, the degree of development of individual lobes, as well as the volume and shape, serve as guidelines for determining the age of the fetus [2, 28, 29]. Recent studies have also confirmed the significant role of the cerebellum in brain development [4, 25].

Functional and morphological changes of the cerebellum are associated with various neurological and psychiatric disorders [7, 12, 14, 22], such as autism, multiple sclerosis, Arnold-Chiari anomaly, cerebellar cognitive-affective syndrome, Parkinson's disease, Alzheimer's disease, and others. Research is being conducted to create criteria for the norm of diagnostic methods of neuroimaging of morphological changes in the cerebellum (linear dimensions, reduction in mass and volume) [26]. However, information about the anatomical norm of the cerebellum, on which these criteria are based, does not take into account the peculiarities of its individual anatomical variability. The variability of the shape of the organ is one of the manifestations of its individual anatomical variability. One of the ways to determine the shape of an organ is to evaluate the ratio of its linear dimensions [17, 21, 30]. Magnetic resonance imaging and other modern neuroimaging research methods make it possible to establish the morphological features of organs during life, while preserving their natural position. Studies of the shape of the cerebellum and its variability are few; they were performed on anatomical preparations of the cerebellum. A comprehensive assessment of the shape of the cerebellum on tomograms has not been carried out before.

The purpose of the work is to develop a method for evaluating the shape of the human cerebellum based on the results of morphometry of MR tomograms.

Materials and methods

Materials

In this work, T2-weighted MR images of the cerebellum were examined. MRI was performed on 30 people (15 men and 15 women aged 20 to 40), and no visible brain pathology was detected. The study was performed on a 1.5 T MRI machine (Siemens Magnetom Symphony, Munich, Germany). Imaging parameters: TE (echo time) 122 ms, TR (repetition time) 4520 ms, and slice thickness 5 mm. The Commission on Bioethics of the Kharkiv National Medical University, Kharkiv (protocol No. 4 dated 15.09.2020) established that the research does not contradict the basic bioethical standards of the Helsinki Declaration, the Council of Europe Convention on Human Rights and Biomedicine (1977), relevant WHO regulations and laws of Ukraine.

The method of determining the size of the cerebellum

When analyzing the MRI images, the dimensions of the cerebellum in the axial, coronal, and sagittal projections were determined as the dimensions of a rectangle that can be constructed to cover the contour of the cerebellum, or its right and left hemispheres, on the MRI image in the corresponding projection (the so-called "bounding rectangle", Fig. 1). The rectangle is oriented in such a way that two of its sides are parallel to the line that appears at the point of intersection of the median plane with the plane of the MRI image in the axial and coronal projections (further - the median line). In the sagittal projection, two sides of the indicated rectangle are parallel to the intercommissural line by Talairach [10]. Thus, two dimensions of the cerebellum were determined in each projection.

In the axial projection (Fig. 1A):

- L_{ax} - the length of the cerebellum is equal to the length of the side of the rectangle parallel to the median line;
- W_{ax} - the width of the cerebellum is equal to the length of the side of the rectangle perpendicular to the median line;

In the coronal projection (see Fig. 1B):

- H_{cor} - the height of the cerebellum is equal to the length of the side of the rectangle parallel to the median line;
- W_{cor} - the width of the cerebellum is equal to the length of the side of the rectangle perpendicular to the median line;

In the sagittal projection, the height and length of the right and left hemispheres were measured (see Fig. 1C):

- L_{sag} - the length of the cerebellum is equal to the length of the side of the rectangle parallel to the intercommissural line;
- H_{sag} - the height of the cerebellum is equal to the length of the side of the rectangle perpendicular to the intercommissural line.

For further analysis, the maximum values of these dimensions were taken into account.

Methods of determining the shape of the cerebellum

To assess the shape of the cerebellum on MR images, shape factors were calculated - the ratio of cerebellum sizes determined in each projection:

in axial projection W_{ax}/L_{ax} (1)

in the coronal projection W_{cor}/H_{cor} (2)

in the sagittal projection L_{sag}/H_{sag} (3)

To assess the shape of the cerebellum as a three-dimensional structure, MR images offer parameters that take into account the ratio of one linear size of the cerebellum to the other two, namely: the *relative width of the cerebellum* (W_r), the *relative length of the cerebellum* (L_r), and the *relative height of the cerebellum* (H_r). They are calculated according to the formulas:

$$W_r=(W_{ax} \times W_{cor}) / (L_{ax} \times H_{cor}) \quad (4)$$

$$L_r=(L_{ax} \times L_{sag}) / (W_{ax} \times H_{sag}) \quad (5)$$

$$H_r=(H_{cor} \times H_{sag}) / (W_{cor} \times L_{sag}) \quad (6)$$

Statistical data processing was carried out in Microsoft

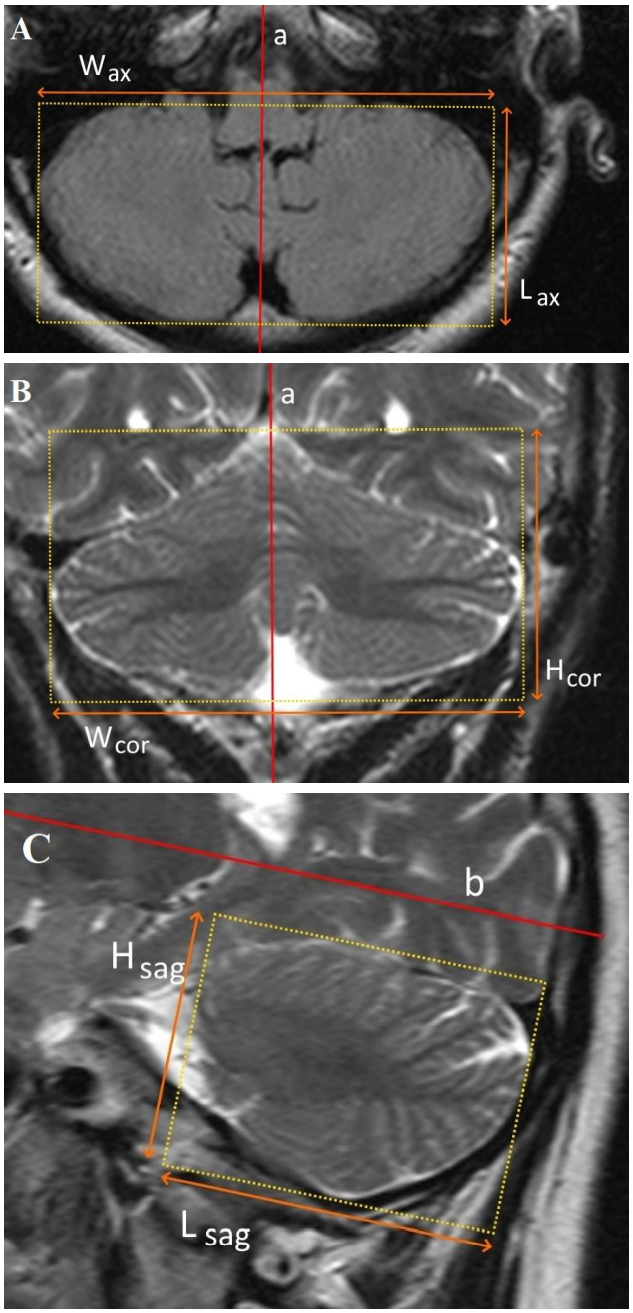

Fig. 1. Determining the linear dimensions of the cerebellum on MRI images of the brain (A - axial, B - coronal, C - sagittal projection): a - a straight line arising at the intersection of the median plane with the plane of the MRI image; b - intercommissural line by Talairach.

Excel 2016. The distribution of values was analyzed according to the Kolmogorov-Smirnov test criterion. It was determined that the distribution of values of all morphometric parameters, both linear and their ratios, does not differ from normal. Further statistical analysis included calculation of the sample mean (M), standard deviation (S), coefficient of variation (Cv), determination of the minimum and maximum value and standard error of the mean (m). Correlation analysis was carried out with the calculation of the Pearson correlation coefficient (r) to establish patterns of individual variability. Parametric methods of testing the significance of differences were used. The values of cerebellum sizes and their ratios were divided by the mean value and standard deviation into three groups: small (from minimum to (M-S)), medium (M±S) and large (from (M+S) to maximum).

Results

Variability of the linear dimensions of the cerebellum. Table 1 (A) shows the values of the height, width, and length of the cerebellum on tomographic images in the corresponding projections.

As can be seen from the data in Table 1 (A), there is variability in the values of the linear dimensions of the cerebellum of the studied sample, but it is insignificant; the greatest variability is observed in Lax (Cv=7.27%), smallest - in Lsag (Cv=4.92%).

Statistical indicators of the distribution of values of the same linear size of the cerebellum, determined in mutually perpendicular tomographic projections, differ; but only the difference in height values is statistically significant. The distribution of these values is shown in Figures 2-4.

As can be seen from the data of Figures 2-4, the width of the cerebellum is determined almost identically in two different projections, the discrepancy is greater when determining the length, the maximum difference in values is found when measuring the height. This fact is fully explained by the complex three-dimensional organization of the cerebellum (see Fig. 1). In addition, the value of the same size in different projections can belong to different

Table 1. Statistical evaluation of the distribution of cerebellar size values, their ratios and relative parameters.

Parameter	Test statistic					
	M	m	S	CV, %	min	max
A. Parameters						
W_{ax}	104.9	1.0	5.5	5.24	94.2	116.6
W_{cor}	106.4	1.0	5.7	5.31	95.8	118.7
L_{ax}	58.61	0.78	4.26	7.27	48.8	67.2
L_{sag}	60.72	0.55	2.99	4.92	54.6	67.8
H_{cor}	58.32*	0.65	3.55	6.08	49.9	63.4
H_{sag}	45.81*	0.55	3.04	6.63	38.7	52.7
B. Proportions						
W_{ax}/L_{ax}	1.796	0.022	0.121	6.72	1.61	2.05
W_{cor}/H_{cor}	1.828	0.021	0.116	6.36	1.62	2.08
L_{sag}/H_{sag}	1.330	0.017	0.094	7.04	1.2	1.57
C. Relative parameters						
W_r	3.290	0.067	0.367	11.15	2.76	4.08
L_r	0.743	0.012	0.066	8.87	0.59	0.86
H_r	0.415	0.007	0.040	9.74	0.33	0.48

Note: * - the difference is statistically significant for $p<0.05$.

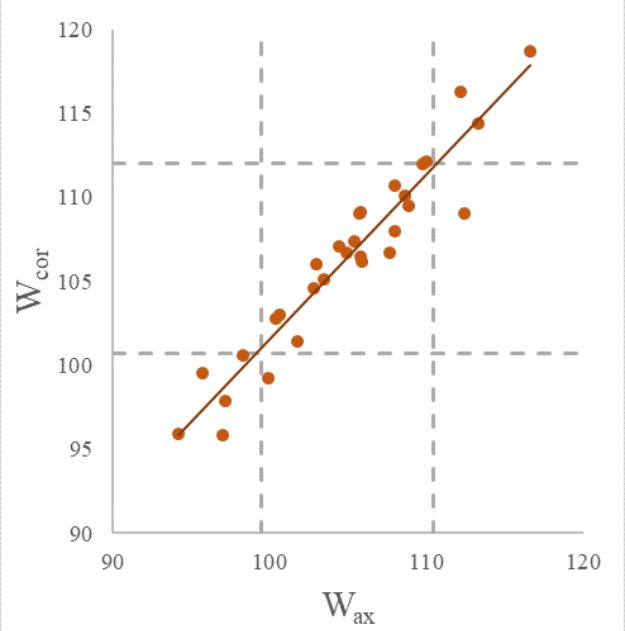

Fig. 2. Distribution of cerebellar width values in axial and coronal projections. Note: dashed lines correspond to M-S and M+S values (here and in Fig. 3-7).

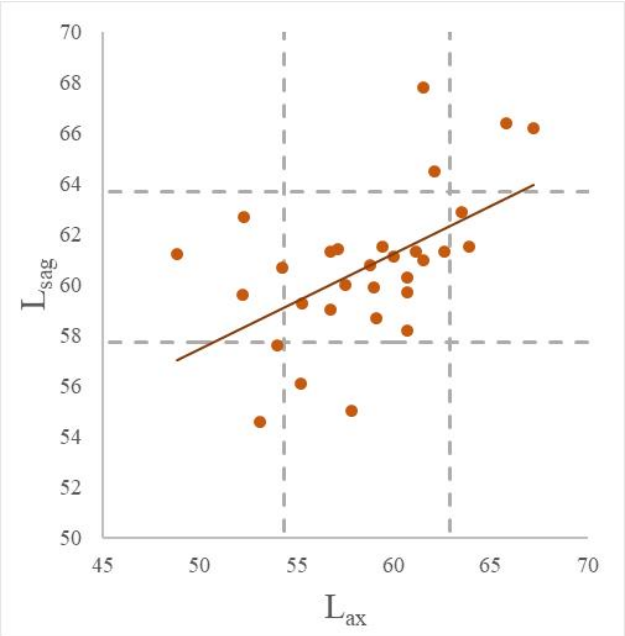

Fig. 3. Distribution of cerebellar length values in axial and sagittal projections.

groups by the value of the sign. Thus, these discrepancies were observed in 3 cerebellums when comparing Wax and Wcor, in 10 cerebellums when comparing Lax and Lsag, and in another 10 cerebellums when comparing Hcor and Hsag.

Figures 5-7 show the distribution of values of mutually perpendicular dimensions in the corresponding projections.

Correlation analysis (Fig. 5-7) showed a statistically

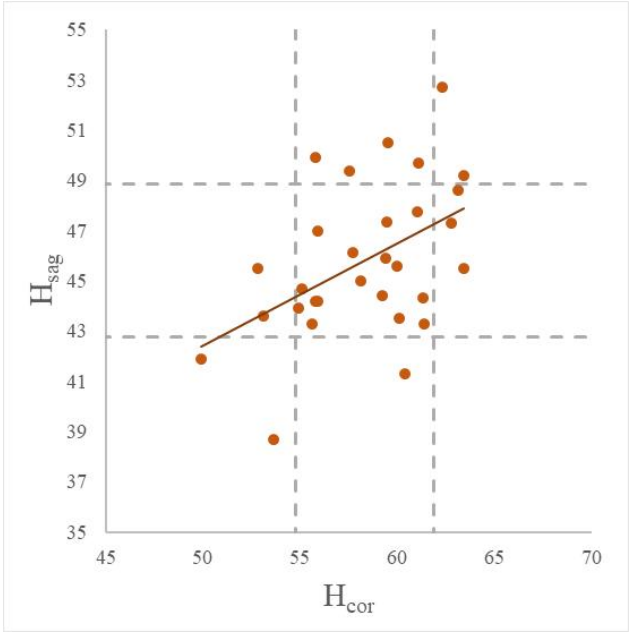

Fig. 4. Distribution of cerebellar height values in coronal and sagittal projections.

significant linear relationship between the values of W_{ax} and L_{ax} (r=0.48; p<0.01); average strength and statistically significant linear relationship between W_{cor} and H_{cor} (r=0.39; p<0.05), as well as average strength, but statistically insignificant linear relationship between L_{sag} and H_{sag} (r=0.33; p>0.05).

Variability of form factors. According to Table 1 (B), the shape of the cerebellum in individual projections can be characterized by the relative value of the shape factor [21]. If the value of the shape factor of the cerebellum under

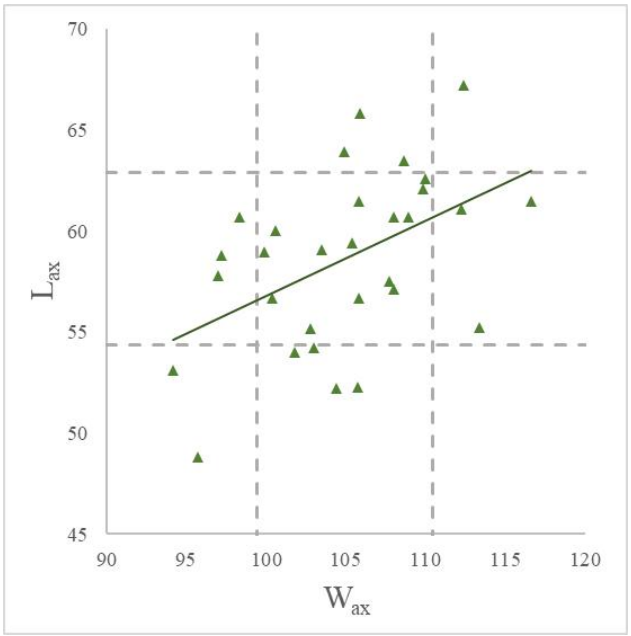

Fig. 5. Distribution of values of the width and length of the cerebellum in the axial projection.

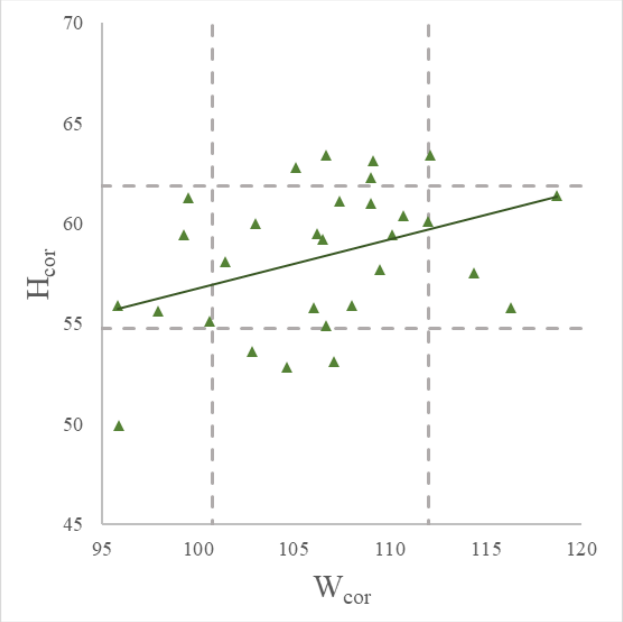

Fig. 6. Distribution of values of the width and height of the cerebellum in the coronal projection.

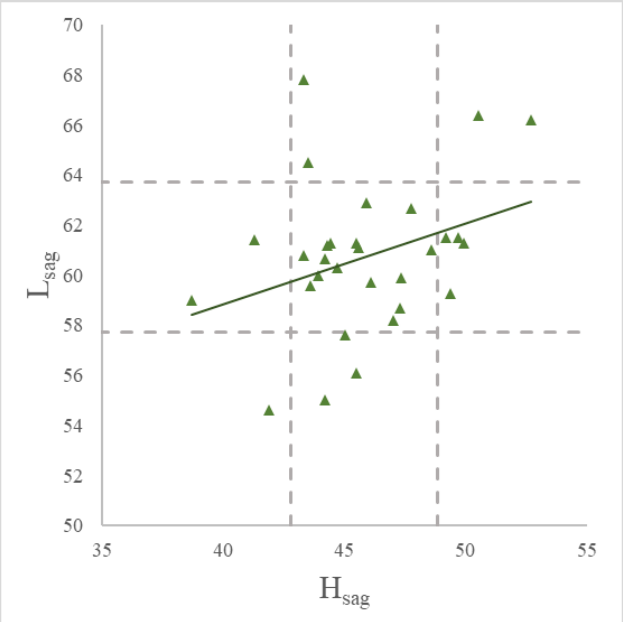

Fig. 7. Distribution of values of the height and length of the cerebellum in the sagittal projection.

study is in the range of average values, such a cerebellum is characterized as proportional, while extreme values indicate disproportionality:

- *relatively wide and short*, with a large ratio value W_{ax} / L_{ax} (1.92÷2.05), or vice versa - *relatively narrow and long*, with a small value of this ratio (1.61÷1.68);
- *relatively wide and low*, with a large ratio value W_{cor} / H_{cor} (1.94÷2.08), or vice versa - *relatively narrow and tall*, with a small value of this ratio (1.62÷1.71);
- *relatively long and low*, with a large ratio value L_{sag} / H_{sag} (1.42÷1.57), or vice versa - *relatively short and tall*, with a small value of this ratio (1.2÷1.24).

According to the ratio of width and length (in the axial projection), 19 cerebellums can be classified as proportional, 4 are relatively wide and short, and 7 are relatively narrow and long. According to the ratio of width and height (in the coronal projection), 21 cerebellums can be classified as proportional, 5 are relatively wide and low, and 4 are relatively narrow and high. According to the ratio of length and height (in the sagittal projection), 21 cerebellums can be classified as proportional, 4 - relatively long and low, 5 - relatively short and high. The distribution of the values of all three form factors by the size of the feature is compared together in Table 2.

As can be seen from the data in Table 2, there is a variety of combinations of variants of the shape of the cerebellum in different projections. 8 cerebellums are proportional in all three shape factors (group 8), 16 have average values of two of the three parameters (groups 3, 5, 7, 9-11). In another 5 cerebellums, only one parameter is in the range of average values (groups 1, 4, 6, 12). Only 1 cerebellum (group 2) belongs to the disproportionate size of all three shape factors.

Relative parameters of the cerebellum. These relative parameters of the cerebellum are shown in Table 1 (C). According to these data, the shape of the cerebellum as a whole can be characterized by the value of the relative parameter. Just as in the analysis of form factors, if the values of the parameters of the cerebellum under study are in the range of average values, such a cerebellum is characterized as proportional, while extreme values indicate disproportionality:

- *relatively wide,* with large value W_r (3.66÷4.08) or vice versa - *relatively narrow* with little value W_r (2.76÷2.92).
- *relatively long*, with large value L_r (0.81÷0.86) or vice versa - *relatively short* with little value L_r (0.59÷0.68).
- *relatively high*, with large value H_r (0.46 ÷ 0.48) or vice

Table 2. Variants of observed cerebellar forms (by form factors).

№	W_{ax} / L_{ax}	W_{cor} / H_{cor}	L_{sag} / H_{sag}	Count
1	Wide and short	Wide and low	Proportional	1
2	Wide and short	Wide and low	Short and high	1
3	Wide and short	Proportional	Proportional	1
4	Wide and short	Narrow and high	Proportional	1
5	Proportional	Wide and low	Proportional	1
6	Proportional	Wide and low	Short and high	2
7	Proportional	Proportional	Long and low	4
8	Proportional	Proportional	Proportional	8
9	Proportional	Proportional	Short and high	2
10	Proportional	Narrow and high	Proportional	2
11	Narrow and long	Proportional	Proportional	6
12	Narrow and long	Narrow and high	Proportional	1
			Total	30

Table 3. Variants of observed cerebellar forms (by relative parameters).

№	Shape variant			Count
	W_r	L_r	H_r	
1	wide	long	low	1
2	wide	medium	low	1
3	wide	short	medium	3
4	medium	medium	low	1
5	medium	long	low	2
6	medium	medium	medium	11
7	medium	long	medium	1
8	medium	short	medium	2
9	medium	medium	high	2
10	narrow	long	medium	2
11	narrow	medium	medium	1
12	narrow	medium	high	3
			Total	30

versa - *relatively small* with little value H_r (0.33÷0.37).

According to the relative width, 19 cerebellums can be classified as proportional, 5 are relatively wide, and 6 are relatively narrow. According to the relative length, 19 cerebellums can be classified as proportional, 6 are relatively long, and 5 are relatively short. According to the relative height, 20 cerebellums can be classified as proportional, 5 are relatively high, and 5 are relatively low. The distribution of the values of all three relative dimensions by the size of the feature is compared together in Table 3.

As can be seen from the data in Table 3, there is a variety of combinations of parameters of the shape of the cerebellum. Eleven cerebellums have average values of each of the three parameters (group 6), seven have average values of two of the three parameters (groups 4, 7, 8, 9, 11). In another 11 cerebellums, only one parameter is in the range of average values (groups 2, 3, 5, 10, 12), and 1 disproportionate cerebellum was also observed (group 1).

Discussion

The method of determining the size of the cerebellum used in this work is similar to the "bounding box" method of L. Xiang for analyzing a three-dimensional model of the brain [27]. The method of orientation of the rectangle in different projections was chosen among the most common methods in stereotaxic neurosurgery, which were the most informative and based on the most stable and visible on MRI images of the brain structure [11]. "Limiting rectangle" can be used as an additional examination of the cerebellum during morphometry of MR tomograms [9].

Measurement of the cerebellum on tomograms makes it possible to assess the size and shape in vivo, in its natural position in the skull cavity, but only in separate tomographic projections. To assess the shape of the cerebellum on MR images, shape factors were calculated - the ratio of cerebellum sizes determined in each projection. In our work, this method of assessing the shape of the cerebellum was adapted for morphometric studies on MR tomograms [21].

As shown in Figure 1, each linear dimension - length, width, height - is defined in two mutually perpendicular projections. Due to the peculiarities of conducting MR tomography (the presence of a "step" when conducting MR "slices" and their orientation in space), on the one hand, as well as the complex three-dimensional shape of the cerebellum, on the other hand, the extreme, most distant points on the surface of the cerebellum, on which the bounding rectangle rests, on mutually perpendicular MR images often do not coincide. As a result, the value of the same size defined in one projection differs from that defined in another projection. Also, the same linear dimension in two different projections is related to two different other linear dimensions. Therefore, to evaluate the shape of the cerebellum as a three-dimensional structure, parameters were proposed on MR images that take into account the ratio of one linear size of the cerebellum to the other two, namely: the *relative width of the cerebellum* (W_r), the *relative length of the cerebellum* (L_r) and the *relative height of the cerebellum* (H_r).

The obtained data on the variability of the linear dimensions of the cerebellum differ from those in [20], where the height was determined to be more variable than the width or length. This is explained by the peculiarities of the measurement technique and sample sizes.

The existence of a statistically significant linear relationship between the values of length and width was previously established when measuring anatomical preparations of the cerebellum [20]. However, the significant linear relationship between Wcor and Hcor found in this study may be due to the peculiarities of measuring cerebellar height on tomograms. The variability of the values of paired linear dimensions measured in one projection and the lack of a functional connection between them lead to the variability of the ratios of linear dimensions, hence the variability of the shape factors (Table 1 B), which characterize the shape of the cerebellum in tomographic projections.

As shown in the study of A. Yu. Stepanenko [21], the size of the form factor determined on an anatomical preparation of the cerebellum affects its external structure in individual projections. In our opinion, the size of the shape factors determined on MR tomograms affects the shape of intracerebellar structures, namely the nuclei of the cerebellum, first of all, the dentate nucleus, which has a complex three-dimensional organization [18].

The analysis of relative indicators allows, in our opinion, to determine which linear size has the greatest influence on the shape of the cerebellum as a whole and, thereby, on the shape of the lobes, the course of the furrows, the three-dimensional organization of its nuclei and other anatomical features. Taking into account the shape of the cerebellum,

in turn, will contribute to the improvement of the diagnosis of its diseases using MRI, will be useful when conducting neuromorphological studies.

Conclusion

1. The proposed complex method of assessing the shape of the cerebellum in the morphometry of tomograms. The method consists in measuring linear dimensions (*width, length and height*) on tomograms in three different projections, calculating their ratios (form factors: *width / length, width / height and length / height ratios*) and relative dimensions (*relative width, length and height cerebellum*) according to formulas.

2. Analysis of the shape of the cerebellum contributes to the intravital determination of the features of its structure, namely: the shape of the lobes, the course of the furrows, the three-dimensional organization of its nuclei, etc.

References

[1] Adamaszek, M., D'Agata, F., Ferrucci, R., Habas, C., Keulen, S., Kirkby, K. C., … & Verhoeven, J. (2017). Consensus Paper: Cerebellum and Emotion. Cerebellum (London, England), 16(2), 552-576. doi: 10.1007/s12311-016-0815-8

[2] Ahmad, N., Singh, D., & Jethani, S. (2023). Role of vermal anteroposterior length and width in age determination of fetus. *Journal of the Anatomical Society of India,* 72(2), 135. doi: 10.4103/jasi.jasi_89_22

[3] Clouchoux, C., Guizard, N., Evans, A. C., du Plessis, A. J., & Limperopoulos, C. (2012). Normative fetal brain growth by quantitative in vivo magnetic resonance imaging. *American Journal of Obstetrics and Gynecology,* 206(2), 173.e1-173.e1738. doi: 10.1016/j.ajog.2011.10.002

[4] D'Mello, A. M., & Stoodley, C. J. (2015). Cerebro-cerebellar circuits in autism spectrum disorder. Frontiers in Neuroscience, 9, 408. doi: 10.3389/fnins.2015.00408

[5] Guell, X., Gabrieli, J. D. E., & Schmahmann, J. D. (2018). Triple representation of language, working memory, social and emotion processing in the cerebellum: convergent evidence from task and seed-based resting-state fMRI analyses in a single large cohort. *Neuroimage,* 172, 437-449. doi: 10.1016/j.neuroimage.2018.01.082

[6] Leto, K., Arancillo, M., Becker, E. B., Buffo, A., Chiang, C., Ding, B., … & Hawkes, R. (2016). Consensus Paper: Cerebellar Development. *Cerebellum* (London, England), 15(6), 789-828. doi: 10.1007/s12311-015-0724-2

[7] Lewis, M. M., Galley, S., Johnson, S., Stevenson, J., Huang, X., & McKeown, M. J. (2013). The role of the cerebellum in the pathophysiology of Parkinson's disease. The Canadian Journal of Neurological Sciences. *Le Journal Canadien des Sciences Neurologiques,* 40(3), 299-306. doi: 10.1017/s0317167100014232

[8] Marien, P., Ackermann, H., Adamaszek, M., Barwood, C. H., Beaton, A., Desmond, J. … & Ziegler, W. (2014). Consensus paper: Language and the cerebellum: an ongoing enigma. *Cerebellum* (London, England), 13(3), 386-410. doi: 10.1007/s12311-013-0540-5

[9] Maryenko, N. I. (2020). *Возрастная динамика фрактальной размерности внешнего контура мозжечка человека по данным магнитно-резонансной томографии [Age dynamics of the fractal dimension of the external contour of the human cerebellum according to magnetic resonance imaging data].* Актуальные проблемы медицины: сборник научных статей Республиканской научно-практи ческой конференции с международным участием, посвященной 30-летнему юбилею Гомельского государственного медицинского университета, Т. 2, стр. 55-57, Гомель: ГомГМУ, 2020. - Actual problems of medicine: collection of scientific articles of the Republican scientific and practical conference with international participation, dedicated to the 30th anniversary of Gomel State Medical University, Vol. 2, pp. 55-57, Gomel: GomSMU, 2020.

[10] Nowinski, W. L. (2001). Modified Talairach landmarks. *Acta Neurochirurgica,* 143(10), 1045-1057. doi: 10.1007/s007010170011

[11] Otake, S., Taoka, T., Maeda, M., & Yuh, W. T. (2018). A guide to identification and selection of axial planes in magnetic resonance imaging of the brain. *The Neuroradiology Journal,* 31(4), 336-344. doi: 10.1177/1971400918769911

[12] Phillips, J. R., Hewedi, D. H., Eissa, A. M., & Moustafa, A. A. (2015). The cerebellum and psychiatric disorders. *Frontiers in public health*, 3, 66. doi: 10.3389/fpubh.2015.00066

[13] Reed, M. D., English, M., English, C., Huff, A., Poliacek, I., Musselwhite, M. N., … & Pitts, T. (2019). The Role of the Cerebellum in Control of Swallow: Evidence of Inspiratory Activity During Swallow. *Lung,* 197(2), 235-240. doi: 10.1007/s00408-018-00192-2

[14] Sathyanesan, A., Zhou, J., Scafidi, J., Heck, D. H., Sillitoe, R. V., & Gallo, V. (2019). Emerging connections between cerebellar development, behaviour and complex brain disorders. *Nature reviews. Neuroscience*, 20(5), 298-313. doi: 10.1038/s41583-019-0152-2

[15] Schmahmann, J. D., Doyon, J., McDonald, D., Holmes, C., Lavoie, K., Hurwitz, A. S. … & Petrides, M. (1999). Three-dimensional MRI atlas of the human cerebellum in proportional stereotaxic space. *NeuroImage,* 10(3 Pt 1), 233-260. doi: 10.1006/nimg.1999.0459

[16] Schmahmann, J. D. (2019). The cerebellum and cognition. *Neuroscience Letters,* 688, 62-75. doi: 10.1016/j.neulet.2018.07.005

[17] Shmarhalov, A., Vovk, O., Ikramov, V., Acharya, Y., & Vovk, O. (2022). Anatomical variations of the parietal foramen and its relations to the calvarial landmarks: a cross-sectional cadaveric study. *Wiadomosci Lekarskie* (Warsaw, Poland:1960), 75(7), 1648-1652. doi: 10.36740/WLek202207106

[18] Shyian, D., Galata, D., Potapov, S., & Gargin, V. (2016). Peculiarities of the cerebellum nuclei in aged persons. *Georgian medical news*, (253), 110-115. PMID: 27249446

[19] Steele, C. J., & Chakravarty, M. M. (2018). Gray-matter structural variability in the human cerebellum: Lobule-specific differences across sex and hemisphere. *NeuroImage,* 170, 164-173. doi: 10.1016/j.neuroimage.2017.04.066

[20] Stepanenko, A. Yu. (2010). Вариантная анатомия и индивидуальная изменчивость макроанатомических показателей мозжечка человека [Variant anatomy and individual variation of human cerebellum macroanatomical indexes]. *Медицина сьогодні і завтра - Medicine Today and Tomorrow,* 47-48 (2-3), 81-87.

[21] Stepanenko, A. Yu. (2012). Индивидуальная изменчивость формы и внешнего вида мозжечка человека [Individual variation of the shape and appearance of human cerebellum].

Медицина сьогодні і завтра - Medicine Today and Tomorrow, 56 (3-4), 48-52.

[22] Stoodley C. J. (2014). Distinct regions of the cerebellum show gray matter decreases in autism, ADHD, and developmental dyslexia. *Frontiers in systems neuroscience,* 8, 92. doi: 10.3389/fnsys.2014.00092

[23] ten Donkelaar, H. J., Lammens, M., Wesseling, P., Thijssen, H. O., & Renier, W. O. (2003). Development and developmental disorders of the human cerebellum. *Journal of Neurology,* 250(9), 1025-1036. doi: 10.1007/s00415-003-0199-9

[24] Tiemeier, H., Lenroot, R. K., Greenstein, D. K., Tran, L., Pierson, R., & Giedd, J. N. (2010). Cerebellum development during childhood and adolescence: a longitudinal morphometric MRI study. *NeuroImage,* 49(1), 63-70. doi: 10.1016/j.neuroimage.2009.08.016

[25] Wang, S. S., Kloth, A. D., & Badura, A. (2014). The cerebellum, sensitive periods, and autism. *Neuron*, 83(3), 518-532. doi: 10.1016/j.neuron.2014.07.016

[26] Wang, Y., Chen, L., Wu, Z., Li, T., Sun, Y., Cheng, J., … & UNC/UMN Baby Connectome Project Consortium (2023). Longitudinal development of the cerebellum in human infants during the first 800 days. *Cell reports,* 42(4), 112281. doi: 10.1016/j.celrep.2023.112281

[27] Xiang, L., Crow, T., & Roberts, N. (2019). Cerebral torque is human specific and unrelated to brain size. *Brain Structure and Function,* 224(3), 1141-1150. doi: 10.1007/s00429-018-01818-0

[28] Xu, F., Ge, X., Shi, Y., Zhang, Z., Tang, Y., Lin, X., … & Liu, S. (2020). Morphometric development of the human fetal cerebellum during the early second trimester. *NeuroImage,* 207, 116372. doi: 10.1016/j.neuroimage.2019.116372

[29] Ye, J., Rong, R., Dou, Y., Jiang, J., & Wang, X. (2020). Evaluation of the development of the posterior fossa in normal Chinese fetuses by using magnetic resonance imaging. *Medicine,* 99(16), e19786. doi: 10.1097/MD.0000000000019786

[30] Zhang, Y., & Wu, X. (2021). Asymmetries of cerebellar lobe in the genus homo. *Symmetry,* 13(6), 988. doi: 10.3390/sym1306098

СПОСІБ ОЦІНЮВАННЯ ФОРМИ МОЗОЧКА ЛЮДИНИ: МРТ ДОСЛІДЖЕННЯ

Калініченко М. О.

Мінливість форми органу є одним із проявів його індивідуальної анатомічної мінливості. Магнітно-резонансна томографія та інші сучасні нейровізуалізаційні методи дозволяють встановити морфологічні особливості органів прижиттєво, при збереженні їх природного положення. Мета роботи - розробити метод оцінювання форми мозочка людини за результатами морфометрії МР томограм. Досліджено МР томограми головного мозку 30 осіб без видимої патології головного мозку (15 чоловіків і 15 жінок у віці від 20 до 40 років). МРТ проводили на апараті МРТ 1,5 Т (Siemens Magnetom Symphony, Мюнхен, Німеччина). Було визначено ширину мозочка в аксіальній (W_{ax}) і корональній (W_{cor}) проекціях, довжину в аксіальній (L_{ax}) і сагітальній (L_{sag}) проекціях, висоту у корональній (H_{cor}) та сагітальній (H_{sag}) проекціях. Встановлено, що ширина мозочка майже однаково визначається у двох різних проекціях, більше розбіжність при визначенні довжини, максимальна різниця значень виявляється при вимірюванні висоти. Було знайдено середній за силою статистично значущий лінійний взаємозв'язок між мінливостями W_{ax} і L_{ax} ($r=0,48$; $p<0,01$), W_{cor} і H_{cor} ($r=0,39$; $p<0,05$). Мінливість значень парних лінійних розмірів, що вимірюються в одній проекції, і відсутність функціонального зв'язку між ними призводять до мінливості їх співвідношень - факторів форми (W_{ax} / L_{ax}, W_{cor} / H_{cor}, L_{sag} / H_{sag}), яка своєю чергою впливає на форму внутрішньомозочкових структур, перш за все - ядер мозочка. Для визначення форми мозочка у цілому запропоновано параметри, що враховують співвідношення одного лінійного розміру мозочка до двох інших, а саме: відносна ширина мозочка ($W_r = (W_{ax}xW_{cor}) / (L_{ax}xH_{cor})$), відносна довжина мозочка ($Lr = (L_{ax}xL_{sag}) / (W_{ax}xH_{sag})$) та відносна висота мозочка ($H_r = (H_{cor}xH_{sag}) / (W_{cor}xL_{sag})$). Подальший аналіз даних параметрів визначає, який із лінійних розмірів більше впливає на форму мозочка, що зумовлює особливості його будови, як-то - форму часточок, хід борозн, тривимірну організацію його ядер та ін. Прижиттєве визначення форми мозочка сприятиме покращенню діагностики його захворювань з використанням МРТ і буде корисним при проведенні нейроморфологічних досліджень.

Ключові слова: *людина, анатомія, мозочок, МРТ, морфометрія.*

DOI: 10.31393/morphology-journal-2023-29(4)-03 Reports of Morphology, Vol. 29, №4, Pages 19-26

ISSN 1818-1295 eISSN 2616-6194

REPORTS OF MORPHOLOGY

Official Journal of the Scientific Society of Anatomists, Histologists, Embryologists and Topographic Anatomists of Ukraine

journal homepage: https://morphology-journal.com

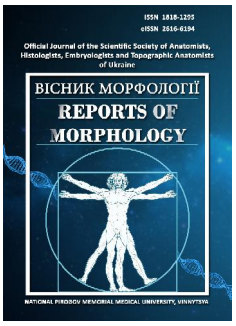

Morphohistological study of regeneration of knee joint cartilage defects in an experimental model under the influence of nuclear magnetic resonance therapy

Fishchenko V. O., Korol A. P., Yusupova D. V.
National Pirogov Memorial Medical University, Vinnytsia, Ukraine

ARTICLE INFO
Received: 19 July 2023
Accepted: 18 September 2023

UDC: 616.728.3-018.3-08:581.148:537.612

CORRESPONDING AUTHOR
e-mail: Daria.plahotna@icloud.com
Yusupova D. V.

CONFLICT OF INTEREST
The authors have no conflicts of interest to declare.

FUNDING
Not applicable.

DATA SHARING
Data are available upon reasonable request to corresponding author.

Despite the variety of modern methods of treatment, the problem of hyaline cartilage regeneration is still relevant. Purpose of the study: to determine the effect of nuclear magnetic resonance therapy on the regenerative ability of simulated defects in the cartilage tissue of the knee joint in rats, to assess the dynamics of microscopic changes in articular cartilage in the main and control groups. The study was performed on 60 sex-mature rats. The defects were created in the area of the articular surfaces of the left knee joint - 30 defects in the main group and 30 defects in the control group. The right knee joint of both study groups was used as the norm. Medical (antibiotics, anti-inflammatory, analgesic) therapy was carried out for 3 days after the surgery. On the 4th day after surgery, rats of the main group were given nuclear magnetic resonance therapy for 60 minutes, for 7 days. After 7, 14, 21, 28 days after therapy, histological analysis of cartilage regenerate was performed. 28 days after the use of nuclear magnetic resonance therapy, the height of cartilage regenerate in rats was 82.12±8.89 μm in the intervention group and 56.34±7.82 μm in the control group. Cartilage regenerate in rats after nuclear magnetic resonance therapy was close to the structure of intact hyaline cartilage. However, complete regeneration did not occur, as evidenced by the smaller thickness of the articular cartilage compared to that in the right knee joint. In the control group, the formation of the regeneration had pronounced signs of dysregeneration. The cartilage tissue in the area of the defect, was predominantly fibrous in the nature with areas of necrosis. Nuclear magnetic resonance therapy contributes to the formation of articular cartilage in the defect - cartilage regenerate, which in its histological structure approaches hyaline cartilage.

Keywords: *nuclear magnetic resonance therapy, rats, cartilage regenerate, chondrocyte proliferation, experiment.*

Introduction

Degenerative joint disease, such as osteoarthritis (OA), is one of the most common pathologies among people, especially after the age of 65, and is a leading cause of disability [4, 10, 15]. Knee joint injuries account for up to 14% of the total number of lower extremity injuries that lead to articular cartilage damage.

Articular cartilage is a type of connective tissue that evenly distributes pressure on the bone, acting as its shock absorber and protection. Given the fact that cartilage tissue is avascular, it is quite difficult for damaged cartilage to recover on its own. Therefore, the restoration of damaged cartilage is achieved due to the proliferation of chondrocytes and the synthesis of the extracellular matrix, which consists of collagen fibers and proteoglycans [5].

The occurrence and progression of degenerative changes in cartilage tissue are associated with various factors, including genetic features, aging, trauma, and environmental exposure [1]. The main pathogenetic factor in the formation of cartilage defects of the knee joint is its destruction, which develops as a result of a mismatch in the distribution of mechanical load and the cartilage's ability to resist it. In case of traumatic damage to articular cartilage tissue, metaplasia or dysregeneration usually occurs, as a result of which hyaline cartilage is replaced by fibrous cartilage [2]. Traumatic damage to articular cartilage leads to degenerative-dystrophic damage to the joint and the occurrence of irreversible secondary arthrotic changes [3, 11]. Despite significant achievements in the study of the

mechanisms of articular cartilage degeneration and the development of new treatment methods, the problem of hyaline cartilage regeneration remains extremely relevant [14, 17, 20].

The purpose of the study: to determine the effect of nuclear magnetic resonance therapy on the regenerative capacity of simulated cartilage tissue defects of the knee joint in rats, to evaluate the dynamics of microscopic changes in articular cartilage in the main and control groups.

Materials and methods

All manipulations with animals were carried out in accordance with the law of Ukraine "On the protection of animals from cruel treatment" dated December 9, 2015 [18]. The experimental animals were cared for in accordance with generally accepted recommendations, requirements and provisions for the care of laboratory animals: the Helsinki Declaration of the General Assembly of the World Medical Association (2000); Provisions of the "European Convention for the Protection of Vertebrate Animals Used for Experiments and Other Scientific Purposes" (Stpacbypg, 1985) [7]. The research protocol was approved at a meeting of the Bioethics Commission of National Pirogov Memorial Medical University, Vinnytsia, Ukraine (protocol No. 7 dated September 16, 2021).

Surgical interventions. The study was performed on 60 sexually mature rats weighing 250.0±50.0 g. In all animals, in aseptic conditions, under intravenous anesthesia with Ketamine solution (50.0 mg/kg), after treating the operative field with Betadine 10 % three times, a skin incision was made and the underlying capsule of the left knee joint through a medial parapatellar approach, measuring ±2-3 mm. Using a scalpel (size 15), a full-layer cartilage defect was created. The open wound was washed with an antiseptic solution of Dekasan, followed by layer-by-layer suturing of soft tissues. The postoperative wound was treated with Sterilium and an aseptic bandage with Betadine 10 % was applied. The first 3 days after damage simulation, all experimental animals were treated with the following drugs: Ceftriaxone, Diclofenac, Analgin. During the surgical intervention, a full-layer cartilage defect was formed with the involvement of the subcartilaginous plate (n=60). After the completion of this stage of the experiment, all animals were divided into 2 groups: the main and control, 30 animals in each.

After medical treatment for the animals of the main group, starting from the 4th day after surgery, a cartilaginous program of nuclear magnetic resonance therapy was carried out daily, for 60 minutes, for 7 days.

Nuclear magnetic resonance therapy was not used for the control group of animals.

For comparative analysis, the right knee joint in both groups of animals was not damaged.

Rats from the main group were removed from the experiment after 7 (group O1), 14 (group O2), 21 (group O3) and 28 (group O4) days (6 animals for each term) after a one-week course of nuclear magnetic resonance therapy by administering lethal dose of anesthetic (sodium thiopental was administered intramuscularly at the rate of 90 mg/kg). In the control group of animals, nuclear magnetic resonance therapy was not performed, but the rats were removed from the experiment at the same time of the study as from the main group, which corresponded to 17 (group K1), 24 (group K2), 31 (group K3) and 38 (group K4) days (6 animals for each period) from the beginning of the operation.

Histological analysis. To evaluate the morphological changes, the knee joints of the left hind limb of rats of the main and control groups, as well as the knee joints of the right hind limb involving the distal part of the femur and the proximal part of the tibia, were isolated, fixed in a 10 % solution of neutral formalin and decalcified. Preparations were prepared according to standard methods, axial histological sections of joints (5 from each animal) with a thickness of 5-7 μm were stained with Weigert's hematoxylin and eosin, as well as Van Gieson's picrofuchsin [22].

Microscopy and photography were carried out using a light microscope EUROMEX microscopes Holland IScope 1153-PLI. Images were acquired and processed using the "ImageFocusAlpha" program.

Animals were withdrawn from the experiment at intermediate stages of articular cartilage regeneration (7, 14, 21, 28 days) to study the dynamics of the recovery process.

Morphometric studies of articular cartilage at the level of the distal part of the femur and the proximal part of the tibia were performed using the "ImageFocusAlpha" software for the "EUROMEX microscopes Holland IScope 1153-PLI" microscope. The total height of the articular cartilage, the height of the surface, intermediate and zone of calcified cartilage were measured. The intermediate (or mid) zone was considered the layer of articular cartilage from the surface zone to the basophilic line (tidemark) according to the recommendations of Gerwin N. and co-authors [8].

In all experimental groups, general and local complications were not observed in the postoperative period.

Statistical studies. The results of the morphometric study were processed using the Microsoft Excel computer program and presented in the form of M±m. Comparison of mean values was performed using Student's t-test.

Results

To compare the structural changes in the articular cartilage after injury, we examined the cartilage structure of the right knee joint of both study groups without injury.

Morphologically, the following zones could be distinguished in the cartilage: the surface layer, separated from the joint cavity by a thin acellular eosinophilic plate, which contained single flat chondrocytes: the middle layer, with rounded and oval chondrocytes, which were evenly

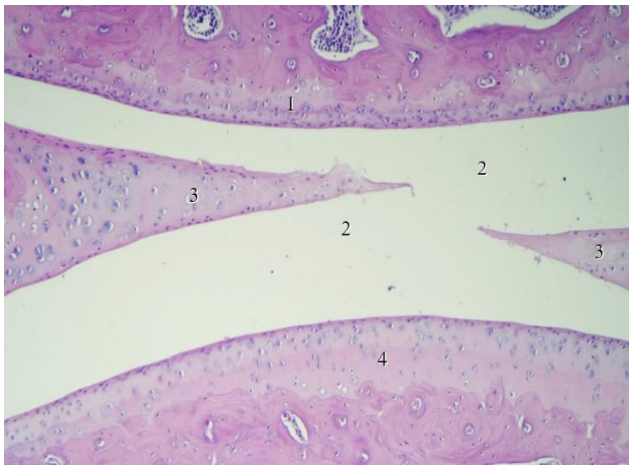

Fig. 1. The structure of the knee joint of an intact rat. 1 - femur cartilage. 2 - articular cavity. 3 - anterior horn of the meniscus. 4 - tibial cartilage. Hematoxylin and eosin staining. Magnification x100.

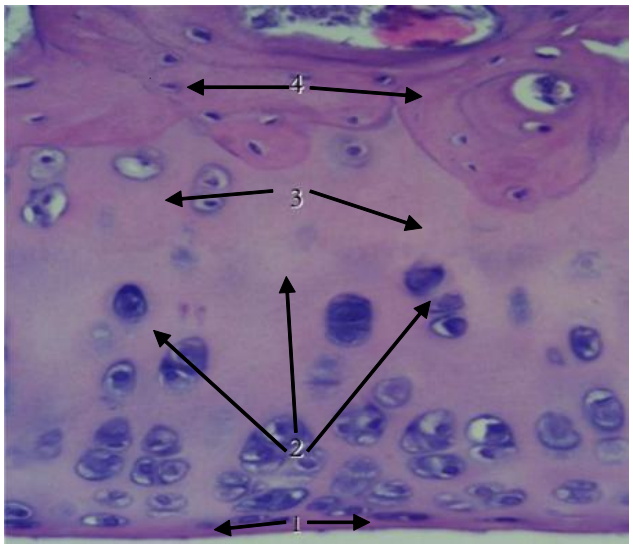

Fig. 2. The structure of the knee joint of an intact rat. 1 - surface zone. 2 - middle zone. 3 - zone of calcification. 4 - subchondral bone tissue. Hematoxylin and eosin staining. Magnification x400.

located in isogenic groups; deep layer where chondrocytes formed columns. The subchondral bone plate was directly adjacent to the deep layer. In the surface layer, elongated chondrocytes, arranged in 2-3 layers along the articular surface, contained large oval hyperchromic nuclei with a thin rim of cytoplasm. The intercellular matrix had a uniform, weakly eosinophilic coloration. In the middle layer, near the surface, isogenic groups of chondrocytes contained 2 to 4 cells. In the deeper layers, chondrocytes formed columns. The basophilic line was visualized along the entire length of the articular surface. The zone of calcified cartilage contained chondrocytes in expanded capsules located at a distance from each other. Such cells had hyperchromic nuclei surrounded by vesicular cytoplasm. Closer to the subchondral bone, chondrocytes had pyknotic nuclei with weakly contoured cytoplasm. Some lacunae did not contain cells. In some places, blood vessels penetrated from the bone tissue to the calcified cartilage (Fig. 1, 2). The described structural features of articular cartilage were characteristic of all articular surfaces of rats that were not traumatized. However, the thickness of the articular cartilage was different, which is related to the long period of the study.

Group O1. In the case of application of nuclear magnetic resonance therapy, a high density of osteoblasts was determined in the newly formed coarse-fiber bone tissue. The central part of the defect was occupied by granulation tissue that completely covered the bottom of the defect and contained a significant number of blood capillaries of various diameters (Fig. 3). The thickness of the regeneration tissue was 33.45±5.17 μm (Table 1).

Group K1. In this research group, the regeneration process was less pronounced. In the regenerate of the bottom of the defect, the formation of bone tissue in the form of coarse-fibered bone trabeculae with a small number of osteocytes was noted. On the outer surface of the bone trabeculae of the subchondral bone, there are numerous osteoblasts in the form of a palisade. The granulation tissue is represented by scattered islands of fibroblastic diferon cells (Fig. 4). The thickness of the regeneration tissue was 20.53±3.07 μm (see Table 1).

In rats that did not undergo MBST, the articular cartilage

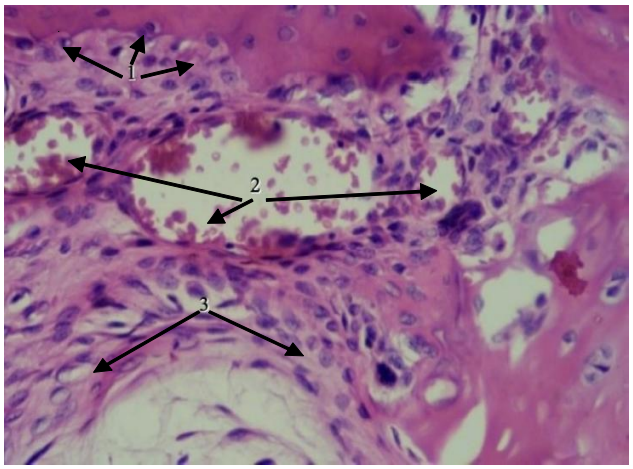

Fig. 3. Regenerative tissue O1. 1 - coarse fibrous bone tissue. 2 - blood vessels. 3 - granulation tissue. Hematoxylin and eosin staining. Magnification x400.

Table 1. The thickness (μm) of the regeneration cartilage of the left knee joint in different experimental groups of animals.

Term, days	Group of animals		p
	Researched	Control	
7	33.45±5.17	20.53±3,07	<0.01
14	48.54±7.03	35.27±6.64	<0.01
21	64.57±7.86	45.42±4.38	<0.01
28	82.12±8.89	56.34±7.82	<0.01

Note: p - the reliability of the differences in the average values of the thickness of the regeneration cartilage of the knee joint of the main group compared to the control group in all terms of the experiment.

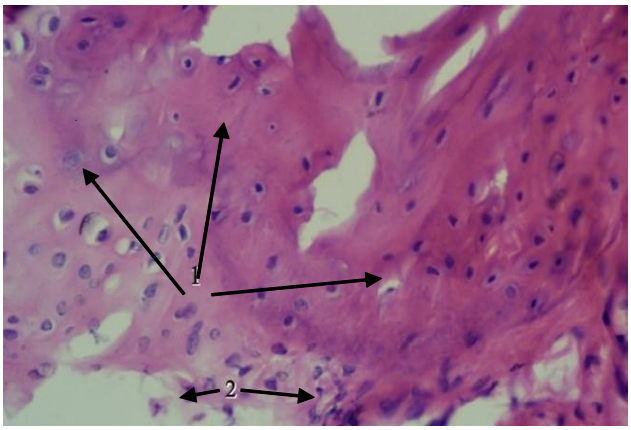

Fig. 4. Regeneration tissue K1. 1 - coarse fibrous bone tissue. 2 - granulation tissue. Hematoxylin and eosin staining. Magnification x400.

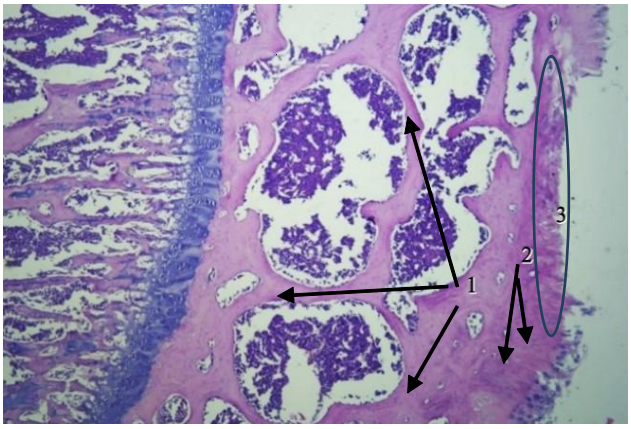

Fig. 5. The structure of articular cartilage K1. 1 - subchondral bone tissue. 2 - intermediate zone of articular cartilage. 3 - absence of chondrocytes in the surface zone of articular cartilage. Hematoxylin and eosin staining. Magnification x100.

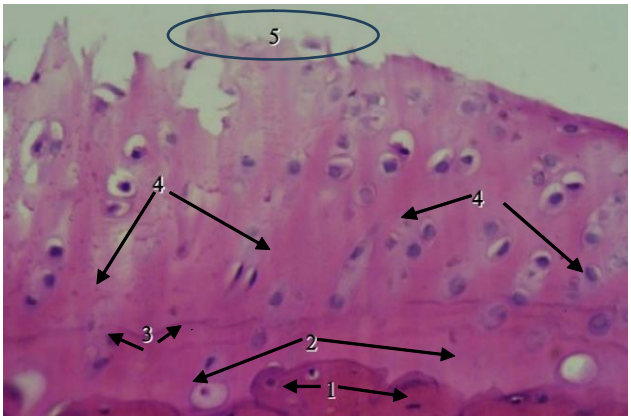

Fig. 6. The structure of articular cartilage K1. 1 - subchondral bone tissue. 2 - zone of calcification of articular cartilage. 3 - basophilic line of articular cartilage. 4 - intermediate zone of articular cartilage. 5 - absence of chondrocytes in the surface zone of the cartilage. Hematoxylin and eosin staining. Magnification x400.

near the injury zone underwent structural changes. In particular, areas of cartilage without chondrocytes were detected in the surface zone, and the matrix was stained eosinophilic. In the middle zone, some isogenic groups did not contain chondrocytes. The basophilic line throughout the area of the articular cartilage covering the femur was uneven and discontinuous. Significant areas without chondrocytes and uneven staining of the matrix were also observed in the zone of calcified cartilage. At a distance from the site of transchondral damage, structural changes in the articular cartilage were less pronounced

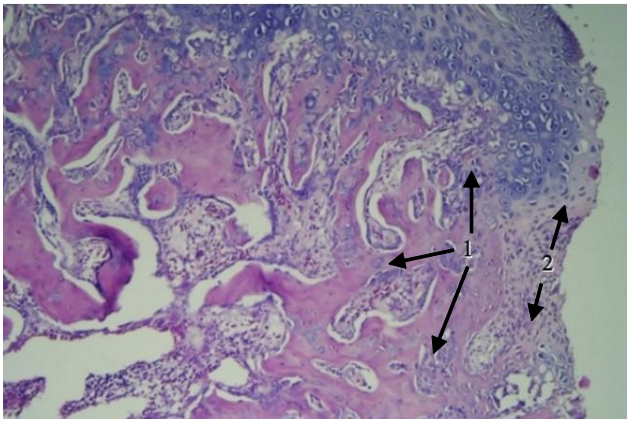

Fig. 7. The structure of regeneration tissue O2. 1 - subchondral bone tissue. 2 - regeneration tissue. Hematoxylin and eosin staining. Magnification x100.

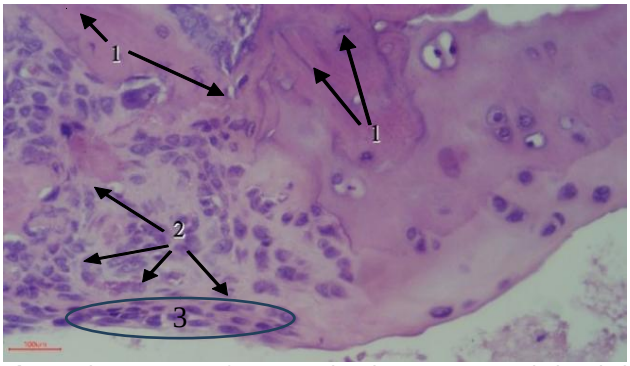

Fig. 8. The structure of regeneration tissue O2. 1 - subchondral bone tissue. 2 - newly formed cartilage tissue. 3 - regeneration tissue. Hematoxylin and eosin staining. Magnification x400.

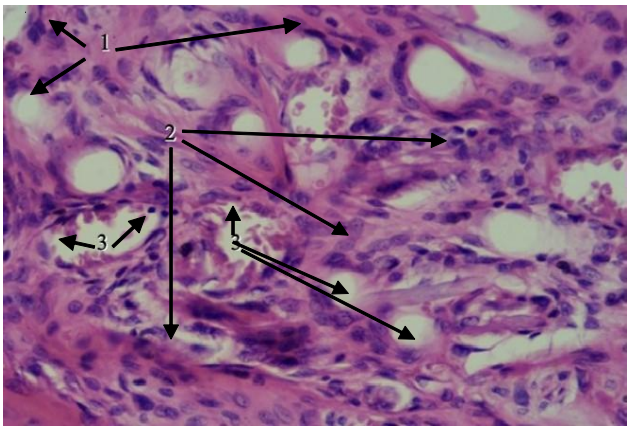

Fig. 9. The structure of articular cartilage K2. 1 - subchondral bone tissue. 2 - dense designed connective tissue. 3 - blood vessels. Hematoxylin and eosin staining. Magnification x400.

and were manifested by a decrease in the density of chondrocytes in the surface zone, inhomogeneity of the color of the matrix, and unevenness of the basophilic line (Fig. 5, 6).

Group O2. In rats, which were subjected to MBST after the articular cartilage defect was applied, the histospecies showed a traumatic injury area filled with lamellar bone tissue, which usually did not differ in structure from the adjacent maternal subchondral bone (Fig. 7). On the surface of the defect, which bordered the cavity of the joint, a formation of uneven thickness of the cartilage layer was found. Chondrocytes, which were densely arranged and formed 2-3 rows of isogenic groups, had 2 cells each. They contained basophilic cytoplasm and large rounded nuclei (Fig. 8). The thickness of the regeneration tissue was 48.54±7.03 μm (see Table 1).

Group K2. In rats that did not undergo MBST after the articular cartilage defect, the regeneration tissue did not completely fill the defect area. The formation of dense connective tissue, which contained numerous fibroblasts, was noted on the surface bordering the joint cavity. Their long axis was directed parallel to the surface. The bone tissue was located along the perimeter of the defect, from the sides of the parent bone to the center, and contained coarse-fibered bone trabeculae with a significant density of osteocytes and osteoblasts on the outer surface (Fig. 9). The number of fibroblasts in the fibrocartilaginous tissue was higher, compared to the same one, in the previous period of the study. The thickness of the regeneration tissue was 35.27±6.64 μm (see Table 1).

Group O3. In the rats treated after the articular cartilage defect was applied, 21 days after nuclear magnetic resonance therapy, in the area of damage, lamellar bone tissue, as in the previous period of the study, did not differ in structure from subchondral bone. On the surface of the defect, which bordered the cavity of the joint, the formation of fibrous cartilage, uneven in thickness, was found. In the middle zone, isogenic groups of cartilage contained 2-3 to 4 chondrocytes, in contrast to the previous period of observation, when isogenic groups contained 2 chondrocytes each. The territorial cartilage matrix is more pronounced in contrast to the previous term of the study. The thickness of the regeneration tissue was 64.57±7.86 μm (see Table 1).

Group K3. In the control group of animals that did not undergo MRI, bone trabeculae were located directly under the fibrocartilage layer, had irregular edges and resorption lacunae with osteoclasts and osteoid layering in other areas. The damaged articular surface was covered with fragments of fibrous cartilage. Most of the chondrocytes were destructively changed. Small foci of chondroblast hyperplasia were detected. Fibrous cartilage also formed on the articular surface adjacent to the defect site, replacing the articular cartilage and, without a clear boundary, transitioning into the connective tissue that was located on part of the surface of the preserved articular cartilage. The

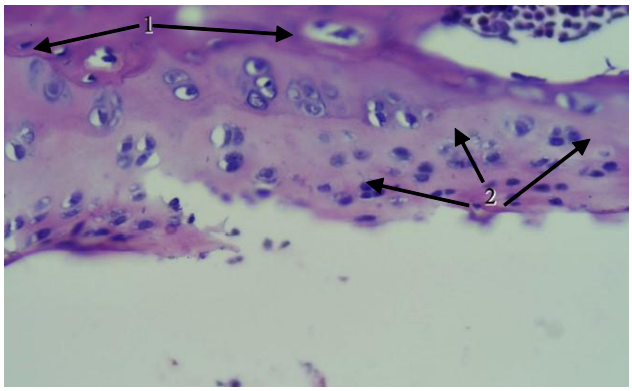

Fig. 10. The structure of articular cartilage K3. 1 - subchondral bone tissue. 2 - fibrous cartilaginous tissue. Hematoxylin and eosin staining. Magnification x400.

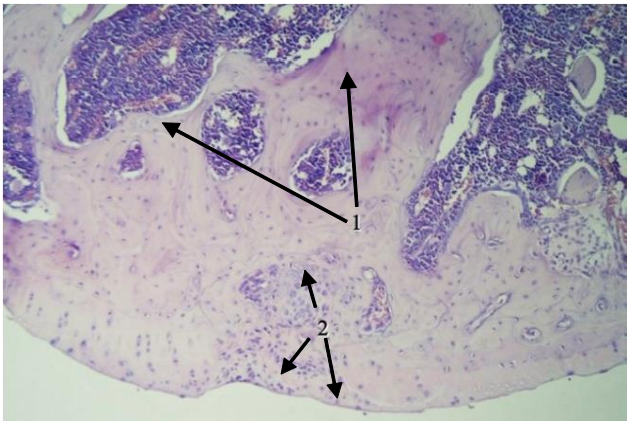

Fig. 11. The structure of articular cartilage O4. 1 - subchondral bone tissue. 2 - area of articular cartilage regeneration. Hematoxylin and eosin staining. Magnification x100.

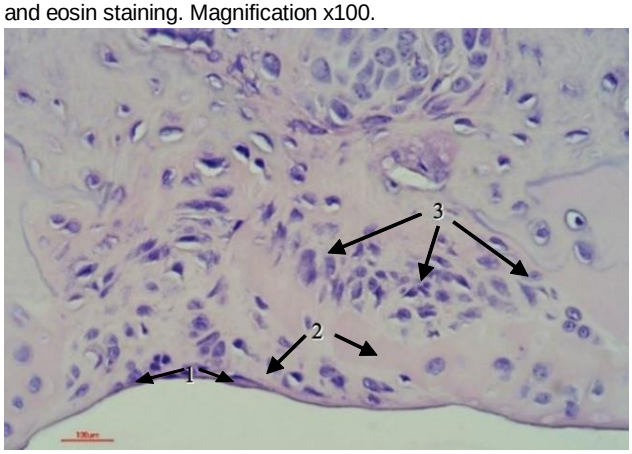

Fig. 12. The structure of articular cartilage O4. 1 - superficial zone of articular cartilage. 2 - intermediate zone of articular cartilage. 3 - deep zone of articular cartilage. Hematoxylin and eosin staining. Magnification x400.

regenerate was filled with fibrous tissue, its average thickness was 45.42±4.38 μm. The fibers were located mainly parallel to the articular surface. The free surface of the fibrous tissue looked smooth, but the tissue itself formed intra-articular growths. In places, foci of destruction (necrosis) were noted in the fibrous tissue. Fibrous tissue

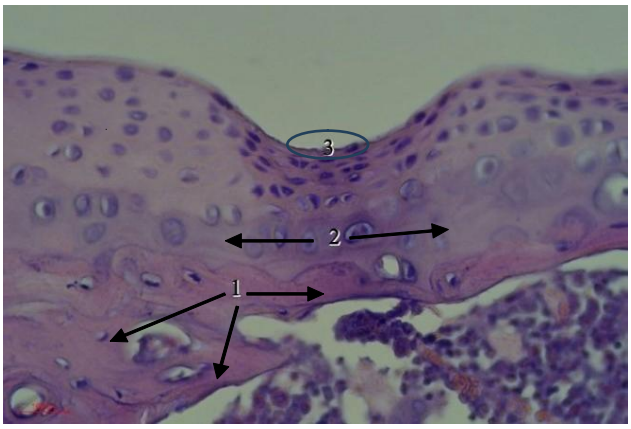

Fig. 13. The structure of articular cartilage K4. 1 - subchondral bone tissue. 2 - deep zone of articular cartilage. 3 - superficial zone of articular cartilage. Hematoxylin and eosin staining. Magnification x400.

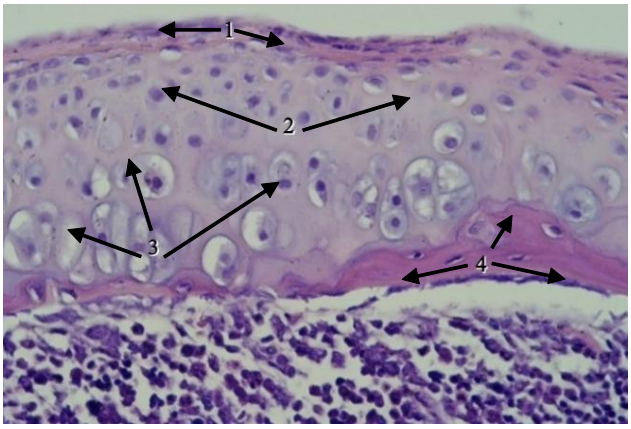

Fig. 14. The structure of articular cartilage K4. 1 - fibrous cartilage tissue in the surface zone of articular cartilage. 2 - intermediate zone of articular cartilage. 3 - deep zone of articular cartilage. 4 - subchondral bone tissue. Hematoxylin and eosin staining. Magnification x400.

contained well-developed blood vessels of the hemomicrocirculatory bed. In addition, on the periphery of the defect area, cells of both damaged and preserved hyaline cartilage were found under the fibrous tissue. That is, excessive (beyond damage to the articular surface) growth of fibrous tissue under which the subchondral bone plate with the applied defect was located was determined (Fig. 10). At the edges of the defect, the plate was unevenly thickened. Because of the bone tissue defect, hemocapillaries and reticular tissue penetrated the area of articular cartilage damage (see Table 1).

Group O4. On the 28th day after nuclear magnetic resonance therapy, in the animals of the main group, histologically, the articular surface at the site of injury was covered with a newly formed coating of cartilage tissue. In the surface zone, chains of flattened chondrocytes are located parallel to the joint gap. With distance from the free surface, chondrocytes formed isogenic groups, which contained 3-4 cells each and did not differ in their structure from chondrocytes of intact areas of articular cartilage. The surface layer turned into a deep, typical articular hyaline cartilage with a weakly basophilic matrix and zonal arrangement of chondrocytes. The deep zone contained full-blooded blood vessels, small areas of granulation tissue.

Thus, in treated animals, cartilaginous tissue was found in the defect zone, which in terms of histological structure approached the structure of articular hyaline cartilage of intact joints. According to the macroscopic (surface, color, density) characteristics, the regenerate had all the properties of the newly formed hyaline articular cartilage (Fig. 11), which was indicated by the increased number of chondroblasts in the deep zone of the cartilage and eosinophilia of the intercellular matrix. However, the superficial zone was represented by one layer of flattened cells oriented parallel to the surface of the joint (Fig. 12). The thickness of the newly formed cartilage tissue was less than the similar tissue in intact joints and was 82.12±8.89 μm (see Table 1).

Group K4. The articular cartilage, near the injury zone, underwent structural changes. In particular, chondrocytes were absent in the surface zone, and the matrix was stained eosinophilic. In the middle zone, the formation of isogenic groups containing 3-4 cells was noted, some isogenic groups did not contain chondrocytes at all. The basophilic line throughout the area of the articular cartilage covering the femur was uneven and discontinuous. Zones without chondrocytes and uneven staining of the matrix were observed in the zone of calcified cartilage. At a distance from the defect site, structural transformations in the articular cartilage were less pronounced and were manifested by a decrease in the density of chondrocytes in the surface zone, heterogeneity of the color of the matrix, and unevenness of the basophilic line. A high density of fibroblasts was determined in it (Fig. 13).

The articular cartilage, located on the edge of the wound, was degeneratively changed, there was a reduced number of chondrocytes and a thickened zone of calcified cartilage. The cells of the surface layer of articular cartilage were destroyed. In the middle layer, chondrocytes were unevenly located in isogenic groups. The deep layer, where the chondrocytes formed columns, the subchondral bone plate was directly adjacent to the deep zone (the zone of calcification was not clearly visualized) (Fig. 14). The thickness of the cartilage was 56.34±7.82 μm (see Table 1).

Discussion

In the course of the histological analysis of defects of the articular cartilage of the knee joint in an experimental model under the influence of nuclear magnetic resonance therapy (MBST), significant morphological changes were found, which testify to the positive role of MBST in cartilage regeneration. At the first stage of the study, it was established that the control group, which did not receive MBST, showed pronounced signs of cartilage

degeneration. In particular, wide zones of necrosis were detected, as well as loss of the cartilage matrix and a decrease in the number of chondrocytes.

In the group of animals subjected to MBST, the articular surface at the site of injury was lined with a newly formed covering of cartilage tissue, and the regenerate had all the properties of hyaline cartilage, which was indicated by an increased number of chondroblasts in the deep zone of the cartilage and eosinophilia of the intercellular matrix. Histological analysis also showed an increased number of living chondrocytes, as well as signs of their greater differentiation compared to the control group, which also indicates stimulation of cartilage regeneration under the influence of MBST.

Our study was also accompanied by a comparative analysis with the work of Gerwin N. and co-authors conducted in 2010 [8]. The authors of this paper recommended using criteria for evaluating histopathological changes in cartilage in osteoarthritis. In our study, we similarly divided the cartilage into three zones: superficial, deep, and calcification zone, and the use of MBST contributed to the improvement of morphological indicators.

In the context of the histological changes found in our study, the molecular aspects mentioned in the study by Chen H. and co-authors [5] should also be taken into account. The maintenance of a higher level of chondrocyte differentiation may be related to the molecular mechanisms that support the proliferation and differentiation of these cells.

Our study in a control group of rats is also consistent with the study by Bets I. G. and co-authors, conducted in 2018 [2], in which the authors showed the stages of articular cartilage regeneration after a full-layer defect of cartilage tissue, resulting in the formation of fibrous cartilage tissue. Restoration of hyaline cartilage at the site of damage did not occur at all stages of the study. However, in our study, in the group of animals that underwent nuclear magnetic resonance therapy, regeneration in the defect zone of subchondral bone tissue and articular cartilage was more pronounced, as indicated by the thickness of regenerated articular cartilage. Also, in the group of animals that underwent nuclear magnetic resonance therapy, the cartilage tissue in the area of regeneration had signs of hyaline cartilage.

In the perspective of further developments, we plan to conduct a study on the restoration of articular cartilage within three months.

Conclusion

1. It has been proven that the use of nuclear magnetic resonance therapy for transchondral damage of articular cartilage contributes to the formation of cartilage regenerate within 28 days in the cartilage defect, which in its structure is close to the structure of intact hyaline cartilage.

2. After transchondral damage to the articular cartilage, it does not fully recover within 28 days, as evidenced by the smaller thickness of the regenerate compared to that of the right knee joint.

3. In the control group of animals without nuclear magnetic resonance therapy, after traumatization of regenerate formation, there were few signs of dysregeneration. The tissue formed in the damaged area had signs of fibrous cartilage with areas of necrosis.

4. The experiment needs a longer period to study the full recovery of articular cartilage.

References

[1] Berenbaum, F., Wallace, I. J., Lieberman, D. E., & Felson, D. T. (2018). Modern-day environmental factors in the pathogenesis of osteoarthritis. *Nat. Rev. Rheumatol.,* 14(11), 674-681. doi: 10.1038/s41584-018-0073-x

[2] Bets, I. G., Ashukina, N. O., Maltseva, V. E., & Nikolchenko, O. A. (2018). Особливості регенерації кісткової та хрящової тканини після травматичних внутрішньосуглобових ушкоджень (експериментальне дослідження) [Peculiarities of regeneration of bone and cartilage tissue after traumatic intra-articular injuries (experimental study)]. *Журнал "Травма" - "Trauma" magazine,* 19(6). doi: 10.22141/1608-1706.6.19.2018.152225

[3] Burianov, O. A., Omelchenko, T. M., Dedukh, N. V., Chornovol, P. A., Vakulich, M. V., & Turchin, O. A. (2019). Застосування клітин кісткового мозку в лікуванні внутрішньосуглобових остеохондральних пошкоджень в експерименті [The use of bone marrow cells in the treatment of intra-articular osteochondral injuries in the experiment]. *Клінічна хірургія - Clinical Surgery,* 86(4), 41-46. doi: 10.26779/2522-1396.2019.04.41

[4] Charlier, E., Deroyer, C., Ciregia, F., Malaise O., Neuville S., Plener Z., & Malaise M. (2019). Chondrocyte dedifferentiation and osteoarthritis (OA). *Biochemical Pharmacology,* 165, 49-65. doi: 10.1016/j.bcp.2019.02.036

[5] Chen, H., Tan, X. N., Hu, S., Liu R. Q., Peng L. H., Li, Y. M., & Wu, P. (2021). Molecular Mechanisms of Chondrocyte Proliferation and Differentiation. *Frontiers in Cell and Developmental Biology,* 9, 664168. doi: 10.3389/fcell.2021.664168

[6] Chijimatsu, R., & Saito, T. (2019). Mechanisms of synovial joint and articular cartilage development. *Cell and Molecular Life Sciences,* 76, 3939-3952. doi: 10.1007/s00018-019-03191-5

[7] European Convention for the Protection of Vertebrate Animals Used for Research and Other Scientific Purposes. Strasbourg, 18 March 1986: Official translation [Electronic resource]. - Access Mode: http: zakon.rada. gov.ua/cgi-bin/laws/main.cgi?nreg=994_137

[8] Gerwin, N., Bendele, A. M., Glasson, S., & Carlson, C. S. (2010). The OARSI histopathology initiative - recommendations for histological assessments of osteoarthritis in the rat. *Osteoarthritis and Cartilage, Supplement,* 3, S24-S34. doi: 10.1016/j.joca.2010.05.025

[9] Grässel, S., & Muschter, D. (2020). Recent advances in the treatment of osteoarthritis. *F1000Research,* 9, 325. doi: 10.12688/f1000research.22115.1

[10] Hermann, W., Lambova, S., & Muller-Ladner, U. (2018). Current Treatment Options for Osteoarthritis. *Current Rheumatology Reviews,* 14(2), 108-116. doi: 10.2174/1573397113666170829155149

[11] Hochberg, M. C., Guermazi, A., Guehring, H., Aydemir, A., Wax, S., Fleuranceau-Morel, P., & Bihlet, A. R. (2019). Effect of Intra-Articular Sprifermin vs Placebo on Femorotibial Joint Cartilage Thickness in Patients with Osteoarthritis: The FORWARD Randomized Clinical Trial. *JAMA,* 322(14), 1360-1370. doi: 10.1001/jama.2019.14735

[12] Huang, X., Das, R., Patel, A., & Nguyen, T. D. (2018). Physical Stimulations for Bone and Cartilage Regeneration. *Regenerative Engineering and Translational Medicine,* 4(4), 216-237. doi: 10.1007/s40883-018-0064-0

[13] Jiang, Y. (2022). Osteoarthritis Year in Review 2021: Biology. *Osteoarthritis and Cartilage,* 30, 207-215. doi: 10.1016/j.joca.2021.11.009

[14] Krpan, D., & Kullich, W. (2017). Nuclear magnetic resonance therapy (MBST) in the treatment of osteoporosis. Case report study. *Clinical Cases in Mineral and Bone Metabolism,* 14(2), 235-238. doi: 10.11138/ccmbm/2017.14.1.235

[15] Lyndin, M., Gluschenko, N., Sikora, V., Lyndina, Y., Hyryavenko, N., Tkach, G. … & Romaniuk, A. (2019). Morphofunctional features of articular cartilage structure. *Folia Med. Cracov.,* 59(3), 81-93. doi: 10.24425/fmc.2019.131138

[16] Liu, Y., Shah, K. M., & Luo, J. (2021). Strategies for Articular Cartilage Repair and Regeneration. *Frontiers in Bioengineer. and Biotechnol.,* 9, 770655. doi: 10.3389/fbioe.2021.770655

[17] Martin, A. R., Patel, J. M., Zlotnick, H. M., Carey, J. L., & Mauck, R. L. (2019). Emerging therapies for cartilage regeneration in currently excluded 'red knee' populations. *npj Regenerative Medicine,* 4(1), 12. doi: 10.1038/s41536-019-0074-7

[18] On the Protection of Animals from Cruelty: Law of Ukraine № 3447-IV dated 21.02.2006 [Electronic resource] /Verkhovna Rada of Ukraine. - Access Mode: http://zakon3.rada.gov.ua/laws/show/3447-15

[19] Onuora, S. (2023). 'Hyalinization' for cartilage regeneration. *Nat. Rev. Rheumatology,* 19(2), 63. doi: 10.1038/s41584-022-00898-x

[20] Pritzker, K. P. H., & Gahunia, H. K. (2020). *Articular Cartilage: Homeostasis, Aging and Degeneration.* In: H. Gahunia, A. Gross, K. Pritzker, P. Babyn, & L. Murnaghan (Eds.), Articular Cartilage of the Knee (pp. 49-78). Springer. doi: 10.1007/978-1-4939-7587-7_3

[21] Ratneswaran, A., Rockel, J. S., & Kapoor, M. (2020). Understanding Osteoarthritis Pathogenesis: A Multiomics System-Based Approach. *Current Opinion in Rheumatology,* 32, 80-91. doi: 10.1097/BOR.0000000000000680

[22] Sarkisov, D. S., & Perov, Yu. L. (1996). *Микроскопическая техника. [Microscopic technique].* М.: Медицина - M: Medicine.

[23] Smith, D. W., Gardiner, B. S., Zhang, L., & Grodzinsky, A. J. (2019). *Cartilage Tissue Homeostasis.* In: A. J. Grodzinsky (Ed.), Articular Cartilage Dynamics (pp. 25-54). Springer. doi: 10.1007/978-981-13-1474-2_2

[24] Steinecker-Frohnwieser, B., Lohberger, B., Eck, N., Mann, A., Kratschmann, C., Leithner, A., … & Weigl, L. (2021). Nuclear Magnetic Resonance Therapy Modulates the miRNA Profile in Human Primary OA Chondrocytes and Antagonizes Inflammation in Tc28/2a Cells. *International Journal of Molecular Sciences*, 22(11), 5959. doi: 10.3390/ijms22115959

[25] Vaysbrot, E. E., Osani, M. C., Musetti, M. C., McAlindon, T. E., & Bannuru, R. R. (2018). Are bisphosphonates efficacious in knee osteoarthritis? A meta-analysis of randomized controlled trials. *Osteoarthritis and Cartilage*, 26(2), 154-164. doi: 10.1016/j.joca.2017.11.013

МОРФОГІСТОЛОГІЧНЕ ДОСЛІДЖЕННЯ РЕГЕНЕРАЦІЇ ДЕФЕКТІВ ХРЯЩА КОЛІННОГО СУГЛОБА В ЕКСПЕРИМЕНТАЛЬНІЙ МОДЕЛІ ПІД ВПЛИВОМ ЯДЕРНОЇ МАГНІТНО-РЕЗОНАНСНОЇ ТЕРАПІЇ

Фіщенко В. О., Король А. П., Юсупова Д. В.

Незважаючи на різноманіття сучасних методів лікування, проблема регенерації гіалінового хряща залишається надзвичайно актуальною. Мета дослідження - визначити вплив ядерної магнітно-резонансної терапії на регенераційну здатність модельованих дефектів хрящової тканини колінного суглоба у щурів, оцінити динаміку мікроскопічних змін суглобового хряща в основній та контрольній групах. Дослідження виконано на 60 статево зрілих щурах. Повношарові дефекти створені в ділянці суглобових поверхонь лівого колінного суглоба - 30 дефектів в основній групі та 30 дефектів в контрольній групі. Правий колінний суглоб обох досліджуваних груп використовували в якості нормативу. Через 3 дні після хірургічного втручання проводили необхідну медикаментозну терапію (антибіотики, протизапальні, аналгезуючі). На четверту добу після операції щурам основної групи застосовували ядерну магнітно-резонансну терапію по 60 хвилин впродовж 7 діб. Через 7, 14, 21, 28 діб після терапії проводили гістологічний аналіз хрящового регенерата. Через 28 діб після застосування ядерної магнітно-резонансної терапії висота хрящового регенерата у щурів становила 82,12±8,89 мкм в основній групі та 56,34±7,82 мкм в контрольній. Хрящовий регенерат у щурів після ядерної магнітно-резонансної терапії за будовою наближався до структури неушкодженого гіалінового хряща. Однак, повної регенерації не відбувалось, про що свідчить менша товщина суглобового хряща порівняно з правим колінним суглобом. У контрольній групі формування регенерату мало виражені ознаки дисрегенерації. Хрящова тканина в ділянці дефекту мала переважно фіброзний характер із зонами некрозу. Ядерна магнітно-резонансна терапія сприяє формуванню в дефекті суглобового хряща хрящового регенерату, котрий за своєю гістологічною будовою наближається до гіалінового хряща.

Ключові слова: *ядерна магнітно-резонансна терапія, щури, хрящовий регенерат, проліферація хондроцитів, експеримент.*

Author's contribution

Fishchenko V. O.: conceptualization, resources, providing equipment for the experiment, supervision.

Korol A. P.: software for morphometric research, histological analysis.

Yusupova D. V.: data visualization, formal analysis and verification, conducting an experiment, project administration, methodology and writing an original draft, review writing and editing, processing of statistical data.

DOI: 10.31393/morphology-journal-2023-29(4)-04 Reports of Morphology, Vol. 29, №4, Pages 27-34

ISSN 1818-1295 eISSN 2616-6194

REPORTS OF MORPHOLOGY

Official Journal of the Scientific Society of Anatomists, Histologists, Embryologists and Topographic Anatomists of Ukraine

journal homepage: https://morphology-journal.com

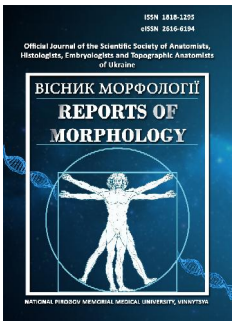

Peculiarities of the parietal bones of the vault of the human skull structure and shape, taking into account sex and craniotype

Voinytska O. M., Vovk O. Yu., Chekanova I. V.
Kharkiv National Medical University, Kharkiv, Ukraine

ARTICLE INFO
Received: 21 July 2023
Accepted: 20 September 2023

UDC: 611.715.4-055.1/.2:572.73

CORRESPONDING AUTHOR
e-mail: oy.vovk@knmu.edu.ua
Vovk O. Yu.

CONFLICT OF INTEREST
The authors have no conflicts of interest to declare.

FUNDING
Not applicable.

DATA SHARING
Data are available upon reasonable request to corresponding author.

The development of neurosurgery and the increase in requirements for the performance of surgical approaches performed through the bones of the skull vault lead to the formation of new requests for detailing and clarification of the craniometric characteristics of the parietal bones. The purpose of our study is to establish the features of the shape and other spatial indicators of the parietal bones of the skull of a mature person, taking into account sex and certain types of craniotype. The study was conducted on 130 studied preparations of bone structures of the head of adults from the collected collection of the Department of Normal Anatomy of the Kharkiv National Medical University, in the amount of 82 bone preparations, including isolated parietal bones, as well as 48 tomograms obtained during the examination of patients. The basis for establishing a craniotype is the principle of calculating the cranial index. For statistical analysis, we used the programs Statistica 13.5.0.17 (trial version) and Microsoft Excel of the corporate package MS 365. To establish the peculiarities of the structure and shape of the parietal bones, the following craniometric indicators were determined: the length and width of the parietal tubers, the parietal chord and the arch, calculated the curvature index of the parietal bone. The obtained data were analyzed for mature people of different genders and three established craniotypes. It has been established that brachycephals are characterized by an expanded and expanded form of the parietal bones, which is associated with the predominance of the transverse dimensions of the entire cerebral skull. For mesocephals, the most typical intermediate-average form depending on the values of the cranial index. Dolichocephals have an elongated and narrowed form of the parietal bones, which is combined with general changes in the cerebral skull. Additional linear parameters of the parietal bones are directly dependent on the established craniotype. The dolichocephalic type is characterized by maximum length values of parietal tubers: $\overline{x}$ =18.43 mm (right) and $\overline{x}$ =18.24 mm (left) with minimum width parameters: up to $\overline{x}$ =15.71 mm and $\overline{x}$ =15.02 mm. Representatives of the brachycranic type are characterized by the minimum indicators of the length of the parietal tubers: from $\overline{x}$ =12.73 mm to $\overline{x}$ =12.81 mm and the maximum indicators for the width - $\overline{x}$ =23.52 mm (right) and $\overline{x}$ =23.04 mm (left). The parietal chord, like the parietal arch, had a similar trend in the distribution of indicators, namely: an increase from dolichocrania to brachycrania. In men with a dolichocephalic type of skull structure, the average values of these parameters were at the level of $\overline{x}$ =108.2 mm (right) and 107.6 mm (left) for the parietal chord, and $\overline{x}$ =114.2 mm and $\overline{x}$ =113.2 mm for the parietal arcs In men with brachycranic type, the parietal chord reached - $\overline{x}$ =116.6 mm (right) and $\overline{x}$ =115.8 mm (left), and the parietal arch reached - $\overline{x}$ =127.8 mm (right) and $\overline{x}$ =126.9 mm (left). In women, a similar principle of size distribution has been established, taking into account a small, 2-3 mm, general decrease in indicators compared to men. The curvature index of the parietal bones was determined: the maximum average values $\overline{x}$ =83.00-83.58 were obtained in dolichocephals, the minimum values were $\overline{x}$ =80.56-81.64 in brachycephals. This indicates an increase in the curvature of bones in brachycephals, given that the absolute value of the index is inversely proportional to the degree of curvature. Thus, the obtained data indicate a stable relationship between the craniotype of the skull and additional parameters of the parietal bones.

Keywords: *craniometry, parietal bone, cranial index, parietal tubers, parietal chord, parietal arch.*

Introduction

It is known that the parietal bone (os parietalis) is a paired bone that forms the lateral (outer) surfaces of the skull vault. They are usually symmetrical and border the frontal bone along the coronal suture (sutura coronalis) from the front, the temporal bone from the bottom through the scaly suture (sutura squamosa), and the lambdoid suture (sutura lambdoidea) from the back - the occipital bone. The left and right parietal bones are connected along the sagittal line by the suture of the same name (sutura sagittalis). The research of the cranial vault has always attracted the attention of a large number of morphologists, as one of the most important areas of the human body from the point of view of performing many neurosurgical interventions when accessing intracranial structures [7, 14, 19, 20]. Classic craniometric works, which were performed using collections of skulls, usually described not only the main parameters of any bone, but also provided a certain characteristic of its shape, structural features, established the existing variability [10, 12, 13, 15]. The parietal bone, as one of the largest structures of the cerebral part of the skull, has a significant dependence on the established craniotype, while there are certain ranges of changes in the main linear parameters, which is confirmed by the studies of a number of authors [3, 16, 17]. However, in modern morphology, greater attention is paid to the intravital study of anatomical structures, including the bones of the human skull, which is made possible by the use of the latest systems of instrumental research [1, 2, 6, 8, 11]. nalyzing a certain amount of information sources, both classical and modern, we came to the conclusion that the issue of detailing the characterization of the shape and structure of the parietal bones from the position of combining classical and modern methods, using not only the basic but also additional craniometric parameters, is extremely insufficiently covered. taking into account craniotype and gender.

Considering the above, *the purpose of our study* is to establish the features of the shape and other spatial indicators of the parietal bones of the skull of a mature person, taking into account sex and certain varieties of craniotype.

Materials and methods

According to the requirements, a bioethical examination of the work was carried out, which was discussed at the meeting of the Committee on Ethics and Bioethics of Kharkiv National Medical University on June 6, 2018 (Protocol №6), according to which it meets international ethical requirements and does not violate ethical norms in science and standards conducting biomedical research.

The research was carried out on 130 studied preparations of bone structures of the head of adults from the collected collection of the Department of Normal Anatomy of the Kharkiv National Medical University, in the amount of 82 bone preparations, including isolated parietal bones, as well as 48 tomograms obtained during the examination of patients. The basis for establishing a craniotype is the basic principle - the calculation of the cranial index, which allows classifying anatomical objects according to the shape of the head structure.

The cranial index is calculated according to the formula:

Ind_{skull}=*(skull width(eu-eu))/(skull length (g-op)) x 100*

According to the obtained indicators of the cranial index: up to 74.9 constitute a group of dolichocephals; at 75.0-79.9 - mesocephals, at 80 and more - brachycephals. In this regard, we distinguished the dolicho-, meso- and brachycephalic forms of the skull, which determine the type of structure of the cranial vault (that is, the cerebral part of the skull).

To identify the existing features of the structure and shape of the parietal bones, we determined the following parameters: the length and width of the parietal tubers, the parietal chord and the arch. A fundamentally important issue for understanding the spatial position of the parietal bone is the establishment of its curvature parameters, which were determined by the formula:

$Ind_{curvature}$=*(chord length (b-l))/(arc length (b-l)) x 100*

The index of curvature (Indcurvature) of the parietal bone was determined as the ratio of the length of the chord (the direct distance between the points bregma (b) and lambda (l), set using a sliding compass or software when working with tomograms) to the length of the arc (the distance between the points b-l on the surface of the bone).

To perform statistical analysis, we used Statistica 13.5.0.17 (trial version) and Microsoft Excel of the MS 365 corporate package. For each sample, we calculated: $\bar{x}$ - arithmetic mean; σ - mean square deviation; $m_{\bar{x}}$ is the error of the arithmetic mean and the interval of variability. Any established patterns were considered reliable under the condition of $p<0.05$, Pearson's correlation analysis was performed among certain categories of samples. In our work, the results of the morphometry of the parietal bone, obtained on a computer tomography, were analyzed. A number of programs were used for this: eFilmLite 4.1.0., Vidar DICOM Viewer 3.0., RadiAnt DICOM Viewer 2023.1., InVesalius 3.1. All this software was used either within the limits of the license granted to the owners of the tomograph, or in terms of the so-called "trial", i.e., free version. Part of the material was studied with the help of the Anatomage table, which is located on the basis of the department of human anatomy of KhNMU with the Launching Table 6.0 Application program installed. This modern system of three-dimensional anatomical visualization allows us to study craniotomograms, which we actively used during the implementation of this dissertation work (Fig. 1).

Fig. 1. Study of craniotomograms using modern means.

Results

Paying attention to the craniotopographic position of the parietal bones in the middle part of the cerebral skull and their bony connection with the frontal and occipital bones, we can talk about a significant variety of forms and configurations of this department and a significant influence of the features of the structure of the parietal bones on the general shape of the skull structure.

This is evidenced by the range of variations in the structure of the cerebral part of the skull found in men and women of mature age (Fig. 2).

Analyzing the obtained array of data of the main linear indices of the parietal bones, we came to the conclusion that there is a certain predominance of longitudinal parameters in turtles of the dolichocephalic type with a significant decrease in the average transverse dimensions, at the same time, in representatives of the established brachycranic type, the diametrically opposite characteristic was observed, the minimum length at maximum average widths.

Accordingly, three main forms of parietal bones should be distinguished depending on the existing three types of skull structure (Fig. 3).

It has been established that the characteristic extended-expanded shape of the parietal bones for brachycephals is associated with the predominance of the transverse dimensions of the entire cerebral skull. For mesocephals, the most typical intermediate-averaged form depending on the values of the cranial index. In dolihocephals, the elongated and narrowed shape of the parietal bones is noted, which is in unity with the general changes of the cerebral skull.

From a practical point of view, the curvature of the parietal bones and the presence of the corresponding parietal tubers, which are pronounced on both sides and very often coincide with the craniometric point eurion (eu), which, in turn, is used to determine the overall width of the head, are of great importance. Naturally, taking into account the individual structure of the cerebral skull, its vault and parietal bones, there are certain osteometric features of these structures (Table 1).

According to our data, the range of variation of the linear parameters of the parietal tubers in people with a brachycephal skull type is between: length from 12.0 mm to 16.0 mm in men and from 10.5 mm to 15.0 mm in women, and width varies from 18.0 mm to 29.0 mm in men and from 17.0 mm to 28.0 mm in women. Accordingly, in representatives of the mesocephal type, the length of the parietal tubers does not exceed 12.0-14.5 mm in men and 12.0-13.5 mm in women, the width decreases to 15.0-25.0 mm in men and 14.0-23.0 mm in women. For people with a dolichocephal type of skull structure, the length of the parietal tubers is slightly increased to 15.0-21.0 mm in men and 14.0-20.0 mm in women, with a tendency to decrease their width to 12.0-18.0 mm and 12.0-17.0 mm, depending on sex.

According to our data, the chord of the parietal bones varies depending on the extreme forms of individual anatomical variability of the structure of the head and skull.

For example, in brachycephals (round-headed people),

Fig. 2. The appearance and position of the parietal bones of a mature person (photos of preparations № 13, 6, 3, 30, 4, 9, 11, 5).

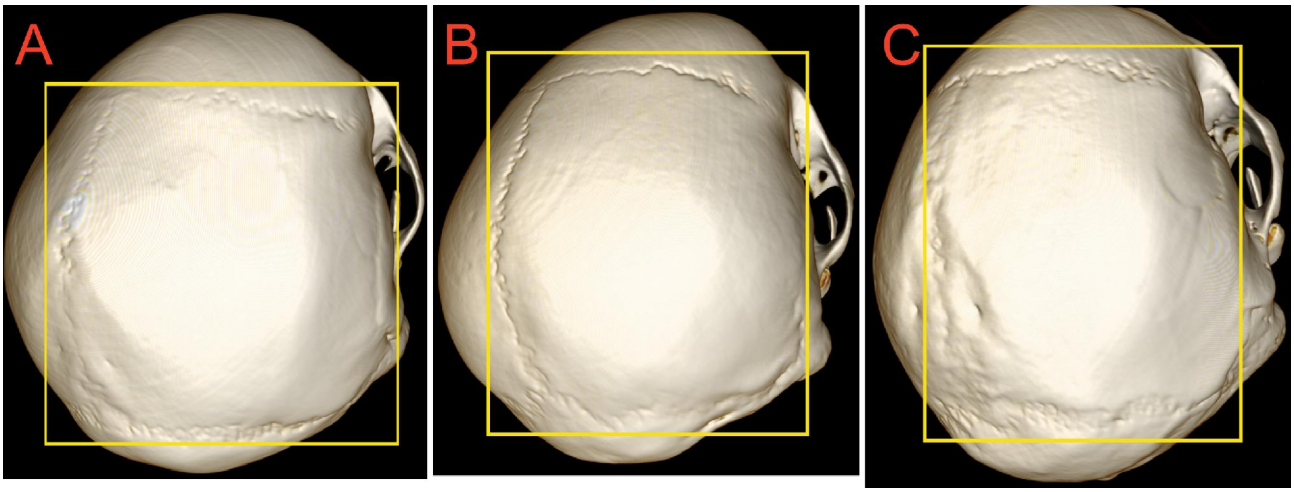

Fig. 3. Three forms of the structure of the parietal bones of a mature person: A - expanded-deployed (CT № 1919); B - intermediate-averaged (KT № 1931); C - elongated-narrowed (CT № 1930).

the chord reaches the maximum values: in men, it is 102.1-130.2 mm (right) and 97.40-130.2 mm on the left, respectively, in women - 98.10-125.8 mm and 99.40-121.8 mm.

In mesocephals (medium-headed people), it gradually decreases to 110.2-120.4 mm and 102.2-126.4 mm (men) and to 103.4-114.7 mm and 103.2-113.8 mm (women). In dolihocephals (long-headed people), a decrease in the bone chord is noted to 96.40-119.8 mm and 90.00-120.2 mm (men), to 95.60-118.6 mm and 86.60-108.4 mm (women).

In addition, the length of the arc of the parietal bones is related to the above measurements. Accordingly, it completely depends on the curvature of the bone body, which is most pronounced in representatives with a brachycephal configuration of the head: 110.2-145.0 mm on the right and 105.7-145.0 mm on the left in men; 106.8-139.0 and 110.0-131.0 mm in women.

In representatives with a mesocephal structure of the head, there is a tendency to decrease the parietal arches to 112.2-132.5 mm and 112.9-135.0 mm (men); to 112.4-125.7 mm and 108.6-123.5 mm (women). Representatives of the dolichocephal structure of the head have the smallest values of parietal arches: 106.2-131.8 mm and 104.5-132.6 (men) and 101.2-128.6 and 104.6-130.5 (women).

To understand the practical value and spatial position of the parietal bones, it is important to calculate the curvature index, which is determined by determining the ratio of chord and arch. This index has certain changes depending on the existing craniotypes.

The obtained measurement results are confirmed by statistical analysis and presented in Table 2.

It is statistically reliable that the length of parietal tubers is the smallest in brachycephals $\bar{x}$ =12.73 mm and $\bar{x}$ =12.81 mm; in mesocephals $\bar{x}$ =13.21 mm and $\bar{x}$ =13.03 mm; in male dolichocephals, the largest $\bar{x}$ =18.43 mm and

Table 1. The range of craniometric indicators of the parietal bones of a mature person (mm).

Studied parameter \ Skull shape		Brachycephals		Mesocephals		Dolichocephals	
		men	women	men	women	men	women
Length of parietal tubers	Right	12.0-16.0	11.0-15.0	12.0-14.0	12.5-13.5	15.0-21.0	14.5-20.0
	Left	12.0-15.0	10.5-14.5	13.0-14.5	12.0-13.5	16.0-21.0	14.0-19.0
Width of the parietal tubers	Right	18.0-29.0	17.0-28.0	15.0-25.0	14.0-23.0	12.0-18.0	12.0-17.5
	Left	18.0-29.0	17.0-28.0	15.0-24.0	14.0-22.0	12.0-18.0	12.0-17.0
Parietal chord	Right	102.1-130.2	98.1-125.8	110.2-120.4	103.4-114.7	96.4-119.8	95.6-118.6
	Left	97.4-130.2	99.4-121.8	102.2-126.4	103.2-113.8	90.0-120.2	86.6-108.4
Parietal arc	Right	110.2-145.0	106.8-139.0	112.2-132.5	112.4-125.7	106.2-131.8	101.2-128.6
	Left	105.7-145.0	110.0-131.8	112.9-135.3	108.6-123.5	104.5-132.6	104.6-130.5
Curvature index	Right	78.36-87.65	76.05-84.10	80.11-83.93	79.50-83.05	81.58-85.35	80.50-84.20
	Left	77.65-85.19	75.80-83.20	81.86-86.76	80.10-84.60	83.13-84.44	82.10-84.00

Table 2. Statistical analysis of craniometric indicators of the parietal bones of mature men.

Studied parameter \ Skull shape		Brachycephals			Mesocephals			Dolichocephals		
		$\bar{x}$	σ	$m_{\bar{x}}$	$\bar{x}$	σ	$m_{\bar{x}}$	$\bar{x}$	σ	$m_{\bar{x}}$
Length of parietal tubers	Right	12.73	0.66	0.17	13.21	0.61	0.18	18.43	0.62	0.27
	Left	12.81	0.64	0.21	13.03	0.70	0.22	18.24	0.58	0.24
Width of the parietal tubers	Right	23.52	0.73	0.11	20.52	0.55	0.19	15.71	0.44	0.15
	Left	23.04	0.19	0.16	21.02	0.66	0.23	15.02	0.55	0.20
Parietal chord	Right	116.6	0.6	0.2	114.2	0.5	0.2	108.2	0.4	0.2
	Left	115.8	0.6	0.2	114.0	0.6	0.2	107.6	0.5	0.1
Parietal arc	Right	127.8	0.8	0.2	122.4	0.4	0.1	114.2	0.8	0.2
	Left	126.9	0.8	0.3	122.0	0.5	0.2	113.2	0.7	0.3
Curvature index	Right	81.23	0.81	0.24	82.55	0.58	0.27	83.44	0.72	0.33
	Left	81.64	0.79	0.21	82.66	0.49	0.32	83.58	0.80	0.28

$\bar{x}$ =18.24 mm.

At that time, the width of the parietal tubers fluctuates with a decreasing trend from brachycephals $\bar{x}$ =23.52 mm (right) and $\bar{x}$ =23.04 mm (left) to $\bar{x}$ =15.71 mm (right) and $\bar{x}$ =15.02 mm (left), established in dolichocephals.

Along with this, it was established that the parietal chord reaches the maximum values of $\bar{x}$ =116.6 mm (right) and $\bar{x}$ =115.8 mm (left) in men with a brachycephal head shape. With the meso- and dolichocephal form, a gradual reduction of the parietal chord is noted to $\bar{x}$ =114.2 mm and $\bar{x}$ =114.0 mm (mesocephals) and $\bar{x}$ =108.2 mm and 107.6 mm (dolichocephals). Accordingly, the arc of the parietal bones depends on the length of the chord and the expressiveness of the curvature. Thus, brachycephals have the largest arc: $\bar{x}$ =127.8 mm (right) and 126.9 mm (left), dolichocephals have the smallest $\bar{x}$ =114.2 mm and $\bar{x}$ =113.2 mm, respectively.

The index of curvature of the parietal bones confirms the established patterns of individual morphometric relationships between the chord and the arch, namely: in mature men with the established brachycephalic type of head structure, a significant expressiveness of the curvature of the bones is noted, which is formed by the growth of their latitudinal (transverse) dimensions of all departments skull, vault and base bones. In men with meso- and dolichocephalic types of head structure, there is a smoothing of the curvature and a gradual decrease in the size of the chord and arch of the parietal bones.

In parallel with this, statistical studies of parietal tubers in mature women were conducted (Table 3).

It was established that the size of the parietal tubers in mature women has a reduced morphometric characteristic for all extreme forms of the head and skull compared to men by an average of 2-3 mm. First of all, this concerns the length and width of the parietal tubers.

In connection with the above, it is necessary to pay attention to the presence of pronounced asymmetry of the parietal tubers and a significant variation of the curvature index depending on the extreme forms of the structure of the head and skull (Fig. 4).

It has been established that brachycephals are more characterized by a gentle but elongated parietal arch, which

Table 3. Statistical analysis of craniometric indicators of the parietal bones of mature women.

Studied parameter \ Skull shape		Brachycephals			Mesocephals			Dolichocephals		
		$\bar{x}$	σ	$m_{\bar{x}}$	$\bar{x}$	σ	$m_{\bar{x}}$	$\bar{x}$	σ	$m_{\bar{x}}$
Length of parietal tubers	Right	12.33	0.81	0.13	13.01	0.75	0.22	16.04	0.78	0.22
	Left	12.21	0.72	0.18	13.21	0.59	0.28	16.33	0.48	0.29
Width of the parietal tubers	Right	21.54	0.80	0.17	19.22	0.70	0.17	14.83	0.80	0.19
	Left	21.04	0.62	0.12	19.03	0.45	0.24	14.62	0.71	0.28
Parietal chord	Right	115.2	0.3	0.2	111.0	0.6	0.2	107.2	0.6	0.2
	Left	114.6	0.6	0.3	110.8	0.2	0.2	106.7	0.5	0.2
Parietal arc	Right	125.5	0.5	0.2	121.0	0.7	0.3	112.0	0.4	0.1
	Left	125.8	0.4	0.2	121.5	0.8	0.3	112.5	0.4	0.2
Curvature index	Right	80.56	0.76	0.32	81.70	0.88	0.23	83.00	0.51	0.22
	Left	80.72	0.62	0.39	81.60	0.76	0.33	83.26	0.61	0.36

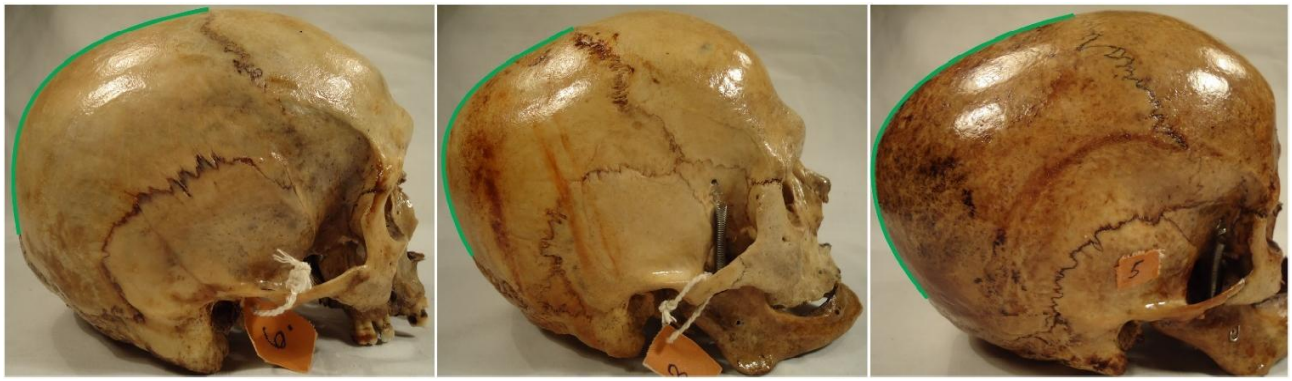

Fig. 4. The characteristic appearance of parietal arches on bone preparations of the skull (photo of the preparations № 6, 3, 5).

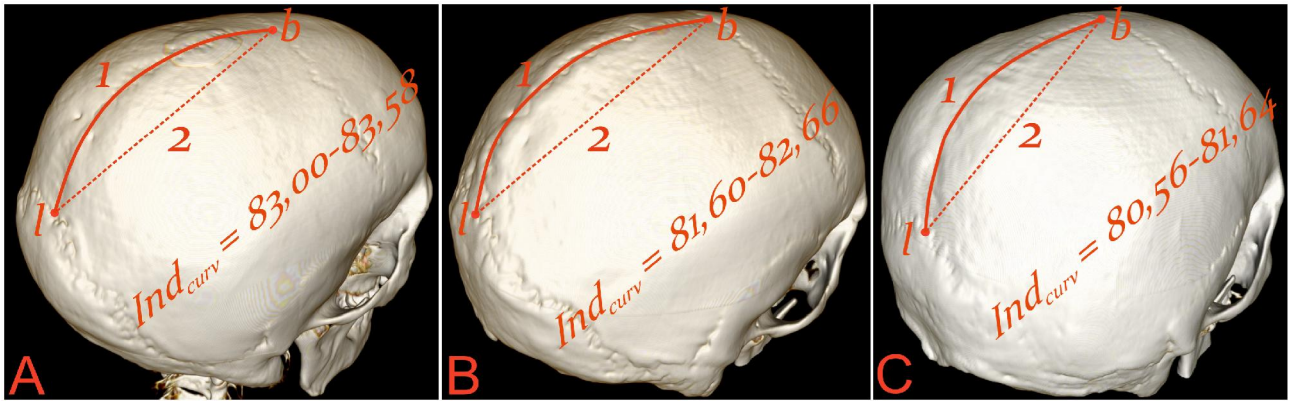

Fig. 5. Schematic ratio of the arc (1), chord (2) and index of curvature of the parietal bones of a mature person: A - in dolichocephals (CT № 1914), B - mesocephals (CT № 1883), C - brachycephals (CT № 1998).

is associated with a gradual and smooth roundness of the skull vault and a predominance of latitudinal dimensions. At the same time, in mesocephals and dolichocephals, the formation of a more convex arch is possible due to an increase in their height indicators of the skull (Fig. 5).

Discussion

At the current stage of the development of morphological science, one of the most promising directions remains the lifelong study of the peculiarities of the structure of the human body with the use of the latest devices and systems, at the same time, the doctrine of individual anatomical variability, which allows systematizing the existing variability of anatomical formations and significantly raising the level, does not lose its relevance individualization of the relationship to the patient [4, 5, 9]. In our work, it was possible to combine classic craniometric methods of research using dry bone preparations of the human skull and analysis of the results of computer tomography with

the use of the latest software and advanced anatomical visualization technologies. The obtained characteristics of the general linear dimensions of the parietal bones and the existing peculiarities of the structure of these structures depending on the gender and craniotype, in general, confirmed the results of the researches of a number of authors known to date [16, 18], at the same time, we proposed for the first time a refined a system for establishing the shape of the parietal bone, a detailed analysis of additional structures (parietal tubers) and measurements (parietal chord and arch) was performed, the index of curvature of the parietal bones was calculated, and the ranges of values of these parameters were provided for each group that was studied. It was established that each of the above indicators has a significant dependence on gender and type of skull structure, even within the same age period. At the same time, it was established that the average values of additional linear parameters of the parietal bones are always greater in men, which logically correlates with the general predominance of men's skull sizes over women's. For the considered craniotypes, there was a tendency to reach the maximum values of longitudinal parameters in dolichocephals, and for transverse dimensions - for brachycephals, regardless of gender, which fits perfectly into the general concept of the doctrine of individual anatomical variability [15, 16].

The accumulated amount of information obtained in combination with the analysis of the existing dynamics of the development of modern morphology allows us to state the perspective of further research, which consists in planning a certain number of works related to the study of the internal structure of the parietal bones, the peculiarities of the relationship with the surrounding structures and the detailing of the form-forming role of this bone in the general structure of the skull.

Conclusion

1. The parietal bones have two extreme forms of individual anatomical variability: expanded-expanded in people with a brachymorphic configuration of the head and skull; elongated-narrowed - in people with a dolichomorphic configuration, between them there are numerous averaged forms noted in people with mesomorphic origin.

2. The linear parameters of the parietal tubers are directly dependent on the established craniotype. The dolichocranic type is characterized by maximum length values at the level of 14.0-21.0 mm with minimum width parameters of 12.0-18.0 mm, in turn, representatives of the brachycranic type had minimum length indicators from 10.5 to 16.0 mm and maximum width indicators - from 17.0 to 29.0 mm.

3. A mature person with a brachycranic type of head structure is characterized by a significant curvature of the parietal bones when the curvature index fluctuates from 78.36 to 87.65 on the right and from 77.65 to 85.19 on the left in men; from 76.05 to 84.10 and from 75.80 to 83.20 in women, due to an increase in the latitudinal (transverse) dimensions of all sections of the cranial vault. In people with a meso- and dolichocranial type of head structure, a decrease in curvature is noted and its smoothing appears over the entire area of the parietal bones.

References

[1] Ajami, S., Rodriguez-Florez, N., Ong, J., Dunaway, D., James, G., Angullia, F., ... & Borghi, A. (2022). Mechanical and morphological properties of parietal bone in patients with sagittal craniosynostosis. *Journal of the Mechanical Behavior of Biomedical Materials,* 125, 104929. doi: 10.1016/j.jmbbm.2021.104929

[2] Alexander, S. L., Rafaels, K., Gunnarsson, C. A., & Weerasooriya, T. (2019). Structural analysis of the frontal and parietal bones of the human skull. *Journal of the Mechanical Behavior of Biomedical Materials*, 90, 689-701. doi: 10.1016/j.jmbbm.2018.10.035

[3] Eisová, S., Rangel de Lázaro, G., Píšová, H., Pereira-Pedro, S., & Bruner, E. (2016). Parietal bone thickness and vascular diameters in adult modern humans: a survey on cranial remains. *The Anatomical Record,* 299(7), 888-896. doi: 10.1002/ar.23348

[4] Gunas, I., Majewski, O., & Makarchuk, I. (2016). Features of somatotype and body weight component composition in patients with acne: boys and girls of Podillya region of Ukraine. *Current Issues in Pharmacy and Medical Sciences,* 29(2), 97-100. doi: 10.1515/cipms-2016-0020

[5] Gunas, I., Prokopenko, S., & Melnik, M. (2016). Sonographic parameters of the pancreas and gall bladder in healthy men from Podillya region of Ukraine of different somatotypes. *Current Issues in Pharmacy and Medical Sciences,* 29(2), 94-96. doi: 10.1515/cipms-2016-0019

[6] Gunas, I. V., Shinkaruk-Dykovytska, M. M., Kotsyura, O. O., Orlovskiy, V. O., Dmytrenko, S. V., Shayuk, A. V., & Glushak, A. A. (2017). Differences of craniotype distribution and types of face among almost healthy men from different regions of Ukraine. *Folia Morphologica,* 76(3), 473-477. doi: 10.5603/FM.a2017.0017

[7] Haut, R. C., & Wei, F. (2017). Biomechanical studies on patterns of cranial bone fracture using the immature porcine model. *Journal of Biomechanical Engineering,* 139(2), 021001. doi: 10.1115/1.4034430

[8] Lillie, E. M., Urban, J. E., Lynch, S. K., Weaver, A. A., & Stitzel, J. D. (2016). Evaluation of skull cortical thickness changes with age and sex from computed tomography scans. *Journal of Bone and Mineral Research,* 31(2), 299-307. doi: 10.1002/jbmr.2613

[9] Marchenko, A. V., Prokopenko, O. S., Dzevulska, I. V., Zakalata, T. R., & Gunas, I. V. (2021). Mathematical modeling of teleroentgenographic parameters according to the method of Schwarz AM depending on the basic cephalometric parameters in Ukrainian young men and young women with different face types. *Wiadomosci Lekarskie*, 74(6), 1488-1492. PMID: 34159943

[10] Pereira-Pedro, A. S., & Bruner, E. (2022). Craniofacial orientation and parietal bone morphology in adult modern humans. *Journal of Anatomy,* 240(2), 330-338. doi: 10.1111/joa.13543

[11] Ray, B., Rajagopal, K. V., Rajesh, T., Gayathri, B. M., D'Souza, A. S., Swarnashri, J. V., & Saxena, A. (2011). Morphometry and CT measurements of useful bony landmarks of skull base. *Rom. J. Morphol. Embryol.,* 52(3), 873-877. PMID: 21892533

[12] Rowbotham, S. K., Mole, C. G., Tieppo, D., Blaszkowska, M., Cordner, S. M., & Blau, S. (2023). Average thickness of the

bones of the human neurocranium: development of reference measurements to assist with blunt force trauma interpretations. *International Journal of Legal Medicine,* 137(1), 195-213. doi: 10.1007/s00414-022-02824-y

[13] Sahoo, N., Roy, I. D., Desai, A. P., & Gupta, V. (2010). Comparative evaluation of autogenous calvarial bone graft and alloplastic materials for secondary reconstruction of cranial defects. *Journal of Craniofacial Surgery,* 21(1), 79-82. doi: 10.1097/SCS.0b013e3181c3ba58

[14] Silva, D. D. D., Paz, A. H. D. R., Portinho, C. P., Lima, E. O. C., Kliemann, L. M., & Collares, M. V. M. (2021). Reconstruction of parietal bone defects with adiposederived mesenchymal stem cells. *Experimental study. Acta Cirurgica Brasileira*, 35, e351201. doi: 10.1590/ACB351201

[15] Shmarhalov, A. (2013). Краніотопографічні особливості потиличної кістки при різних формах будови черепа [Craniotopographic features of the occipital bone in different forms of skull structure]. *Український журнал клінічної та лабораторної медицини - Ukrainian Journal of Clinical and Laboratory Medicine,* 8(3), 89-93.

[16] Stepanenko, A. Yu. (2011). Вариантная анатомия и закономерности индивидуальной изменчивости мозгового черепа человека [Variant anatomy and patterns of individual variability of the human brain skull]. *Український морфологічний альманах - Ukrainian Morphological Almanac*, 9(3, suppl.), 39-42.

[17] Thulung, S., Ranabhat, K., Bishokarma, S., & Gongal, D. N. (2019). Morphometric measurement of cranial vault thickness: A Tertiary hospital based study. *JNMA: Journal of the Nepal Medical Association,* 57(215), 29-32. doi: 10.31729/jnma.3949

[18] Tubbs, R. S., Bosmia, A. N., & Cohen-Gadol, A. A. (2012). The human calvaria: a review of embryology, anatomy, pathology, and molecular development. *Child's Nervous System*, 28, 23-31. doi: 10.1007/s00381-011-1637-0

[19] Urban, J. E., Weaver, A. A., Lillie, E. M., Maldjian, J. A., Whitlow, C. T., & Stitzel, J. D. (2016). Evaluation of morphological changes in the adult skull with age and sex. *Journal of anatomy,* 229(6), 838-846. doi: 10.1111/joa.12247

[20] Zwirner, J., Safavi, S., Scholze, M., Li, K. C., Waddell, J. N., Busse, B., ... & Hammer, N. (2021). Topographical mapping of the mechanical characteristics of the human neurocranium considering the role of individual layers. *Scientific Reports,* 11(1), 3721. doi: 10.1038/s41598-020-80548-y

ОСОБЛИВОСТІ БУДОВИ ТА ФОРМИ ТІМ'ЯНИХ КІСТОК СКЛЕПІННЯ ЧЕРЕПА ЛЮДИНИ З УРАХУВАННЯМ СТАТІ ТА КРАНІОТИПУ

Войницька О. М., Вовк О. Ю., Чеканова І. В.

Розвиток нейрохірургії та підвищення вимог до виконання оперативних доступів, що виконують через кістки склепіння черепа, призводить до формування нових запитів щодо деталізації та уточнення краніометричної характеристики тім'яних кісток. Метою нашого дослідження є встановлення особливостей форми та інших просторових покажчиків тім'яних кісток черепу людини зрілого віку з урахуванням статі та певних різновидів краніотипу. Дослідження проведено на 130 вивчених препаратах кісткових структур голови дорослих людей зі зібраної колекції кафедри нормальної анатомії Харківського національного медичного університету, в кількості 82 кісткових препаратів, включаючи ізольовані тім'яні кістки, а також 48 томограм, отриманих при обстеженні пацієнтів. В основу встановлення краніотипу покладено принцип обчислення черепного індексу. Для статистичного аналізу ми використовували програми Statistica 13.5.0.17 (trial version) та Microsoft Excel корпоративного пакету MS 365. Для встановлення особливостей будови та форми тім'яних кісток визначили такі краніометричні покажчики: довжина та ширина тім'яних горбів, тім'яна хорда та дуга, розрахували індекс кривизни тім'яної кістки. Отримані дані проаналізовані для людей зрілого віку різного гендеру та трьох встановлених краніотипів. Встановлено, що для брахікранів характерна розширено-розгорнута форма тім'яних кісток, пов'язана з переважанням поперечних розмірів всього мозкового черепа. Для мезоцефалів найбільш типова проміжно-усереднена форма залежно від значень черепного індексу. У доліхокранів - подовжено-звужена форма тім'яних кісток, котра об'єднана із загальними змінами мозкового черепа. Додаткові лінійні параметри тім'яних кісток знаходяться в прямій залежності від встановленого краніотипу. Для доліхокранічного типу характерні максимальні значення довжини тім'яних горбів: $\overline{x}$ =18,43 мм (справа) та $\overline{x}$ =18,24 мм (зліва) при мінімальних параметрах ширини: до $\overline{x}$ =15,71 мм та $\overline{x}$ =15,02 мм. Для представників брахікранічного типу характерні мінімальні покажчики довжини горбів: від $\overline{x}$ =12,73 мм до $\overline{x}$ =12,81 мм та максимальні для ширини - $\overline{x}$ =23,52 мм (справа) і $\overline{x}$ =23,04 мм (зліва). Тім'яна хорда, як і тім'яна дуга, мали схожу тенденцію розподілу показників, а саме: збільшення від доліхокранії до брахікранії. У чоловіків з доліхокранічним типом будови черепа середні значення цих параметрів знаходились на рівні $\overline{x}$ =108,2 мм (справа) та 107,6 мм (зліва) для тім'яної хорди, та $\overline{x}$ =114,2 мм та $\overline{x}$ =113,2 мм для тім'яної дуги. У чоловіків з брахікранічним типом тім'яна хорда досягала - $\overline{x}$ =116,6 мм (справа) та $\overline{x}$ =115,8 мм (зліва) а тім'яна дуга досягала - $\overline{x}$ =127,8 мм (справа) та $\overline{x}$ =126,9 мм (зліва). У жінок встановлено аналогічний принцип розподілу розмірів з урахуванням невеликого, 2-3 мм, загального зменшення показників відносно чоловіків. Визначили індекс кривизни тім'яних кісток: у доліхокранів отримані максимальні значення середніх $\overline{x}$ =83,00-83,58, мінімальні - у брахікранів $\overline{x}$ =80,56-81,64. Це свідчить про збільшення кривизни кісток у брахікранів, враховуючи що абсолютна величина індексу має обернено пропорційну залежність від ступеня кривизни. Таким чином, отримані дані свідчать про встановлену стійку залежність між краніотипом черепу та додатковими параметрами тім'яних кісток.

Ключові слова: *краніометрія, тім'яна кістка, черепний індекс, тім'яні горби, тім'яна хорда, тім'яна дуга.*

Author's contribution:

Voinytska O.M.: conceptualization, research, review writing and editing, methodology and writing of the original draft. formal analysis and validation.

Vovk O.Y.: supervision, project administration.

Chekanova I.V.: data visualization. resources. software.

DOI: 10.31393/morphology-journal-2023-29(4)-05 Reports of Morphology, Vol. 29, №4, Pages 35-40

ISSN 1818-1295 eISSN 2616-6194

REPORTS OF MORPHOLOGY

Official Journal of the Scientific Society of Anatomists, Histologists, Embryologists and Topographic Anatomists of Ukraine

journal homepage: https://morphology-journal.com

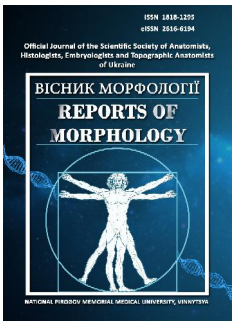

Peculiarities of the microscopic structure of rat testis under the influence of vipera berus berus venom

Niyazmetov T. S.
Bogomolets National Medical University, Kyiv, Ukraine

ARTICLE INFO
Received: 24 July 2023
Accepted: 26 September 2023

UDC: 61:612.4:615.9.616.4:616-099

CORRESPONDING AUTHOR
e-mail: timur_X007@icloud.com
Niyazmetov T. S.

CONFLICT OF INTEREST
The authors have no conflicts of interest to declare.

FUNDING
Not applicable.

DATA SHARING
Data are available upon reasonable request to corresponding author.

Morpho-functional changes in the organs of the male reproductive system are usually associated with injuries, infectious diseases, age, lifestyle, the presence of bad habits (abuse of alcohol, drugs), the influence of environmental factors, etc. However, the action of natural toxins, in particular those that are components of animal venoms, including the venoms of snakes and vipers, is no less important. The aim of the research is to study the features of the microscopic structure of the testis of rats under the influence of Vipera berus berus venom. Experimental studies were carried out on white non-linear male rats. Animals were conditionally divided into two groups - control and experimental, 10 individuals in each. Experimental rats were injected intraperitoneally with a semi-lethal dose (LD^{50}) (1.576 mg/g^{-1}) of Vipera berus berus venom in physiological solution. Animals of the control group were injected intraperitoneally with only saline solution. Rats were removed from the experiment 24 hours after exposure of the venom, anesthetized by cervical dislocation. Testis samples were taken for microscopic examination. Fixation of the material and preparation of paraffin blocks were carried out according to generally accepted methods. Staining of histological preparations of the testis was carried out with hematoxylin and eosin. Histological preparations were studied using a SEO SCAN light microscope. Administration of Vipera berus berus venom to rats leads to the development of pathogistological changes in the parenchymal elements of the testis of animals, among which desquamation and disorganization of all stages of spermatogenic cells development, disruption of spermatogenesis processes were the most pronounced. Spermatogenic cells of the seminiferous tubules of the testis were distinguished by changes in morphology and location, lost the regularity of their placement, and their number decreased. The cells detached from the basement membrane and did not form a continuous layer. A characteristic feature was the presence of clusters of erythrocytes in the lumen of the seminiferous tubules, which may indicate the development of hemorrhagic complications. In addition, an increase in the number of Leydig cells was detected, which is probably the cause of changes in the hormonal regulation of the organ's function.

Keywords: *vipers, testis, spermatogenesis, seminiferous tubules, rats.*

Introduction

To date, it has been established that the venom of snakes and vipers includes about 50-200 different components, which usually belong to four main families of toxins: phospholipases A2 (PLA2), metalloproteinases (SVMPs), serine proteases (SVSPs), three-finger toxins (3FTXs) [13, 15, 16, 17]. The composition of the venom can vary at the interspecies and intraspecies levels and depends on such factors as features of ontogenesis, nutrition, sex, adaptation to living conditions [14, 19, 20].

Among the many venoms of other animals, the composition of the venom of the scorpion Leiurus macroctenus, which mainly consists of inorganic salts, nucleotides, amino acids, lipids, enzymes and peptides, attracts attention [19].

The most common in European countries are vipers of the Viperidae family, the bites of which are associated with numerous fatal consequences or the development of hemotoxic, cytotoxic, neurotoxic disorders. Among all species of this family, Vipera berus berus and Vipera berus nikolskii are also common in Ukraine [11, 21].

The spectrum of clinical manifestations of snake and viper bites is extremely wide. The analysis of scientific literature shows that the most common are local tissue damage, pain, lymphadenitis, hemorrhagic disorders, damage of the nervous, urinary systems, etc [4, 5, 10].

Enzymes present in the venom enhance the process of poisoning and the spread of the venom by destroying the extracellular matrix. An increase in enzymatic activity during poisoning leads to increased tissue permeability and provides a systemic inflammatory response since poison toxins can quickly spread between all organs and tissues [8, 9].

Morpho-functional changes in the organs of the male reproductive system are usually associated with injuries, infectious diseases, age, lifestyle, the presence of bad habits (abuse of alcohol, drugs), the influence of environmental factors, etc. However, the action of natural toxins, in particular those that are components of animal venom, including the venom of snakes and vipers, is not less important. This problem is currently a subject of interest of scientists. The facts of the development of pronounced violations in the structural organization of the male reproductive system under the influence of snake venom, namely Crotalus durissus ssp. and Daboia russelli are proven. In the scientific literature, no data were found regarding the effect of Vipera berus berus venom on organs of the male reproductive system, which determines the relevance of the chosen direction of research.

The aim of the research is to study the features of the microscopic structure of the testis of rats under the influence of Vipera berus berus venom.

Materials and methods

Experimental studies were carried out on white non-linear male rats. For preliminary acclimatization, the animals were kept for 7 days in the animal facility of Taras Shevchenko National University of Kyiv, and then kept in laboratory conditions at constant temperature (22±3°C), humidity (60±5 %) and light (12 h light/12 h dark cycle), being fed standard rodent food and water ad libitum [6]. All experiments were conducted in accordance with the National Institutes of Health Guidelines for the care and use of laboratory animals and the European Council Directive of 24 November 1986 for the Care and Use of Laboratory Animals (86/609/EEC). The research was approved and confirmed by the Bioethics Commission of the NSC "Institute of Biology and Medicine" of the Taras Shevchenko National University of Kyiv (protocol No. 2 dated August 19, 2021).

Vipera berus berus venom was obtained from the V. N. Karazin Kharkiv National University. The lyophilized crude venom was stored at -20°C and then dissolved in saline solution immediately before the experiment.

The animals were conditionally divided into two groups - a control and an experimental group of 10 individuals in each. Experimental rats were injected intraperitoneally with a semi-lethal dose (LD^{50}) (1.576 mg/g^{-1}) of Vipera berus berus venom in saline solution. Animals of the control group were injected intraperitoneally with only saline solution. Rats were removed from the experiment 24 hours after exposure to the venom, anesthetized by cervical dislocation.

Testis samples from animals of all groups were taken for microscopic examination. The pieces were fixed in a 10 % formalin solution for 1 day. Further the pieces were dehydrated in alcohols of increasing concentration and embedded in paraffin blocks. Histological preparations of testis were stained with hematoxylin and eosin [12]. Histological specimens were studied using a SEO SCAN light microscope.

Results

A morphological study of the testis of animals from the group injected with Vipera berus berus venom showed a lower reactivity of stromal elements damage compared to parenchymatous elements. The dense connective tissue of the capsule and trabeculae does not undergo noticeable changes: the septa do not thicken and do not undergo delamination. Small and medium-diameter blood vessels in the interstitium are characterized by full blood and aggregation of red blood cells in the lumen (Fig. 1 A, Fig. 2 D). In general, the shape of the seminiferous tubules does not change and remains quite regular (see Fig. 1 B).

Sometimes the interstitium was characterized by an increased number of Leydig cells, which may indicate a violation in the hormonal regulation of the organ (see Fig. 2 A, 2 D).

Unlike the stroma, the parenchymal components of the testis are characterized by various microscopic signs of damage. In particular, a general examination of the contents of the seminiferous tubules demonstrates detachment and disorganization of spermatogenic cells at all stages of their development. The lumens of some tubules are empty, which indicates a radical disruption of spermatogenesis processes in them (see Fig. 1 B, 1 C). Such emptiness is most likely determined by the incomplete stop of spermatocytes in the spermatogenesis pathway in such tubules. In the case of spermatogenic hypoplasia, the tubules have a reduced population of germ cells and a poor order of spermatogenesis.

In other tubules, desquamation and disorganization indicate that spermatogenesis is disordered and the tubule lumen is filled with desquamated immature cells (see Fig. 1 D).

Spermatogenic cells in seminiferous tubules of animals are characterized by changes in morphology and location. In contrast to animals from the control group, in rats, after the injection of Vipera berus berus venom, spermatogonia lose the regularity of their location and decrease in number (see Fig. 2 A, 2 B). Cells are separated from the basement membrane and do not form a single layer. It is likely that their location below the blood-testicular barrier makes them most vulnerable to venom. In some tubules, spermatogonia are

practically not visible (see Fig. 2 B), which indicates the loss of the ability to renew the population of male germ cells, because only spermatogonia can divide by mitosis and perform this function.

Primary spermatocytes are slightly less exposed to snake venom, their general presence in the lumen of the tubules practically does not change, but their location becomes disorganized, they are largely shifted to the center of the seminiferous tubules, where they "mix" with more mature forms of spermatogenic cells (see Fig. 2 C, 2 B). Inside the first line spermatocytes, vacuolization is often seen around the nucleus (see Fig. 2 A). Presumably, this can be explained by the origin of these vacuoles - they are expanded cisterns of the rough endoplasmic reticulum, which try to ensure detoxification processes in the cell.

Spermatids in their location shift to the center of the seminiferous tubules, presumably losing their connection with Sertoli cells. Closer to the center of the tubule lumen, they form an eosinophilic amorphous mass together with mature spermatozoa. An interesting feature is the presence of erythrocytes clusters in the lumen of the tubules, which probably indicates hemorrhages under the influence of snake venom (see Fig. 2 B, 2 C).

In conclusion, it should be noted that the content of seminiferous tubules in research group of animals is characterized by a partial inhibition of proliferation and differentiation of spermatocytes, spermatogenic hypoplasia.

Discussion

The study of the effect of snake venom on the testis is related to their important functions, which have complex mechanisms of regulation. Factors such as active mitosis, the presence of a barrier between the blood and testicles, the spermatogenic cycle and hormonal control complicate the response of this organ to external toxic factors.

However, the general mechanisms of the types of

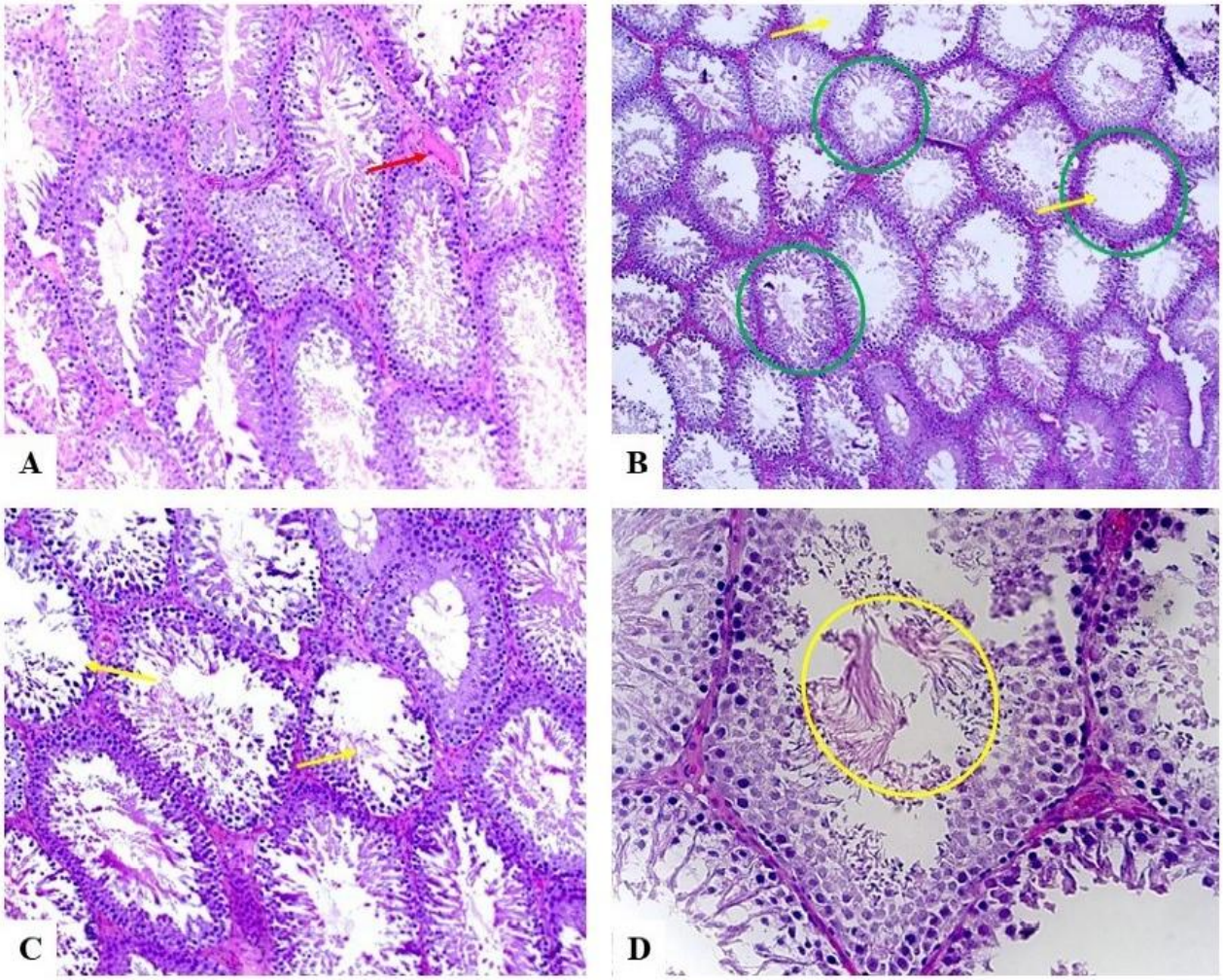

Fig. 1. The stroma and seminiferous tubules of the testis of rats in the experimental group with the introduction of Vipera berus berus venom. A: full blood vessels with aggregated blood elements in the lumen (red arrow); B: seminiferous tubules of regular shape (green ovals); B, C: gaping space of seminiferous tubules without spermatogenic cells (yellow arrows); D: desquamated immature cells in the lumen of tubules (yellow oval). Staining with hematoxylin and eosin; A, B x200, C x100, D x400.

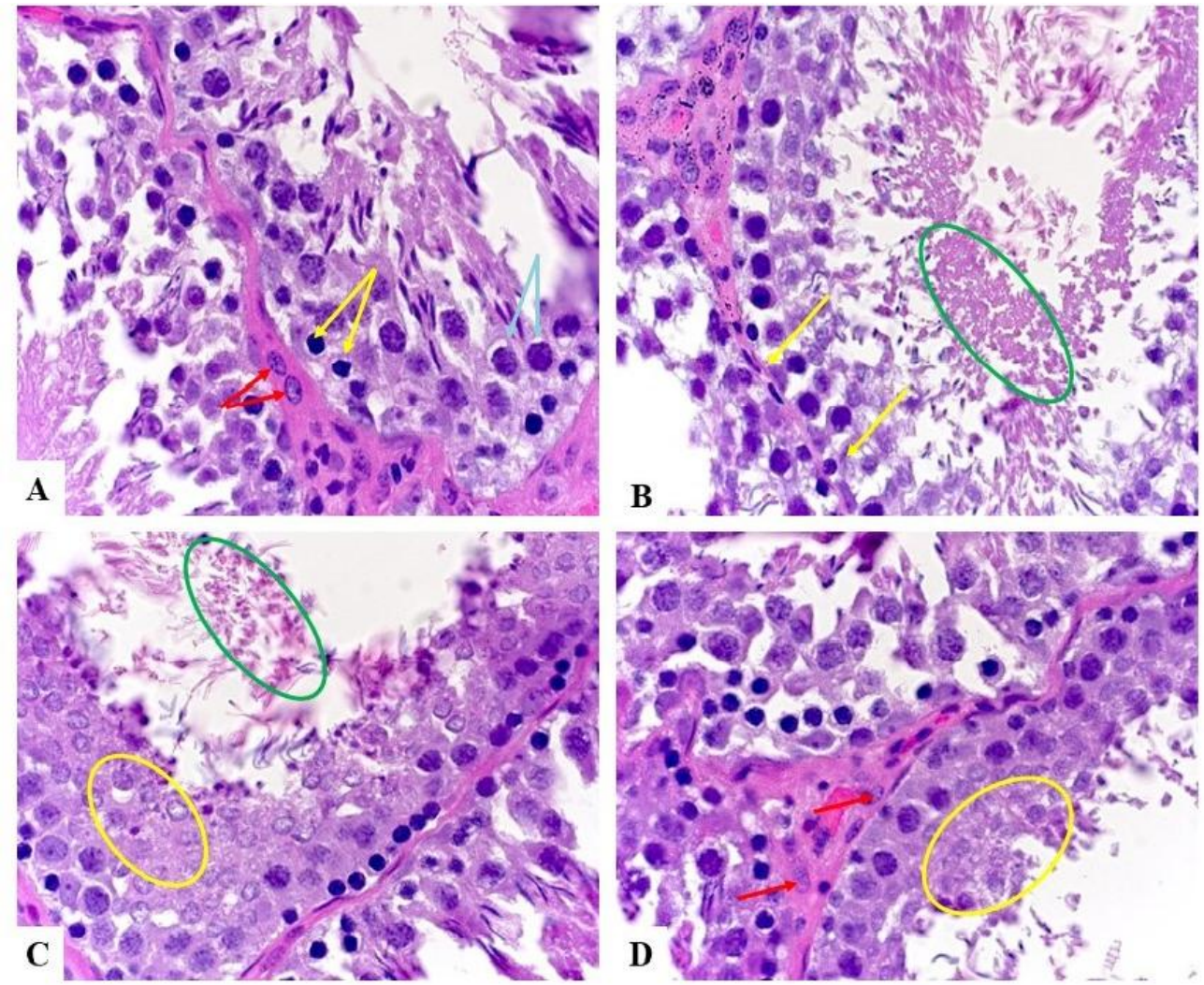

Fig. 2. The stroma and seminiferous tubules of the testis of rats in the experimental group with the introduction of Vipera berus berus venom. A: vacuolization around the nucleus of spermatocytes (blue arrows); A, B: a small number of irregularly placed spermatogonia (yellow arrows); A, D: Leydig cells in the interstitium (red arrows); B, C: erythrocytes within the amorphous mass in the lumen of seminiferous tubules (green ovals); C, D: cell mass from spermatogenic cells of various degrees of maturity with blurred edges (yellow ovals). Staining with hematoxylin and eosin; x 1000.

testicular toxicity can be classified according to certain developmental mechanisms. It is necessary to analyze the primary toxicity - the direct effect of the venom on the spermatogenic epithelium. In addition, there are several indirect factors of the effect of the venom on this organ, related to the regulation of its functions and blood supply. In particular, indirect hormonal influence on spermatogenesis and impaired blood circulation in the testicle can also lead to pathological changes. In the histological assessment of testicular toxicity, histological models of toxic lesions caused by various model chemicals, classified on the basis of their mechanisms of action, are very useful [18].

Studies of the effects of toxic compounds on the structure and function of the testis strongly suggest that the early changes, rather than those that occur later are particularly useful for understanding their mechanisms of action. This observation correlates with our research, because we study the morphology of the testes 24 hours after the injection of snake venom.

B. S. Ajisebiola et al. established that the venom of Naja nigricollis causes the development of morphological and biochemical changes in testicular tissue of experimental animals. In rats, under these conditions, atrophy of the tubular epithelium of the testis, a significant decrease in the number of spermatogenic cells, their necrosis, and distortion of the structure of the germinal epithelium were detected. In the tissue of the organ, a decrease in the activity of catalase, glutathione peroxidase and an increase in the level of malondialdehyde, IL-1β, TNF-α were noted [1].

According to scientists, toxins from the venom of Echis ocellatus snakes cause the development of an inflammatory process in the tissue of the testis of rats, degenerative

changes in the germinal epithelium and the epithelium of seminiferous tubules, and tubular atrophy [2].

C. Alberto-Silva and co-authors [3] in experiments on rats injected with Bothrops jararaca snake venom observed a violation of the integrity of the epithelial lining of the seminiferous tubules, the absence of spermatids in them. In some places, degenerative changes of the seminiferous tubules, an increase in their diameter, and an expansion of the lumens were detected. The number of pachytene spermatocytes, rounded spermatids and pluripotent spermatocytes also decreased. At the same time, the general resistance capacity of Sertoli cells also underwent changes. Research of other scientists regarding the effect of the toxic venom components of these snakes demonstrated the presence of microscopic changes in the structure of the germinal epithelium in the adlumenal part of testis, atypical multinucleated cells were present in the lumen of the seminiferous tubules [7].

Conclusions

Injection of Vipera berus berus venom to rats leads to the development of pathogistological changes in the parenchymal elements of the testis of animals, among which desquamation and disorganization of spermatogenic cells of all stages of development, disruption of spermatogenesis processes were the most pronounced. Spermatogenic cells of the seminiferous tubules of the testis were distinguished by changes in morphology and location, lost the regularity of their placement, and their number decreased. The cells detached from the basement membrane and did not form a continuous layer. A characteristic feature was the presence of clusters of erythrocytes in the lumen of the seminiferous tubules, which may indicate the development of hemorrhagic complications. In addition, an increase in the number of Leydig cells was detected, which is probably the cause of changes in the hormonal regulation of the organ.

References

[1] Ajisebiola, B. S., Adeniji, O. B., James, A. S., Ajayi, B. O., & Adeyi, A. O. (2022). Naja nigricollis venom altered reproductive and neurological functions via modulation of pro-inflammatory cytokines and oxidative damage in male rats. *Metabol Open,* (14), 100188. doi: 10.1016/j.metop.2022.100188

[2] Ajisebiola, B. S., Alamu, P. I., James, A. S., & Adeyi, A. O. (2022). Echis ocellatus Venom-Induced Reproductive Pathologies in Rat Model; Roles of Oxidative Stress and Pro-Inflammatory Cytokines. *Toxins* (Basel), 14(6), 378. doi: 10.3390/toxins14060378

[3] Alberto-Silva, C., Franzin, C. S., Gilio, J. M., Bonfim, R. S., & Querobino, S. M. (2020). Toxicological effects of bioactive peptide fractions obtained from Bothrops jararaca snake venom on the structure and function of mouse seminiferous epithelium. *J Venom Anim Toxins Incl Trop Dis*, (26), e20200007. doi: 10.1590/1678-9199-JVATITD-2020-0007

[4] Burin, S. M., Menaldo, D. L., Sampaio, S. V., Frantz, F. G., & Castro, F. A. (2018). An overview of the immune modulating effects of enzymatic toxins from snake venoms. *Int J Biol Macromol,* (109), 664-671. doi: 10.1016/j.ijbiomac.2017.12.101

[5] Canas, C. A., Castro-Herrera, F., & Castano-Valencia, S. (2021). Clinical syndromes associated with Viperidae family snake envenomation in southwestern Colombia. *Trans R Soc Trop Med Hyg,* 115(1), 51-56. doi: 10.1093/trstmh/traa081

[6] Dobrelia, N. V., Boitsova, L. V. & Danova, I. V. (2015). Правова база для проведення етичної експертизи доклінічних досліджень лікарських засобів з використанням лабораторних тварин [Legal basis for ethical examination of preclinical studies of drugs using laboratory animals]. *Фармакологія та лікарська токсикологія - Pharmacology and drug toxicology,* (2), 95-100.

[7] Gilio, J. M., Portaro, F. C., Borella, M. I., Lameu, C., Camargo, A. C., & Alberto-Silva, C. (2013). A bradykinin-potentiating peptide (BPP-10c) from Bothrops jararaca induces changes in seminiferous tubules. *J Venom Anim Toxins Incl Trop Dis*, 19(1), 28. doi: 10.1186/1678-9199-19-28

[8] Gunas, V., Maievskyi, O., Raksha, N., Vovk, T., Savchuk, O., Shchypanskyi, S., & Gunas, I. (2023). Protein and peptide profiles of rats' organs in scorpion envenomation. *Toxicology Reports,* 10, 615-620. doi: 10.1016/j.toxrep.2023.05.008

[9] Gunas, V., Maievskyi, O., Raksha, N., Vovk, T., Savchuk, O., Shchypanskyi, S., & Gunas, I. (2023). The Activity of Metalloproteases and Serine Proteases in Various Organs after Leiurus macroctenus Envenomation. *Journal of Toxicology,* 2023, 5262729. doi: 10.1155/2023/5262729

[10] Gutierrez, J. M., Calvete, J. J., Habib, A. G., Harrison, R. A., Williams, D. J., & Warrell, D. A. (2017). Snakebite envenoming. Nat Rev Dis Primers, 3, 17063. doi: 10.1038/nrdp.2017.63

[11] Hermansen, M. N., Krug, A. H., Tjønnfjord, E., & Brabrand, M. (2019). Envenomation by the common European adder (Vipera berus): a case series of 219 patients. *Eur J Emerg Med*, 26(5), 362-365. doi: 10.1097/MEJ.0000000000000577

[12] Horalskyi, L. P., Khomych, V. T., & Kononskyi, O. I. (2011). *Основи гістологічної техніки і морфофункціональні методи досліджень у нормі та при патології [Fundamentals of histological technique and morphofunctional research methods in normal and pathology].* Житомир, Полісся - Zhytomyr: Polissya.

[13] Makarova, Y. V., Kryukova, E. V., Shelukhina, I. V., Lebedev, D. S., Andreeva, T. V., Ryazantsev, D. Y., … Utkin, Y. N. (2018). The First recombinant viper three-finger toxins: Inhibition of muscle and neuronal nicotinic acetylcholine receptors. *Dokl Biochem Biophys,* 479(1), 127-130. doi: 10.1134/S1607672918020205

[14] Malina, T., Krecsák, L., Westerström, A., Szemán-Nagy, G., Gyémánt, G., M-Hamvas, M., … Vasas, G. (2017). Individual variability of venom from the European adder (Vipera berus berus) from one locality in Eastern Hungary. *Toxicon,* (135), 59-70. doi: 10.1016/j.toxicon.2017.06.004

[15] Modahl, C. M., Saviola, A. J., & Mackessy, S. P. (2021). Integration of transcriptomic and proteomic approaches for snake venom profiling. *Expert Rev Proteomics,* 18(10), 827-834. doi: 10.1080/14789450.2021.1995357

[16] Nirthanan, S. (2020). Snake three-finger alfa-neurotoxins and nicotinic acetylcholine receptors: molecules, mechanisms and medicine. *Biochem Pharmacol,* (181), 114168. doi: 10.1016/j.bcp.2020.114168

[17] Serrano, S. M. T., Zelanis, A., Kitano, E. S., & Tashima, A. K. (2018). Analysis of the snake venom peptidome. *Methods Mol Biol,* (1719), 349-358. doi: 10.1007/978-1-4939-7537-2_23

[18] Shah, W., Khan, R., Shah, B., Khan, A., Dil, S., Liu, W., … Jiang, X. (2021). The Molecular Mechanism of Sex Hormones on

Sertoli Cell Development and Proliferation. *Front Endocrinol* (Lausanne), (12), 648141. doi: 10.3389/fendo.2021.648141

[19] Zanetti, G., Duregotti, E., Locatelli, C. A., Giampreti, A., Lonati, D., Rossetto, O., ... Pirazzini, M. (2018). Variability in venom composition of European viper subspecies limits the cross-effectiveness of antivenoms. *Sci Rep,* 8(1), 9818. doi: 10.1038/s41598-018-28135-0

[20] Zelanis, A., Menezes, M. C., Kitano, E. S., Liberato, T., Tashima, A. K., Pinto, A. F., ... Serrano, S. M. (2016). Proteomic identification of gender molecular markers in Bothrops jararaca venom. *J Proteomics,* (139), 26-37. doi: 10.1016/j.jprot.2016.02.030

[21] Zinenko, O., Tovstukha, I., & Korniyenko, Y. (2020). PLA2 inhibitor varespladib as an alternative to the antivenom treatment for bites from Nikolsky's viper Vipera berus nikolskii. *Toxins* (Basel), 12(6), 356. doi: 10.3390/toxins12060356

ОСОБЛИВОСТІ МІКРОСКОПІЧНОЇ СТРУКТУРИ ЯЄЧОК ЩУРІВ ЗА УМОВ ВПЛИВУ ОТРУТИ ГАДЮКИ VIPERA BERUS BERUS

Ніязметов Т. С.

Морфо-функціональні зміни органів чоловічої статевої системи зазвичай асоціюються з травмами, інфекційними захворюваннями, віком, способом життя, наявністю шкідливих звичок (зловживання алкоголем, наркотиками), впливом факторів навколишнього середовища, тощо. Однак не менш вагомою є дія природних токсинів, зокрема тих, що є компонентами тваринних отрут, в тому числі отрут змій та гадюк. Метою дослідження є вивчення особливостей мікроскопічної структури яєчок щурів за умов впливу отрути гадюки Vipera berus berus. Експериментальні дослідження проводили на білих нелінійних щурах самцях. Тварин умовно розподіляли на дві групи - контрольну і дослідну по 10 особин в кожній. Дослідним щурам внутрішньоочеревинно вводили напівлетальну дозу (LD50) (1,576 мг/г$^{-1}$) отрути Vipera berus berus на фізіологічному розчині. Тваринам контрольної групи внутрішньоочеревинно вводили лише фізіологічний розчин. Виводили щурів з експерименту через 24 години після впливу отрути, знеживлюючи шляхом цервікальної дислокації. Для мікроскопічного дослідження забирали зразки яєчок. Фіксація матеріалу та приготування парафінових блоків проводили за загальноприйнятими методиками. Забарвлення гістологічних препаратів яєчок здійснювали гематоксиліном та еозином. Гістологічні препарати вивчали за допомогою світлового мікроскопа SEO SCAN. Введення щурам отрути гадюк Vipera berus berus призводить до розвитку патогістологічних змін паренхіматозних елементів яєчок тварин, серед яких найбільш виразними були десквамація та дезорганізація сперматогенних клітин всіх стадій розвитку, порушення процесів сперматогенезу. Сперматогенні клітини звивистих канальців яєчок відрізнялись змінами у морфології та розташуванні, втрачали регулярність свого розміщення, знижувалась їх чисельність. Клітини відшаровувались від базальної мембрани і не формували суцільного шару. Характерною особливістю була наявність скупчень еритроцитів в просвітах сім'яних канальців, що може свідчити про розвиток геморагічних ускладнень. Крім того, виявляли зростання кількості клітин Лейдіга, що, ймовірно, є причиною зрушень гормональної регуляції роботи органу.

Ключові слова: *гадюки, яєчка, сперматогенез, сім'яні канальці, щури.*

DOI: 10.31393/morphology-journal-2023-29(4)-06 Reports of Morphology, Vol. 29, №4, Pages 41-49

ISSN 1818-1295 eISSN 2616-6194

REPORTS OF MORPHOLOGY

Official Journal of the Scientific Society of Anatomists, Histologists, Embryologists and Topographic Anatomists of Ukraine

journal homepage: https://morphology-journal.com

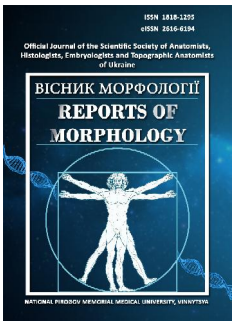

Rats' thyroid gland histological and ultrastructural changes throughout the experimental thermal injury dynamics on the background of HAES-LX 5 % colloid-hyperosmolar solution injection

Tiron O. I., Vastyanov R. S.
Odesa National Medical University, Odesa, Ukraine

ARTICLE INFO
Received: 20 July 2023
Accepted: 28 September 2023

UDC: 616.441:599.323.4:615.459

CORRESPONDING AUTHOR
e-mail: chekina.o@ukr.net
Tiron O. I.

CONFLICT OF INTEREST
The authors have no conflicts of interest to declare.

FUNDING
Not applicable.

DATA SHARING
Data are available upon reasonable request to corresponding author.

The urgency of the burn injury problem is determined by frequent thermal injuries of patients of different ages, the complexity and duration of treatment, long-term disability and relatively high mortality. Depending on the area and depth of the lesion, a burn wound causes multiple and long-lasting disturbances in homeostasis, which cause organs and systems dysfunction. We are interested in the intrathyroid changes that occur during thermal burns, as thyroid gland plays one of the leading roles in the endocrine regulation of organisms' majority functions. When researching the issue of pharmacological correction of thyroid gland damage after a burn injury, we proceed from the classical fundamental concept regarding its pathogenetic validity. Taking into account the known pathogenetic mechanisms of burn disease with consecutive (and sometimes simultaneous) hypoproteinemia and haemoconcentration manifestations, intoxication formation, inflammatory and autoimmune reaction, we came to a conclusion regarding the reasonability of colloid solutions efficacy testing to attempt the pharmacocorrection in case of thyroid gland both structure and function burning. The purpose of the work is to establish histological and ultrastructural changes in the thyroid gland of experimental rats that were injected with colloidal hyperosmolar solution HAES-LX 5 % in the dynamics of skin thermal damage. Experimental studies were conducted on 90 white male rats. Skin thermal burns were simulated using four copper plates application to previously depilated lateral surfaces of the rats' body for 10 s. Rats were injected with colloidal hyperosmolar solution HAES-LX 5 % into the vena cava inferior during the first 7 days of the post-burn period. Thyroid gland pieces were fixed in a 10 % neutral formalin solution, dehydrated in alcohols of increasing concentration and embedded in paraffin blocks. The prepared sections of 5-6 μm thickness were stained with hematoxylin-eosin. For electron microscopic studies, pieces of the thyroid gland were taken, fixed in a 2.5% glutaraldehyde solution, and postfixed with a 1% osmium tetroxide solution in a phosphate buffer. Semi-thin sections were stained with methylene blue. Ultrathin sections were contrasted with uranyl acetate, lead citrate according to the Reynolds method and studied in a PEM-125K electron microscope. Colloidal hyperosmolar solution HAES-LX 5 % administration within 7 days of the post-burn period to correct the thermal injury effects has an expressed positive effect on burned animals thyroid gland histo- and ultrastructure. A significant improvement of the structural state of the stromal and parenchymal components of the organ and their relative normalization in the late period under the influence of the applied solution was established in the dynamics of the experiment. The colloidal hyperosmolar solution HAES-LX 5 % positive effects were expressed by cellular walls of the vessels and follicles dystrophic and destructive changes reduction the structural components of the organ restoration during the entire period of the study up to the 30th day of the trial. The first signs of the intraglandular environment recovery after colloidal hyperosmolar solution HAES-LX 5 % use were proved to start registered from the 7th day of the post-burn period and were maximally expressed from the 21st day until the end of the experiment. The authors are sure that colloidal hyperosmolar HAES-LX 5 % solution protective action possible mechanism is the generalized catabolic reaction

inhibition and the membrane-protective effect development. A complex of colloidal hyperosmolar solution HAES-LX 5 % protective, adaptive, adaptive, compensatory and regenerative effects were realized throughout the 30 days of the post-burn period, which efficacy exceeds the thyroid gland parenchyma and surrounding tissues destructive, decompensatory and necrotic changes. The authors consider the use of colloidal hyperosmolar solution HAES-LX 5 % to be one of the burn treatment regimen components as a restorative therapy drug and secondary cytoprotection aimed at the vascular wall and tissue defects integrity restoring.
Key words: *thyroid gland, thermal burn, post-burn period, morphological changes, ultrastructural changes, colloid-hyperosmolar solution HAES-LX 5 % restorative processes, pathogenetically based paharmacological correction.*

Introduction

Burn injuries are among the most common and severe diseases in humans, second only to transport injuries [10, 14, 20]. The urgency of the burn injury problem is determined by frequent thermal injuries of patients of different ages, the complexity and duration of treatment, long-term disability and relatively high mortality. Depending on the area and depth of the lesion, a burn wound causes multiple and long-lasting disturbances in homeostasis, which cause organs and systems dysfunction [3, 9, 13].

We are interested in the intrathyroid changes that occur during thermal burns, as thyroid gland plays one of the leading roles in the endocrine regulation of organisms' majority functions [15]. The thyroid gland, taking into account the wide range of thyroid hormones physiological activity, its structural and functional organization and morphofunctional features, as well as large-scale redundant regulatory feedback mechanisms, is one of the first to be subject to damaging thermal effects [9, 20]. Thyroid gland and other organs of the body dysfunction or pathological dysregulation arising as a result of thermal exposure "triggers" systemic dysfunctions via the "vicious circle" mechanisms, positive feedback and systemic-antisystemic regulation, outside of which there cannot be disorders of most organs and organ systems functioning, the pathogenetic mechanisms of which, firstly, are initiated by the general fundamental mechanisms of hypoxic and/or free radical cell death, secondly, are chains of pathophysiological processes provoked by thyroid pathology, and, thirdly, have not been sufficiently studied [9].

Despite significant advances achieved in the treatment of this pathology, mortality among severely burned victims remains high, especially with critical (40-50 % of the body surface) and supercritical (more than 50 %) deep burns [3, 17]. Therefore, while investigating the idea of thyroid gland burning pharmacological correction we used the classical fundamental concept of its pathogenetic validity. For this purpose, the pathophysiological mechanisms of the formation of endocrine disorders of the thyroid gland, pituitary gland and adrenal glands, the intensification of lipid peroxidation processes with the antioxidant system functional activity inhibition, blood rheological properties disruption with pronounced changes in red blood cells, as well as parenchymal organs involvement in this pathological process mediation were established.

Additionally, we carefully studied the morphological changes in the thyroid gland and adjacent tissues, starting from the first day of the postburn period, during the 30th day of the trial. Thyroid gland structural changes during the early post-burn period were concerned mainly the structure of its vascular component, its stroma and parenchyma and were predominantly of the nature of adaptation and/or compensation. Thyroid gland pathomorphological changes trend starting from the 21st day until the end of the trial was complex, on the one hand, with destructive and decompensatory nature, and, on the other hand, having an adaptive-compensatory, restorative and regenerative character. These data allowed us to believe the development of compensatory and restorative morphological changes in the thyroid gland and in surrounding organs and systems when prescribing pathogenetically based pharmacological correction.

According to fundamental concepts, hypohydration is one of the thermal damage leading clinical manifestation. Taking this into account, we tried to eliminate the thyroid gland parenchyma and cellular composition damage using 0.9 % physiological NaCl solution, which turned out to be unsuccessful. Taking into account the known pathogenetic mechanisms of burn disease with consecutive (and sometimes simultaneous) hypoproteinemia and haemoconcentration manifestations, intoxication formation, inflammatory and autoimmune reactions [18], we came to a conclusion regarding the reasonability of colloid solutions efficacy testing to attempt the pharmacocorrection in case of thyroid gland both structure and function burning.

The aim of the research is to establish histological and ultrastructural changes in the thyroid gland of experimental rats that were injected with HAES-LX 5 % colloidal hyperosmolar solution in the dynamics of skin thermal damage.

Materials and methods

Experimental trials were performed on 90 white male rats weighing 160-180 g (obtained from the vivarium of the Institute of Pharmacology and Toxicology of the National Academy of Medical Sciences of Ukraine) on the basis of the Research Center of National Pirogov Memorial Medical University. Animals keeping, handling and manipulation was carried out in accordance with the "General Ethical Principles of Animal Experiments" adopted by the "General

Ethical Principles of Animal Experiments" adopted by the Fifth National Congress on Bioethics (Kyiv, 2013) and was guided by the recommendations of the European Convention for the Protection of Vertebrate Animals for Experimental and Other Scientific Purposes (Strasbourg, 1985) and guidelines of the State Pharmacological Center of the Ministry of Health of Ukraine on "Preclinical studies of drugs" (2001) as well as rules of humane treatment of experimental animals and conditions approved by the Committee on Bioethics of National Pirogov Memorial Medical University (protocol № 1 from 14.01.2010).

Thermal skin burns of 2-3 degrees were modeled by four copper plates (each surface area equal to 13.86 cm^2) preheated for 6 min in water with a temperature of 100 °C applying to rats depilated side surfaces for 10 sec [5]. Rats were infused with hyperosmolar colloidal HAES-LX 5 % solution (10 ml/kg) into the lower femoral vein via catheter once per day throughout the first 7 days (the first administration was done 1 hr after the skin burn) after the skin burn during 5-6 min. Shaving, venous catheterization, skin burns and decapitation of rats were performed under propofol (i.v., 60 mg/kg) anesthesia.

Tissues for microscopic studies were collected 1, 3, 7, 14, 21 and 30 days after the skin thermal injury according to accepted methods [8]. The thyroid gland samples were fixed in a 10 % neutral formalin solution, dehydrated in alcohols of increasing concentration, and embedded in paraffin blocks. The prepared sections, 5-6 μm thick, were stained with hematoxylin-eosin [8].

The histological sections were examined under the MIKROmed SEO SCAN light microscope ("Sumy Electron Optics", Sumy, Ukraine), the photomicrographs were taken with the Vision CCD Camera with an image output system for histological specimens. The thyroid gland samples collected for electron microscopic examination were fixed with 2.5 % glutaraldehyde solution, and then post-fixed with 1 % osmium tetroxide prepared with phosphate buffer. Further processing was done according to used method [8]. Semi-thin sections were stained with methylene blue. Ultrathin sections made on an LKB-3 ultramicrotome were contrasted with uranyl acetate and lead citrate according to Reynolds method and then studied using PEM-125K electron microscope.

All morphological researches were performed under the Agreements on Scientific Cooperation among the Histology, Cytology and Embryology Department of Odesa National Medical University and Research Center of National Pirogov Memorial Medical University (from 01.01.2018) and Histology and Embryology Department of I. Horbachevsky Ternopil National Medical University (from 01.01.2019).

Results

Light-optical studies of micropreparations of the animals` thyroid gland on first day after experimental thermal injury and injection of colloid-hyperosmolar HAES-LX 5 % solution showed presence of interstitial swelling both in the capsule of the organ and in the interstitial septa; stasis in small calibre vessels and hyperemia in the arteries and veins. The follicles were polymorphic, some were in the active stage, others were overextended, lined with flat thyrocytes in the stage of hypofunction (Fig. 1A).

Histological examination of the thyroid gland after 3 days after HAES-LX 5 % injections for thermal injury correction showed a decrease both of stasis of the thyroid vessels and in interstitial and perivascular swelling in the organ. A majority of the follicles is lined with flat thyrocytes (see Fig. 1B).

Submicroscopic changes in the thyroid gland during three days of HAES-LX 5 % colloidal hyperosmolar solution usage to correct the effects of thermal injury were manifested by minor changes in the ultrastructure of the vessel wall, especially of small caliber, which were more pronounced on the first day and gradually subsided until

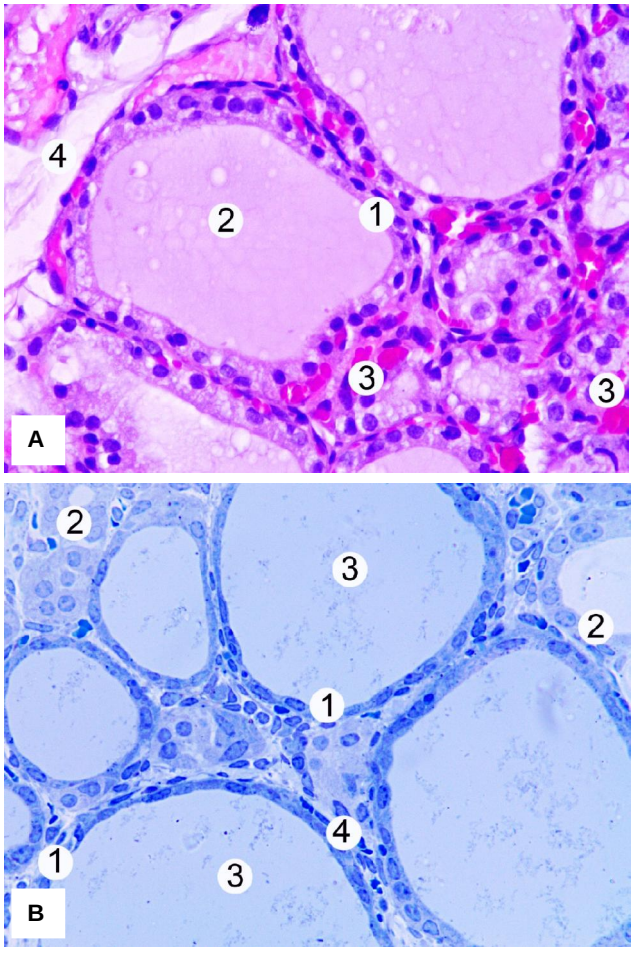

Fig. 1. Histological changes in the animal's thyroid gland after 1day (fragment A) and after 3 days (fragment B) after the cutaneous burn was treated with HAES-LX 5 % solution use. **A**: 1 - thyrocytes, 2 - colloid, 3 - capillary stasis, 4 - interstitial swelling. Hematoxylin-eosin staining. Increase x400. **B**: 1 - flat thyrocytes, 2 - cubic thyrocytes, 3 - colloid, 4 - hemocapillaries. Semi-thin cut. Methylene blue staining. Increase x400.

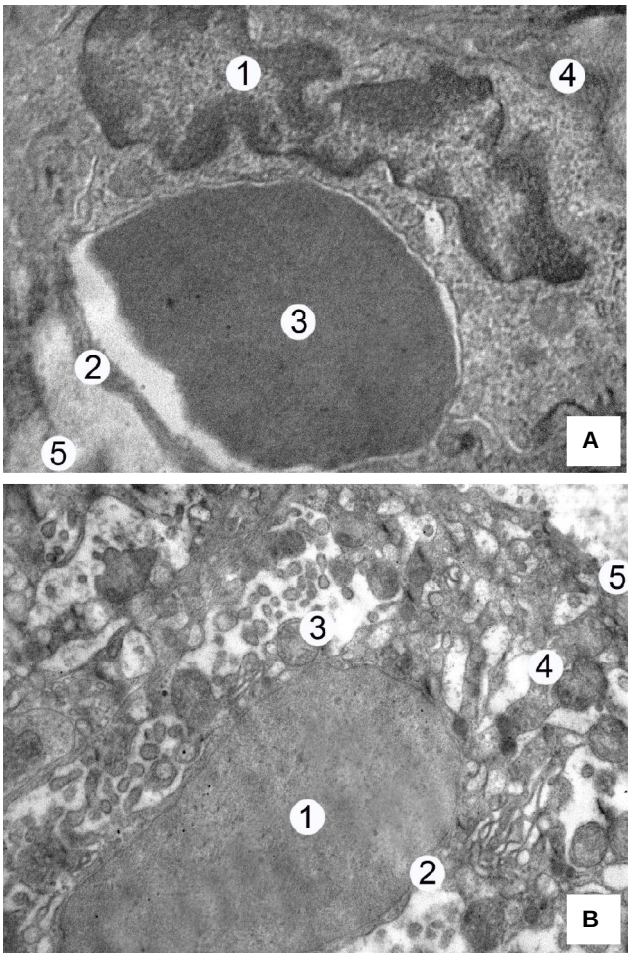

Fig. 2. Submicroscopic changes in the hemocapillary of the thyroid gland of an animal (fragment A) and thyrocytes of the thyroid gland (fragment B) after 1 day and 3 days, respectively, after experimental thermal skin injury with HAES-LX 5 % solution use. **A**: 1 - endotheliocyte nucleus, 2 - peripheral zone of endotheliocyte cytoplasm, 3 - erythrocyte in capillary lumen, 4 - unevenly thickened basement membrane, 5 - perivascular edema. Electronogram. Magnification x9000. **B**: 1 - thyrocyte nucleus, 2 - swelling of the perinuclear space, 3 - mitochondrion, 4 - hypertrophied tubules of the granular endoplasmic reticulum, 5 - apical surface with microvilli. Electronogram. Magnification x15000.

the third day. Locally thickened basement membrane, narrowing of fenestrae and a small number of microvesicles and caveolae in the peripheral zone of endotheliocytes were presented in electronograms analysis at these times of the trial (Fig. 2A).

Submicroscopically, on the 1st - 3rd days of the experiment, the HAES-LX 5 % solution was used as a corrective factor after thermal injury, and swelling of the perinuclear space was observed in thyrocytes. Large vacuole-like structures were visible in their cytoplasm, some mitochondria were characterized by disorganization of cristae, and tubules of the granular endoplasmic reticulum were characterized by hypertrophy. On the apical surface of the cells, the number of microvilli was insignificant (see Fig. 2B).

The analysis of histological preparations of the thyroid

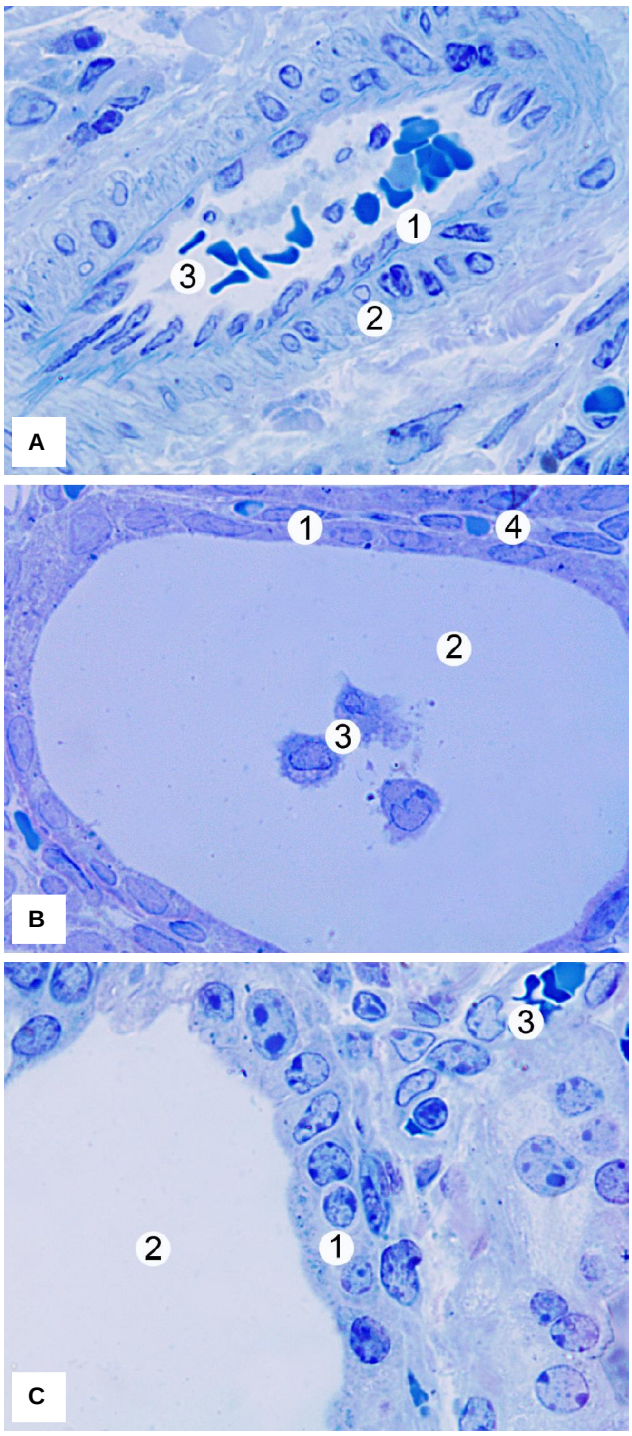

Fig. 3. Microscopic changes in the vessels of the thyroid gland of an animal in 7 days (fragments A B) and in 14 days (fragment C) after experimental thermal skin injury under the conditions of HAES-LX 5 % solution use. Semi-thin cut. Staining with methylene blue. Magnification x1000. **A**: 1 - endothelium, 2 - smooth myocytes of the media, 3 - lumen of arteriole. **B**: 1 - flat thyrocytes, 2 - colloid, 3 - desquamated thyrocytes. **C**: 1 - prismatic thyrocytes, 2 - colloid, 3 - hemocapillary.

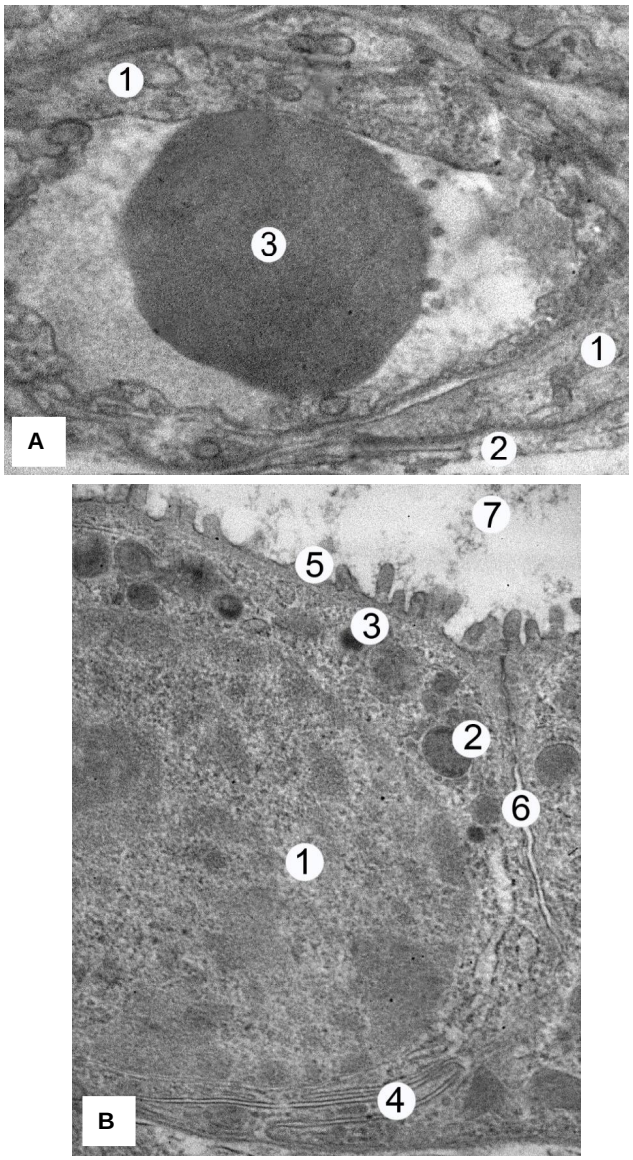

Fig. 4. Submicroscopic changes in the hemocapillary of the thyroid gland of an animal (fragment A) and thyrocytes of the thyroid gland (fragment B) after 7 days and 14 days, respectively, after experimental thermal skin injury with HAES-LX 5 % solution use. **A**: 1 - peripheral zone of endotheliocyte cytoplasm, 2 - basement membrane, 3 - erythrocyte in capillary lumen. Electronogram. Magnification x9000. **B**: 1 - thyrocyte nucleus, 2 - mitochondria, 3 - lysosome, 4 - tubules of granular endoplasmic reticulum, 5 - apical surface with microvilli. Electronogram. Magnification x17000.

gland 7-14 days after the seven-day administration of the HAES-LX 5 % solution for the correction of thermal injury consequences showed the absence of edematous manifestations in the stroma of the organ. The vessels in the stroma were moderately moderately blood-filled vessel (Fig. 3A).

Majority of the follicles in these terms of the experiment are lined with cubical or prismatic epithelium with clearly contoured basophilic nuclei. Mostly, on the 7th day, isolated overstretched follicles on the periphery of the organ and follicles with the manifistation of desquamation of thyrocytes in their lumen were detected (see Fig. 3B, 3C).

Submicroscopically, on the 7-14th day of the experiment, after a seven-day usage of the HAES-LX 5 % solution for the thermal injury effects correction, it was found that the capillaries of the organ have a preserved ultrastructure. The nuclei of endotheliocytes are oval in shape with shallow invaginations of the karyolemma and small lumps of heterochromatin located marginally. The peripheral zone of the cytoplasm of these cells was in some degree thickened, and a large number of micropinocytotic vesicles and vesicles were observed in it, which indicates the processes of active transendothelial exchange (Fig. 4A).

Ultrastructurally, thyrocytes of the thyroid gland at 7-14 days after experimental thermal injury for the seven-day usage of colloid-hyperosmolar injection of HAES-LX 5 % solution for its correction were characterized by the presence of a round or oval nucleus with the predominance of euchromatin and structured mitochondria, osmiophilic lysosomes, clearly contoured granular tubules of endoplasmic reticulum, microvesicles in the cytoplasm. At the apical pole of the follicular cells there was a significant number of microvilli, which were involved in the process of endocytosis of thyroglobulin (see Fig. 4B). These signs of the morphology preservation of follicular cells on a submicroscopic level indicate the expression of the cytoprotective effect of HAES-LX 5 % solution.

Microscopic studies of the thyroid gland of animals in 21-30 days after experimental thermal injury under the conditions of a seven-day injection of colloidal hyperosmolar HAES-LX 5 % solution for its correction showed that the histostructure of the organ is close to the normal state. No signs of connective tissue edema were recorded in the stromal component, and the vessels of the capsule and interlobular trabeculae corresponded to their

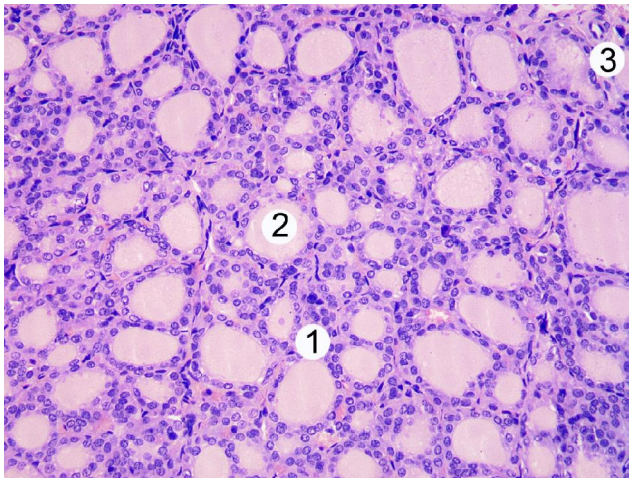

Fig. 5. Microscopic changes in the thyroid gland of an animal in 30 days after experimental thermal skin injury under the conditions of HAES-LX 5 % solution use. Hematoxylin-eosin staining. Magnification x200. 1 - thyrocytes, 2 - colloid, 3 - arteriole.

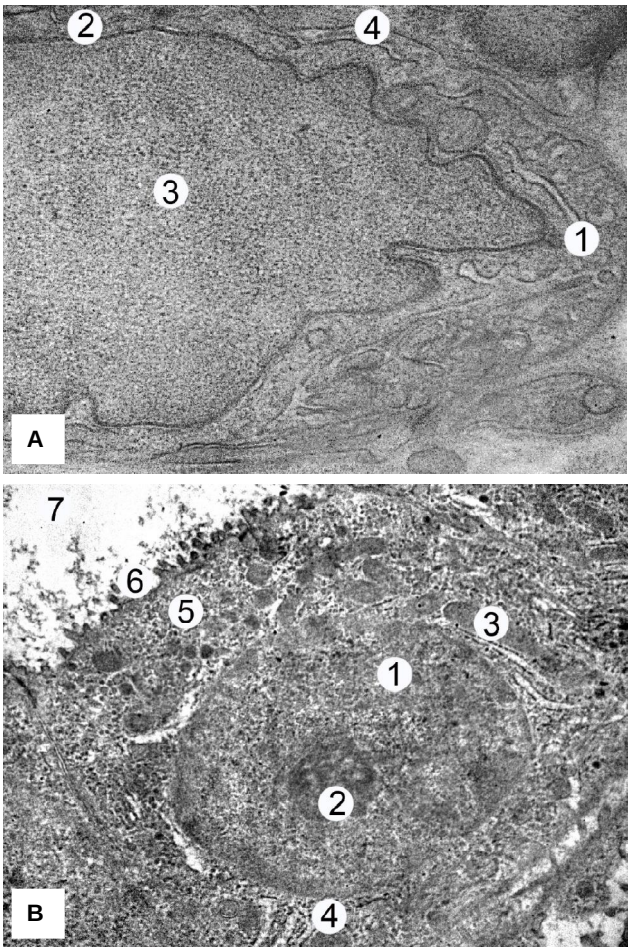

Fig. 6. Submicroscopic changes in the hemocapillary of the thyroid gland of an animal (fragment A) and thyrocytes of the thyroid gland (fragment B) in 21 days and 30 days, respectively, after experimental thermal skin injury under the conditions of HAES-LX 5 % solution use. **A**: 1 - organelle zone of endotheliocyte cytoplasm, 2 - peripheral zone of endotheliocyte cytoplasm, 3 - capillary lumen, 4 - basement membrane. Electronogram. Magnification x12000. **B**: 1 - nucleus and 2 - nucleolus of thyrocyte, 3 - mitochondrion, 4 - tubules of granular endoplasmic reticulum, 5 - microvesicles, 6 - apical surface with microvilli, 7 - colloid. Electronogram. Magnification x14000.

typical morphology. The blood supply of the vascular bed of the thyroid gland is moderate. Follicles in the composition of the lobes were mostly isomorphic and lined with cuboidal epithelium. A significant number of interfollicular islands were observed (Fig. 5).

Electromicroscopic studies of the structure of hemocapillaries of the thyroid gland on 21-30 days of the experiment in the conditions of correction of thermal injury with infusions of HAES-LX 5 % solution established the integrity of the endothelial lining of the wall, the clear contouring of the cells` plasmolemma, and the moderate thickness of the basement membrane. In the peripheral zone of the cytoplasm of endotheliocytes, numerous micropinocytotic vesicles and caveolae were detected, and in the zone of organelles - well-structured general purpose organelles (Fig. 6A).

The ultrastructure of thyrocytes in these terms of the experiment, under the conditions of correction of thermal injury by the introduction of HAES-LX 5% solution, corresponded to the normal state. The predominantly cubic-shaped cells contained a centrally located rounded nucleus with an osmiophilic structured nucleolus. In their cytoplasm, organelles of protein-synthesizing and energy apparatus were well developed. The apical pole was profusely filled with small microvesicles, and the plasmalemma formed numerous microvilli, which indicates the manifistation of active endocytosis of thyroglobulin and synthesis of thyroid hormones (see Fig. 6B).

Discussion

Thus, the obtained data indicate that the HAES-LX 5 % colloidal hyperosmolar solution administration within 7 days of the post-burn period to correct the thermal injury consequences has an expressed positive influence on burned animals thyroid gland histo- and ultrastructure. A significant improvement of the structural state of the stromal and parenchymal components of the organ and their relative normalization in the late period under the influence of the applied solution was established in the dynamics of the experiment. The colloidal hyperosmolar solution HAES-LX 5 % positive effects were expressed by cellular walls of the vessels and follicles dystrophic and destructive changes reduction the structural components of the organ restoration during the entire period of the study up to the 30th day of the trial.

The first signs of intraglandular environment recovery were proved to start from the 7th day of the post-burn period, and the maximally expressed HAES-LX 5 % colloidal hyperosmolar solution influence was observed from the 21st day until the end of the trial. Making parallels with the stages of burn disease classification, we note that the correction we applied showed effectiveness starting from the toxemia stage, and this positive histological dynamic lasted throughout the 30 days.

We conducted trials with thyroid gland and its microenvironment morphological state pharmacological corrections taking into account the pathogenetic mechanisms of burn disease. Our choice of HAES-LX 5 % colloidal hyperosmolar solution was due to the ineffectiveness of hypovolemia and oxygen deficiency correction by 0.9 % physiological NaCl solution introduction [19].

We believe that we have chosen a sufficiently effective compound for thyroid gland parenchyma, stroma and vascular environment thermally induced morphological disorders correction - HAES-LX 5 % colloidal hyperosmolar solution, created on the basis of HAES-LX 5 % hydroxyethylated starch, which influence on the body revealed the encouraging results in experimental [12] and clinical conditions [16]. HAES-LX 5 % colloidal-hyperosmolar solution (Institute of Blood Pathology and

Transfusion Medicine of the National Academy of Medical Sciences of Ukraine) contains as a colloid base poly (0-2-hydroxyethyl) starch - 5 %, as well as xylitol - 5 %, sodium lactate - 1.5 %, sodium chloride - 0.8 %, potassium chloride - 0.03 %, calcium chloride - 0.02 %, magnesium chloride - 0.01 %. The drug has a multiionic composition: Na^+ - 270.7 mmol/l, K^+ - 4.0 mmol/l, Ca^{2+} - 1.8 mmol/l, Mg^{2+} - 1.1 mmol/l, Cl^- - 146.6 mmol/l, $CH_3CH(OH)COO^-$ - 133.8 mmol/l [11].

Both small intestine and thymus morphological structure case of a burn injury were shown to be restored under the influence of HAES-LX 5 % colloidal-hyperosmolar solution [2, 4]. Stimulation of thymus cells synthetic processes according to the main indicators of the cellular cycle were proved under the influence of this drug in burn injury conditions [1]. Also in the studies of Gunas I.V. et al. [6] it was found that the administration of HAES-LX-5% solution for 7 days in rats after a burn injury of the skin reduces pathological changes in the stroma and parenchyma of the lungs in the early period of burn disease.

Our experiments on HAES-LX 5 % colloidal hyperosmolar solution use together with lactoprotein with sorbitol hyperosmolar solution as corrective compounds in case of thyroid gland burning, which are currently ongoing, highlight a practically comparable profile of their protective action in terms of thyroid morphological changes normalization, pituitary gland, thyroid gland, parathyroid gland and adrenal glands hormonal activity recovery as well as in the aspect of lipoperoxidation inhibition in the tissue of the thyroid gland, pancreas and liver.

An important aspect of this work and the obtained data analysis we consider not only to receive the array of encouraging pathomorphological results, but also to establish the mechanism of positive/protective effect of the applied colloid-hyperosmolar solution realization under the conditions of thyroid gland and the whole body burning. Taking into account the applied solution multicomponent ionic composition and the complete predominance of catabolic and necrotic processes in the post-burn period dynamics, we consider the inhibition of the generalized catabolic reaction to be one of the mechanisms of HAES-LX 5 % colloidal hyperosmolar solution protective effect. In this case, the efficacy of the applied solution we suppose to be identical to the membrane-protective effect.

The proven thyroid gland structure almost complete cytomorphological restoration within 30 days of the post-burn period is not final, given the thermal factor powerful alterating effect, which is why we assume the implementation of self-sustaining functional cellular activity under the influence of the HAES-LX 5 % solution. This type of activity lasts for 30 days. We believe that under these conditions a complex of protective, adaptive, adaptive, compensatory and regenerative effects are realized, the total efficacy of which exceeds destructive, decompensatory and necrotic changes within the thyroid gland parenchyma and surrounding tissues. This probably occurs due to the excessive permeability restoration of histo-hematic barrier, which functional breakdown occurs under the investigated pathological conditions [17, 18].

Abovementioned speculations cannot fully explain the 30-day long-term protective effect of HAES-LX 5 % colloidal hyperosmolar solution use in conditions of thyroid gland thermal damage. Therefore, upon ascertaining the fact of the thyroid gland follicles and the vascular component integrity histological and ultrastructural signs restoration, we stress the necessity of experiments continuation aimed at HAES-LX 5 % colloidal hyperosmolar solution protective effects mechanisms implementation in case of thyroid gland burning.

The obtained data analysis allows recommending the HAES-LX 5 % colloidal hyperosmolar solution use as one of the components of the burn treatment regimen as a restorative therapy drug, secondary cytoprotection aimed at restoring the integrity of the vascular wall and tissue defects.

Conclusions

1. Colloidal hyperosmolar solution HAES-LX 5 % administration within 7 days of the post-burn period to correct the thermal injury effects has an expressed positive effect on burned animals thyroid gland histo- and ultrastructure.

2. A significant improvement of the structural state of the stromal and parenchymal components of the organ and their relative normalization in the late period under the influence of the applied solution was established in the dynamics of the experiment.

3. The colloidal hyperosmolar solution HAES-LX 5 % positive effects were expressed by cellular walls of the vessels and follicles dystrophic and destructive changes reduction the structural components of the organ restoration during the entire period of the study up to the 30th day of the trial.

4. The first signs of the intraglandular environment recovery after colloidal hyperosmolar solution HAES-LX 5 % use were proved to start registered from the 7th day of the post-burn period and were maximally expressed from the 21st day until the end of the experiment.

5. Colloidal hyperosmolar HAES-LX 5 % solution protective action possible mechanism is the generalized catabolic reaction inhibition and the membrane-protective effect development.

6. A complex of colloidal hyperosmolar solution HAES-LX 5 % protective, adaptive, adaptive, compensatory and regenerative effects were realized throughout the 30 days of the post-burn period, which efficacy exceeds the thyroid gland parenchyma and surrounding tissues destructive, decompensatory and necrotic changes.

7. Colloidal hyperosmolar solution HAES-LX 5 % use seems to be one of the burn treatment regimen components as a restorative therapy drug and secondary cytoprotection aimed at the vascular wall and tissue defects integrity restoring.

References

[1] Cherkasov, E. V. (2015). Клітинна смерть і клітинний цикл в тимусі при експериментальній опіковій хворобі у щурів в умовах її лікування інфузією комбінованих гіперосмолярних розчинів [Cell death and cell cycle in the thymus during experimental burn disease in rats under the conditions of its treatment by infusion of combined hyperosmolar solutions]. *Український науково-медичний молодіжний журнал - Ukrainian scientific and medical youth magazine*, (2), 68-75.

[2] Cherkasov, V. G., Dzevulska, I. V., Cherkasov, E. V., Kaminsky, R. F., Pastukhova, V. A., Kovalchuk, O. I., & Trofimenko, Yu. Yu. (2017). Influence of HAES-LX-5 % infusion solution on the DNA content of endocrine glands cells against the background of thermal burn of skin in rats. *Світ медицини та біології - World of Medicine and Biology,* 4(62), 168-173. doi: 10.26724/2079-8334-2017-4-62-168-173

[3] Chernyakova, H. M., Minukhin, V. V., & Voronin, Ye. P. (2016). Сучасний погляд на місцеве лікування опіків з інфекційною складовою [A modern view of the local treatment of burns with an infectious component]. *Вісник проблем біології і медицини - Herald of problems of biology and medicine,* 4(133), 68-72.

[4] Gavryluk, A. O., Galunko, G. M., Chereshniuk, I. L., Tikholaz, V. O., Cherkasov, E. V., Dzevulska, I. V., & Kovalchuk, O. I. (2018). Indicators cell cycle and DNA fragmentation in cells of small intestine mucosa 14, 21 and 30 days after skin burns on the background of preliminary infusion of solution lactoprotein with sorbitol or HAES-LX 5 %. *Світ медицини та біології - World of Medicine and Biology,* 1(63), 104-108. doi: 10.26724/2079-8334-2017-4-62-104-108

[5] Gunas, I., Dovgan, I., & Masur, O. (1997). *Method of thermal burn trauma correction by means of cryoinfluence. Abstracts are presented in zusammen mit der Polish Anatomical Society with the participation of the Association des Anatomistes Verhandlungen der Anatomischen Gesellschaft, Olsztyn*. Jena - Munchen : Der Urban & Fischer Verlag, 105.

[6] Gunas, I. V., Yakovleva, O. O., & Ocheretniuk, A. O. (2012). Корекція гістологічних змін в легенях щурів при застосуванні інфузійного розчину HAES-LX-5% в перші 7 діб після опіку шкіри [Correction of histological changes in rats' lungs with HAES-LX-5% infusion solution usage in the period of 7 days after skin burn]. Світ медицини та біології - World of Medicine and Biology, 8(4), 73-76.

[7] Hamblin, M. R. (2019). Novel pharmacotherapy for burn wounds: what are the advancements. *Expert Opin Pharmacother,* 20(3), 305-321. doi: 10.1080/14656566.2018.1551880

[8] Horalskyi, L. P., Khomych, V. T., & Kononskyi, O. I. (2019) *Основи гістологічної техніки і морфофункціональні методи досліджень у нормі та при патології [Basics of histological technique and morphofunctional research methods in normal and pathological conditions].* Житомир : ЖНАЕУ - Zhytomyr: ZhNAEU, 286.

[9] Jeschke, M. G., Gauglitz, G. G., Kulp, G. A., Finnerty, C. C., Williams, F. N., Kraft, R., … & Herndon, D. N. (2011). Long-Term Persistance of the Pathophysiologic Response to Severe Burn Injury. *PLoS One,* 6(7), e21245. doi: 10.1371/journal.pone.0021245

[10] Jeschke, M. G., van Baar, M. E., Choudhry, M. A., Chung, K. K., Gibran, N. S., & Logsetty, S. (2020). Burn injury. *Nat Rev Dis Primers*, 6(1), 11. doi: 10.1038/s41572-020-0145-5

[11] Kondratskyi, B. O., Novak, V. L., & Kondratskyi, Ya. B. (2011). Комплексний колоїдно-гіперосмолярний інфузійний препарат [Complex colloid-hyperosmolar infusion preparation]. Патент України №93776 - Patent of Ukraine N 93776. Бюл. № 5 - Byul N5, 12.

[12] Maievskyi, O. Ye., Mironov, Ye. V., Bobruk, S. V., & Gunas, I. V. (2018). Dynamics of histochemical changes in the skin of rats within a month after the burning of II-III degrees on the background of the injection first 7 days HAES-LX-5% solution. *Світ медицини та біології - World of Medicine and Biology,* 4(66), 180-184. doi: 10.26724/2079-8334-2018-4-66-180-184

[13] Mehta, K., Arega, H., Smith, N. L., Li, K., Gause, E., Lee, J., & Stewart, B. (2022). Gender-based disparities in burn injuries, care and outcomes: A World Health Organization (WHO) Global Burn Registry cohort study. *Am J Surg,* 223(1), 157-163. doi: 10.1016/j.amjsurg.2021.07.041

[14] Opriessnig, E., Luze, H., Smolle, C., Draschl, A., Zrim, R., Giretzlehner, M., … & Nischwitz, S. P. (2023). Epidemiology of burn injury and the ideal dressing in global burn care - Regional differences explored. *Burns,* 49(1), 1-14. doi: 10.1016/j.burns.2022.06.018

[15] Sawicka-Gutaj, N., Zawalna, N., Gut, P., & Ruchala, M. (2022). Relationship between thyroid hormones and central nervous system metabolism in physiological and pathological conditions. *Pharmacol Rep,* 74(5), 847-858. doi: 10.1007/s43440-022-00377

[16] Semenenko, A. I., Khrebtii, H. I., Malyk, S. L., Dmytriiev, D. V., Bodnar, R. Y., Zheliba, L. M., … & Alsalama, M. W. O. (2020). Influence of different qualitative composition of infusion solutions on cerebral hemodynamics in patients with acute ischemic stroke. *Wiad Lek,* 73(2), 272-277. doi: 10.36740/WLek202002112

[17] Smolle, C., Cambiaso-Daniel, J., Forbes, A. A., Wurzer, P., Hundeshagen, G., Branski, L. K., … & Kamolz, L. P. (2017). Recent trends in burn epidemiology worldwide: A systematic review. *Burns,* 43(2), 249-257. doi: 10.1016/j.burns.2016.08.013

[18] Stanojcic, M., Abdullahi, A., Rehou, S., Parousis, A., & Jeschke, M. G. (2018). Pathophysiological Response to Burn Injury in Adults. *Ann Surg,* 267, 576-584. doi: 10.1097/SLA.0000000000002097

[19] Wang, Y., Beekman, J., Hew, H., Jackson, S., Issler-Fishe, A., Parungao, R., … & Maitzet, P. K. M. (2018). Burn injury: challenges and advances in burn wound healing, infection, pain and scarring. *Adv Drug Deliv Rev,* 123, 3-17. doi: 10.1016/j.addr.2017.09.018

[20] Zarutskyi, Ya. L., & Bilyi, I. Ya. (2018). *Воєнно-польова хірургія [Military field surgery].* Київ : ФЕНІКС - Kyiv: PHOENIX, 544.

ГІСТОЛОГІЧНІ ТА УЛЬТРАСТРУКТУРНІ ЗМІНИ ЩИТОПОДІБНОЇ ЗАЛОЗИ ЩУРІВ В ДИНАМІЦІ ЕКСПЕРИМЕНТАЛЬНОЇ ТЕРМІЧНОЇ ТРАВМИ ПРИ ВВЕДЕННІ КОЛОЇДНО-ГІПЕРОСМОЛЯРНОГО РОЗЧИНУ HAES-LX 5 %

Тірон О. І., Вастьянов Р. С.

Актуальність проблеми опікової травми визначається частими термічними ураженнями різних вікових контингентів пацієнтів, складністю та тривалістю лікування, довготривалою втратою працездатності та порівняно високою летальністю. Залежно від площі та глибини ураження, опікова рана викликає множинні й тривалі порушення гомеостазу, які спричиняють дисфункції органів і систем. Нас зацікавили зміни, що виникають при термічному опіку, в щитоподібній залозі,

оскільки їй відводиться одна з провідних ролей в ендокринній регуляції більшості функцій організму. При дослідженні питання фармакологічної корекції ураження щитоподібної залози після опікової травми ми виходимо із класичної фундаментальної концепції стосовно її патогенетичної обґрунтованості. Зважаючи на відомі патогенетичні механізми опікової хвороби з послідовними (а інколи - із одночасними) проявами гіпопротеїнемії, гемоконцентрації, формуванням інтоксикаційного синдрому, запальної та аутоімунної реакції, ми дійшли висновку стосовно доцільності тестування колоїдних розчинів з намаганнями фармакокорекції індукованих термічним подразненням структури та функції щитоподібної залози. Мета роботи - встановлення гістологічних та ультраструктурних змін щитоподібної залози щурів, яким в динаміці термічного ураження шкіри вводили колоїдно-гіперосмолярний розчин HAES-LX 5 %. Експериментальні дослідження проводили на 90 білих щурах-самцях. Термічні опіки шкіри моделювали шляхом притискання чотирьох мідних пластин до завчасно депільованих бокових поверхонь тіла щурів протягом 10 с. Протягом перших 7 діб післяопікового періоду щурам у нижню порожнисту вену вводили колоїдно-гіперосмолярний розчин HAES-LX 5 %. Шматочки щитоподібної залози фіксували в 10 % нейтральному розчині формаліну, проводили дегідратацію в спиртах зростаючої концентрації, заливали у парафінові блоки. Виготовлені зрізи, товщиною 5-6 мкм, забарвлювали гематоксиліном-еозином. Для електронномікроскопічних досліджень вилучали шматочки щитоподібної залози, фіксували їх у 2,5 % розчині глютаральдегіду, постфіксували 1 % розчином тетраокису осмію на фосфатному буфері. Напівтонкі зрізи забарвлювали метиленовим синім. Ультратонкі зрізи контрастували уранілацетатом, цитратом свинцю згідно методу Рейнольдса та вивчали в електронному мікроскопі ПЕМ-125К. Введення протягом 7 діб післяопікового періоду колоїдно-гіперосмолярного розчину HAES-LX 5 % для корекції наслідків термічної травми спричиняє виражений позитивний ефект на гісто- та ультраструктуру щитоподібної залози обпечених тварин. В динаміці досліду встановлено суттєве покращення структурного стану стромального та паренхіматозного компонентів органу та їх відносну нормалізацію у пізні терміни під впливом застосованого розчину. Позитивні ефекти застосування колоїдно-гіперосмолярного розчину HAES-LX 5 % були виражені зменшенням дистрофічних і деструктивних змін клітин стінок судин та стінки фолікулів у період інфузій з відновленням та нормалізацією морфології структурних компонентів органу протягом всього терміну дослідження до 30-ї доби досліду. Доведено, що перші ознаки відновлення внутрішньозалозистого оточення виникають, починаючи з 7-ї доби післяопікового періоду, а максимально виражений проективний ефект від застосування колоїдно-гіперосмолярного розчину HAES-LX 5 % спостерігався, починаючи з 21-ї доби і до кінця досліду. Ймовірним механізмом реалізації захисної дії колоїдно-гіперосмолярного розчину HAES-LX 5 % є гальмування генералізованої катаболічної реакції та розвиток мембранопротекторного ефекту. Протягом 30 діб післяопікового періоду реалізується комплекс захисних, адаптаційних, пристосувальних, компенсаторних та регенераторних ефектів колоїдно-гіперосмолярного розчину HAES-LX 5 %, ефективність яких перевищує деструктивні, декомпенсаторні та некротичні зміни в паренхімі щитоподібної залози та оточуючих тканинах. Застосування колоїдно-гіперосмолярного розчину HAES-LX 5 % доцільно як одного із компонентів схеми лікування при опіках в якості препарату відновлювальної терапії, вторинної цитопротекції, спрямованої на відновлення цілісності судинної стінки та дефектів тканин.

Ключові слова: *щитоподібна залоза, термічний опік, післяопіковий період, морфологічні зміни, ультраструктурні зміни, колоїдно-гіперосмолярний розчин HAES-LX 5 %, відновлювальні процеси, патогенетично обумовлена фармакологічна корекція.*

Author's contribution

Tiron O. I.: conceptualization, research, methodology and writing of the original draft, formal analysis and validation, data visualization, resources.

Vastyanov R. S.: conceptualization, review writing and editing, supervision, project administration.

DOI: 10.31393/morphology-journal-2023-29(4)-07 Reports of Morphology, Vol. 29, №4, Pages 50-57

ISSN 1818-1295 eISSN 2616-6194

REPORTS OF MORPHOLOGY

Official Journal of the Scientific Society of Anatomists, Histologists, Embryologists and Topographic Anatomists of Ukraine

journal homepage: https://morphology-journal.com

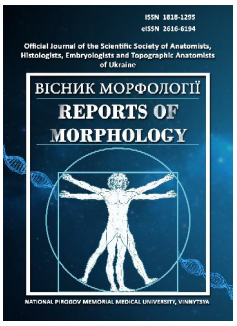

A comprehensive study of dura mater biomineralization: morphological, crystallographic, and immunohistochemical aspects

Denysenko A. P.[1], Piddubnyi A. M.[2], Tkachenko I. A.[2], Shubin P. A.[2], Tarabarov S. I.[3], Moskalenko R. A.[1]

[1]Sumy State University, Sumy, Ukraine
[2]Umea University, Umea, Sweden
[3]Sumy Regional War Veterans Clinical Hospital, Sumy, Ukraine

ARTICLE INFO

Received: 24 July 2023
Accepted: 4 October 2023

UDC: 616.831.9-003.84-076

CORRESPONDING AUTHOR

e-mail: r.moskalenko@med.sumdu.edu.ua
Moskalenko R. A.

CONFLICT OF INTEREST

The authors have no conflicts of interest to declare.

FUNDING

This research has been performed with the financial support of grants of the Ministry of Education and Science of Ukraine № 0112U100471 "Condition of mineralized tissues using new composites with Ag+ and Cu2+ nanoparticles".

DATA SHARING

Data are available upon reasonable request to corresponding author.

Biomineralization is a process of formation of biominerals widespread among living organisms. This phenomenon occurs in the central nervous system in normal and pathological conditions. Typically, this can manifest age-related changes, and the prevalence of biominerals increases with age. At the same time, it can be a sign of pathology - tumour growth, dystrophy, metabolic disorders, etc. This work aims to study the morphological features of the dura mater with signs of biomineralization. In this work, we examined 30 samples of the dura mater with signs of biomineralization (group I) and 30 samples without these signs (group II) obtained during autopsies in the pathology department of the Sumy Regional Clinical Hospital. For the morphological characteristics of the dura mater, we used histological, histochemical and immunohistochemical methods, as well as scanning electron microscopy. Statistical processing of the results of the immunohistochemical study was carried out in the GraphPad Prism 8.0 statistical package using parametric and non-parametric research methods. To divide the samples into groups, we relied on the histological method - staining with hematoxylin-eosin. Histochemical methods (alizarin red staining, von Koss method) confirmed the presence of calcium compounds in the studied group. Van Gieson staining visualized the collagen fibres of the dura mater, and the PAS reaction did not reveal the presence of glycosaminoglycans in the mineral deposits. Immunohistochemical examination of the dura mater with antibodies against osteopontin revealed a significant difference between the study and control groups ($p<0.001$), confirming the critical role of osteopontin in the biomineralization process in this tissue. With the help of scanning electron microscopy, it was found that biominerals in the dura mater are represented by tens to hundreds of formations of various shapes (rounded, oval and irregular), varying from tens of nanometers to 50 micrometres. Their composition was analyzed using maps and spectra of energy-dispersive X-ray spectroscopy and most probably corresponded to calcium hydroxyapatite. So, the dura mater is characterized by biomineralization, manifested by the formation of microscopic calcium hydroxyapatite composites.

Keywords: *calcification, dura mater, osteopontin, calcium hydroxyapatite, histology, histochemistry, scanning electron microscopy with energy dispersive X-ray spectroscopy.*

Introduction

Biomineralization is a process of formation of biominerals widespread among living organisms. Pathological biomineralization refers to the deposition of calcium compounds outside the tissues of the skeleton and teeth [12].

Biomineralization of the dura mater is observed in 12.5 % of the population, mainly in men with an average age of 53 years. Moreover, in more than 75 % of cases, biomineralization of the vascular plexus is simultaneously observed [25]. Most often, calcifications are localized in the sickle of the brain (26.8 %), the petrocline ligament (13.2 %) and the tent of the cerebellum (6.8 %) [11].

In children, biomineralization of the dura mater is extremely rare (less than 1 % among patients examined by

CT) and is more often localized in the tent of the cerebellum. Moreover, in each case, there was a history of craniotomy, craniocerebral injury or headache [24].

The phenomenon of calcification is also characteristic of tumours of the dura mater - meningiomas. They usually have an expansive nature of growth and are considered histologically benign [14]. Calcifications are found in 20-25 % of meningiomas, but since they are often found in meninges, the problem of differential diagnosis between relatively "normal" tissue of meninges and calcified meningiomas arises [1, 16].

There is no unequivocal opinion about the mechanism and significance of meningioma calcification. Perhaps it is related to the process of tumour cell degeneration and serves as a barrier against the further spread of the tumour [8].

After neurosurgical interventions for the removal of tumours, traumatic brain damage or other reasons, it is necessary to reconstruct the dura mater to minimize the risks of complications: fistulas, infections, brain keels, scars and adhesions [4, 13].

There is data on autografts, for example, temporal fascia. This method has advantages: ease of material processing, price and good biocompatibility. However, the autograft cannot be used when the size of the defect is significant; this method requires an additional operation and creates a risk of complications at the removal site [2, 6].

The use of homografts today is not a good option due to the risks of prion infection transmission [9, 21].

A promising solution is using synthetic materials, including nanomaterials, to create an artificial dura mater. Obstacles can be insufficient biocompatibility or neurotoxicity, so these materials require detailed study before possible use [5, 17, 19, 23].

Therefore, the study of the morphological features of the biomineralization of the dura mater can create a basis for the development of new models of artificial dura mater and can also contribute to improving the diagnosis of tumours of the meninges and the central nervous system.

This work aims to study the morphological features of the dura mater with signs of biomineralization.

Materials and methods

Protocol of the Ethics Commission

This study was approved by the Commission on compliance with bioethics in conducting experimental and clinical research at the Academic and Research Medical Institute of Sumy State University (protocol № 2/12 dated December 8, 2022). All studies used the Declaration of Helsinki (6th edition, revised 2008, Seoul) and the Universal Declaration of Bioethics and Human Rights (2006).

Sample collection

The research was conducted on tissues obtained during autopsies in the pathology department of the Sumy Regional Clinical Hospital (Sumy, Ukraine). 30 samples of dura mater with signs of biomineralization (group I) and 30 samples without these signs (group II) were examined. Group I contained 15 samples from female patients and 15 from male patients. Group II included 14 samples from female patients and 16 samples from male patients. To detect pathological biomineralization, the tissue of the dura mater was examined using histological, histochemical, and immunohistochemical methods and scanning electron microscopy with energy-dispersive X-ray spectroscopy.

Histological examination (hematoxylin-eosin staining)

We removed dura mater samples from the falx cerebri area and fixed them in a 10% buffered formalin solution (CAS № 50-00-0) for 24 hours. After that, we cut out strips measuring 2.0 x 0.5 x 0.1 cm, dehydrated and embedded in paraffin in the ATM-4M carousel-type apparatus (Ukraine). Paraffin blocks were cut at a thickness of 7 microns using a Shandon Finesse 325 rotary microscope (Thermo Scientific, Waltham, MA, USA). After that, the paraffin sections were stained with hematoxylin-eosin. All photos were taken using a Zeiss Primo Star microscope with a Zeiss Axiocam ERc 5s camera and "Zen 2.0" software (Carl Zeiss, Jena, Germany).

Based on the results of the histological examination, we divided the dura mater samples into two groups (30 samples each): with signs of biomineralization (group I) and without them (group II).

Histochemical study by the von Kossa method

Staining of dura mater samples by the von Koss method began with deparaffinization (twice for 5 min in a solution of xylene (CAS № 95-47-6)) and dehydration (twice for 5 min in a solution of 96 % ethanol (CAS № 64-17-5), 10 min in a solution of 70 % ethanol (CAS № 64-17-5)) to distilled water. Then, the samples were placed in a beaker with a 5 % solution of silver nitrate (CAS № 7761-88-8) under intense illumination (in front of a 60-watt lamp, having previously wrapped the beaker in foil) for 1 hour. To remove silver nitrate residues, the samples were washed three times with distilled water and placed in a sodium thiosulfate solution (CAS № 10102-17-7) for 5 min. The samples were washed with tap and distilled water. The samples were then stained in a 0.1 % solution of nuclear fast red (CAS № 6409-77-4) for 5 min. The samples were washed with tap and distilled water. Dehydration, clarification, and synthetic coating were then performed.

Histochemical study with alizarin red S (Dahl-McGee modification)

Staining of dura mater samples with alizarin red S began with deparaffinization (twice for 5 min in a solution of xylene (CAS № 95-47-6)) and dehydration (twice for 5 min in a solution of 96 % ethanol (CAS № 64-17-5), 10 min in a solution of 70 % ethanol (CAS № 64-17-5)) to distilled water. Then, the samples were stained for 2 min with a solution of alizarin red S. To prepare the solution, 0.5 g of alizarin red S (CAS № 130-22-3) was dissolved in 45 ml of distilled water, and the pH was adjusted to 6.3-6.5 for 10 % NH_4OH solution (CAS № 1336-21-6). The samples were then

rinsed with distilled water for 5-10 sec and treated with acidified ethanol (CAS № 7647-01-0) for 15 sec. Dehydration, clarification, and synthetic coating were then performed.

Histochemical study by the Van Gieson method

Staining of dura mater samples by the Van Gieson method began with deparaffinization (twice for 5 min in a solution of xylene (CAS № 95-47-6)) and dehydration (twice for 5 min in a solution of 96 % ethanol (CAS № 64-17-5), 10 min in a solution of 70 % ethanol (CAS № 64-17-5)) to distilled water. Then Weigert's hematoxylin (50 drops of Weigert's solution I per 25 drops of Weigert's solution II) was dripped onto the samples. Weigert's solution I is a mixture of 1 g of hematoxylin (CAS № 517-28-2) and 100 ml of 96 % ethanol (CAS № 64-17-5). Weigert solution II is a mixture of 4 ml of ferric chloride (CAS № 7705-08-0), 1 ml of concentrated HCl (CAS № 7647-01-0), and 95 ml of distilled water. Then the samples were washed in 2 portions of water and treated with a solution of acidified ethanol (CAS № 7647-01-0) until the background became clear. Then a solution of picrofuchsin (a mixture of 10 ml of a saturated aqueous solution of picric acid (CAS № 88-89-1) with 1 ml of a 1 % aqueous solution of acid fuchsin (CAS № 3244-88-0)) was dripped onto the samples. Dehydration, clarification, and synthetic coating were then performed.

Histochemical study by PAS reaction method

The PAS method started with the preparation of Schiff's reagent. For this, 1 g of basic fuchsin (CAS № 569-61-9) was added to 200 ml of boiling distilled water and boiled for 5 min with constant stirring. Then the solution could cool to 60-70 °C and filtered through a paper filter. Then the solution could cool to 50 °C. 20 ml of 1 N hydrochloric acids (mixture of 16.4 ml of concentrated HCl (CAS № 7647-01-0) and 3.6 ml of distilled water) was added and allowed to cool to 20-25 °C. Then 1 g of sodium bisulfite (CAS № 7631-90-5) was added. The solution is stored for the first three days in a dark place at room temperature, then in the refrigerator.

Staining of dura mater samples by the PAS reaction method began with deparaffinization (twice for 5 min in a solution of xylene (CAS № 95-47-6)) and dehydration (twice for 5 min in a solution of 96 % ethanol (CAS № 64-17-5), 10 min in a solution of 70 % ethanol (CAS № 64-17-5)) to distilled water.

Then the dura mater samples were dewaxed to distilled water. The samples were then treated with a 1 % solution of periodic acid (CAS № 10450-60-9) for 10 min at room temperature in the dark. The samples were washed in tap water (5 min) and distilled water (2 min). Then cold Schiff's reagent was dripped onto the samples for up to 10 min at room temperature and under light illumination until they turned pink. The samples were washed in tap water (several times until the water turned red) and distilled water (2 min). After that, the samples were stained with a hematoxylin solution (CAS № 517-28-2) for 4 minutes. The samples were washed twice in tap water. Dehydration, clarification, and synthetic coating were then performed.

Immunohistochemical study with antibodies against osteopontin

Serial sections of dura mater tissue with a thickness of 3-4 microns, made from prepared histological paraffin blocks, were applied to SuperFrost adhesive slides (Thermo Scientific) and dried at 37 °C for 18 hours. Deparaffinized sections were subjected to unmasking of antigens by the thermal method by heating the sections in a citrate buffer (pH 6.0) at a 95-98 °C. To visualize the results of an immunohistochemical (IGH) study, the detection system "UltraVision Quanto Detection System HRP Polymer" (Thermo Scientific) was used, which involved blocking endogenous peroxidase activity with 3 % hydrogen peroxide, blocking non-specific background staining using "Ultra V Block", enhancing the reaction "Primary Antibody Amplifier Quanto". Diaminobenzidine (DAB) was used as a chromogen. Antibodies against osteopontin - OPN (Thermo Fisher Scientific, PA5-34579, dilution 1:300) were used. Active (use of tissue, with a predetermined positive and negative reaction) and passive control of the obtained results were carried out as quality control of the conducted IHC research.

Scanning electron microscopy (SEM) with energy-dispersive X-ray spectroscopy (EDX)

Histological sections with a thickness of 10-12 microns were made from paraffin blocks of dura mater tissue, which were placed on a table made of spectrally pure graphite. For maximum attachment of the biological material to the microscope stage and melting of the paraffin, the sections were kept in a thermostat at a temperature of 60 °C for 30 min. To remove paraffin, the samples were covered with xylene three times for 3-4 min, then with 96 % ethanol three times for 5-6 min and rinsed with distilled water. After that, the sample of biological material was additionally grounded with conductive tape wrapped around the stage. The prepared preparations were examined on a scanning microscope SEO-SEM Inspect S50-B (SEO, Sumy, Ukraine) with an energy dispersive spectrometer AZtecOne with an X-MaxN20 detector (Oxford Instruments plc, Abingdon, UK).

Statistical analysis

Statistical processing and graphic presentation of the statistical analysis results was performed using GraphPad Prism 8.0. The results of the immunohistochemical study were checked for normal distribution using the Shapiro-Wilk test. In the case of the non-normal distribution of digital indicators, the Mann-Whitney test was used to assess statistical significance. If the data samples had a correct distribution, they were compared using the Student's parametric t-test. The results were considered statistically significant, with a probability of more than 95 % ($p<0.05$).

Results

A total of 60 samples were examined, including 30 dura mater samples with pathological biomineralization (group I) and 30 control samples without signs of biomineral

Fig. 1. Dura mater tissue.

deposits (group II). The average age of patients in the group I was 67.00±2.33 years. When studying the distribution of patients by gender in group I, the average age of men was 61.93±3.54 years, and of women 72.07±2.49 years. The average age of patients in the group II was 62.97±3.12 years. When studying the distribution of patients by gender in group II, the average age of men was 57.81±4.45 years, and women - 68.85±3.93 years.

Histological and histochemical study

Macroscopically, it was not possible to confirm or deny the presence of biominerals in the dura mater (Fig. 1). Histologically, the tissue of the dura mater, which was removed from the area of the sickle of the brain, represented a dense connective tissue, the inner surface of which was covered with a single-layer flat epithelium. The samples were divided into two groups according to the results of histological examination (hematoxylin-eosin staining).

Group I included 30 samples of the dura mater with signs of biomineralization - small formations of various sizes and irregular shapes (Fig. 2A). These signs were not detected in the control group samples (Fig. 3A).

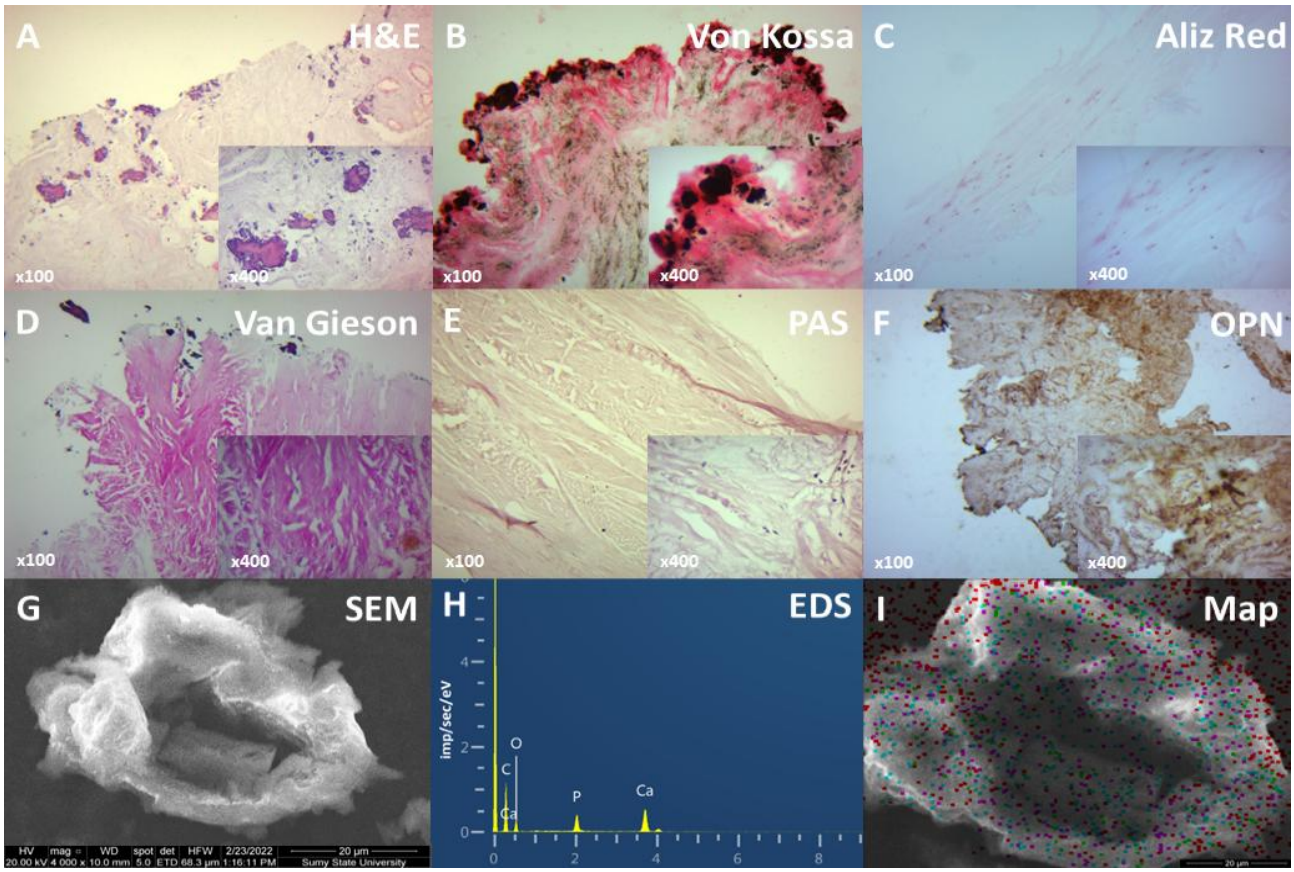

Fig. 2. Study of the tissue of the dura mater with signs of biomineralization (group I). A - histological examination of the tissue of the dura mater (hematoxylin-eosin staining). B - histochemical staining of dura mater calcifications using the von Koss method. C - histochemical staining of dura mater calcifications using the alizarin red S method. D - histochemical staining of the dura mater tissue using the Van Gieson method. E - histochemical staining of the dura mater tissue using the PAS reaction. F - immunohistochemical study of dura mater tissue with anti-osteopontin antibodies. Drawings in the insets A-F correspond to the magnified area of this drug. G - SEM of the calcified area of the dura mater. H - EDS spectrum. I - physicochemical study of group I dura mater calcifications using EDS mapping: carbon ions are marked in red, oxygen in green, calcium in blue, and phosphorus in purple.

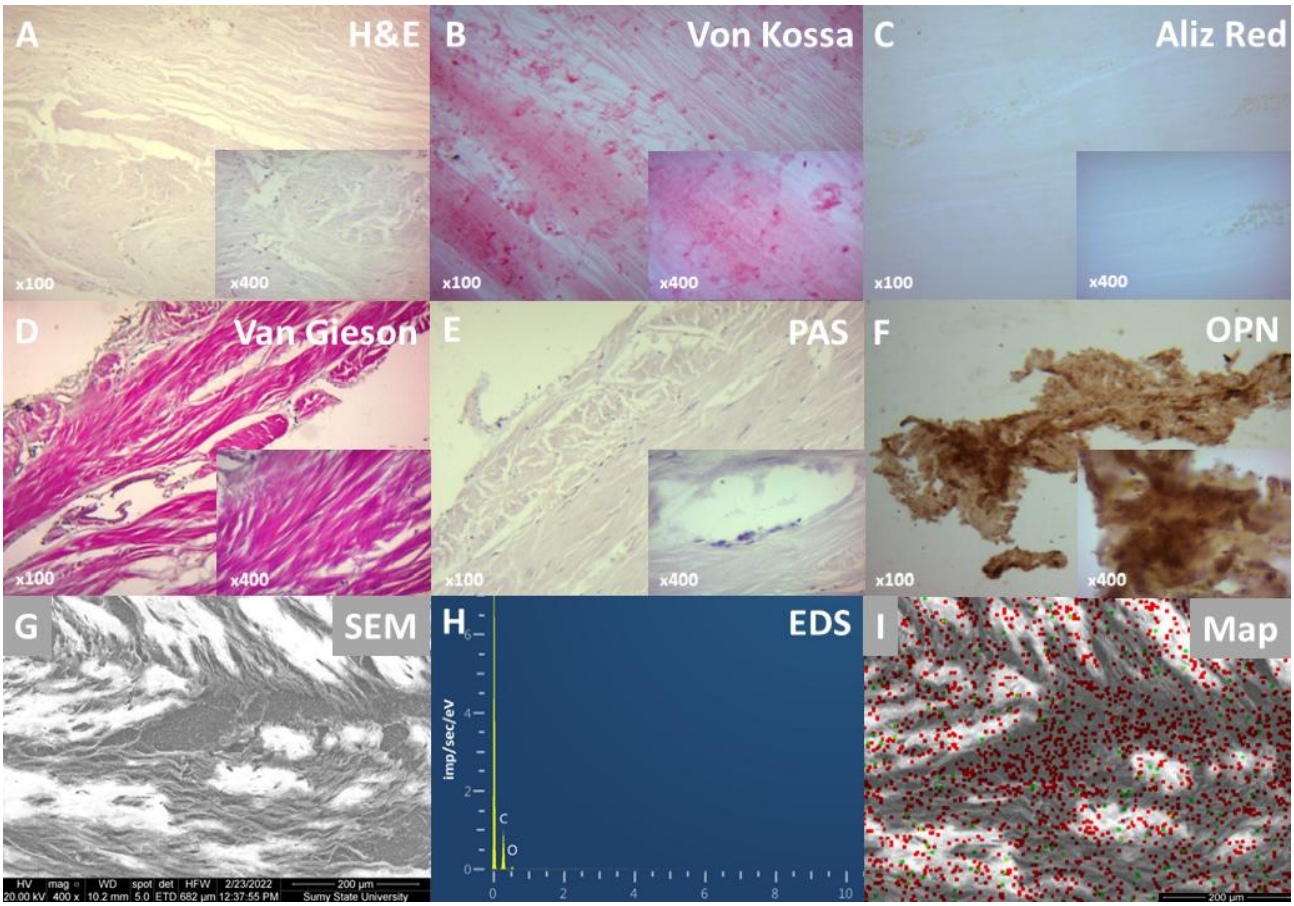

Fig. 3. Examination of the tissue of the dura mater without signs of biomineralization (group II). A - histological examination of the tissue of the dura mater (hematoxylin-eosin staining). B - histochemical staining of the dura mater using the von Koss method. C - histochemical staining of the dura mater using the alizarin red S method. D - histochemical staining of the dura mater tissue using the Van Gieson method. E - histochemical staining of the dura mater tissue using the PAS reaction. F - immunohistochemical study of dura mater tissue with anti-osteopontin antibodies. Drawings in the insets A-F correspond to the magnified area of this drug. G - SEM of the dura mater tissue. H - EDS spectrum. I - physicochemical study of the dura mater of group II using EDS mapping: carbon ions are marked in red, oxygen in green.

The result of the examination of the dura mater tissue using the von Koss method was the staining of mineral deposits in brown colour, which confirmed the presence of calcium phosphate compounds in the samples from group I (see Fig. 2B). In the control group, such staining did not occur (see Fig. 3B).

Staining of the dura mater tissue with alizarin red S confirmed the presence of calcium compounds (orange-red colour) and inorganic iron (purple colour) in the samples of group I (see Fig. 2C). In the samples of group II, we found only iron deposits (see Fig. 3C).

Staining of the dura mater tissue by the Van Gieson method showed the presence of a noticeable amount of collagen fibres (purple-red colour) in the structure of the dura mater of samples of group I (see Fig. 2D) and group II (see Fig. 3D).

Staining of the dura mater with the help of the PAS reaction showed the absence of glycosaminoglycans in the composition of mineral deposits (see Fig. 2E). In the dura mater tissue itself, single PAS-positive cells around vessels were visualized (see Fig. 3E).

Immunohistochemical study

Immunohistochemical examination of group I dura mater tissue with anti-osteopontin (OPN) antibodies showed the prominent presence of this protein (see Fig. 2F). The greatest accumulation was observed on the mineral deposits themselves and in the surrounding tissues. An increased level of background chromogen staining (DAB) was also observed. Immunohistochemical examination of the dura mater tissue of group II showed a minimal level of OPN presence in the tissues (see Fig. 3F). The presence of OPN in meningioma tissues of the control group corresponded to 15.08±1.18 cells and it was significantly less than in the studied group 25.29±2.39 cells ($p<0.001$) (Fig. 4).

Scanning electron microscopy (SEM) with energy-dispersive X-ray spectroscopy (EDX)

SEM examination of the dura mater tissue of group I

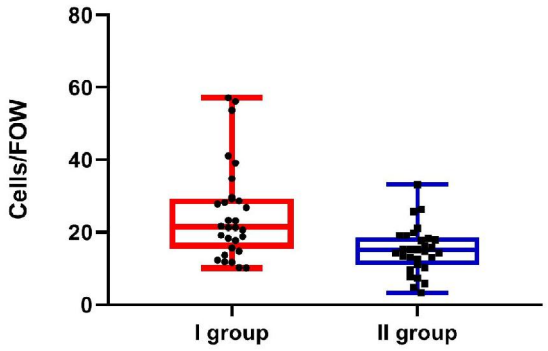

Fig. 4. Results of an immunohistochemical study of the dura mater with antibodies against osteopontin. I - group of samples with calcification, II - control group.

revealed that biominerals in the dura mater are represented by tens to hundreds of formations of various shapes (rounded, oval, and irregular), the sizes of which vary from tens of nanometers to 50 micrometres (see Fig. 2G).

According to the data of the element distribution maps and the Ca/P ratio obtained from the spectra (see Figs. 2H, 2I), the mineral of the dura mater deposits is calcium phosphate of apatite composition.

Scanning electron microscopy of dura mater samples of the control group did not reveal signs of biomineral deposits (see Fig. 3G). These data were also confirmed by spectra and element distribution maps (see Fig. 3H, 3I).

Discussion

Biomineralization occurs in the central nervous system in normal and pathological conditions. Normally, this can be a manifestation of age-related changes. At the same time, it can be a sign of pathology: tumour growth, dystrophy, metabolic disorders, inflammation, intoxication or congenital pathology [20].

Intracranial biominerals are common in non-contrast computed tomography (CT) in children and adults. According to the statistics of CT results, their prevalence varies from 1 % in the young population to 20 % in the elderly. According to the results of autopsies, including microscopic findings during histological examination, biominerals are found in the skull cavity in more than 70 % of patients [10].

In some patients, intracranial biominerals appear as asymptomatic findings on CT; in others, they cause various neurological and cognitive disorders of varying degrees of severity, such as tremors, convulsions, parkinsonism, dementia, psychosis, behavioural disorders, and others [7].

The phenomenon of calcification is characteristic of tumours of the dura mater - meningiomas. They are usually benign neoplasms with an expansive nature of growth. The origin of meningiomas from the dura helps to distinguish them from cancer metastases because the latter is usually intracerebral [18].

But since calcifications are often found in the meninges, the problem of differential diagnosis between relatively "normal" meningeal tissue and calcified meningiomas arises.

In this work, we investigated the dura mater with and without signs of biomineralization using histological, histochemical, and immunohistochemical methods and scanning electron microscopy with energy-dispersive X-ray spectroscopy.

During the histological examination, the samples were divided into two groups based on the presence/absence of signs of biomineralization - small formations of different sizes and irregular shapes. Histochemical methods helped us, to some extent, investigate the composition of these formations. The von Kossa method helped narrow down to calcium phosphate compounds, and alizarin red S staining helped separate iron deposits. The Van Gieson method visualized collagen fibres; the PAS reaction did not reveal glycosaminoglycans in the composition of mineral deposits.

Osteopontin (OPN) is a noncollagenous, sialic acid-rich glycosylated phosphoprotein that regulates osteoblast function during bone formation. In addition, it is also present in various tissues and plays a vital role in inflammation, immune reactions, and bone mineralization [3].

Furthermore, OPN plays an important role in the formation of several human cancers due to the regulation of apoptosis, proliferation, adhesion, migration, invasion, metastasis and angiogenesis. Although staining of OPN has been correlated positively with the development of psammoma bodies in meningiomas, its correlation with clinical recurrence of meningiomas is still largely unknown [15].

In our study, biomineralization is positively correlated with OPN overexpression. We believe a significant amount of OPN is present in connection with remodelling in the calcification process, as this acidic glycoprotein is attracted to hydroxyapatite crystals [22].

SEM data indicate that biominerals in the dura mater are represented by tens to hundreds of formations of various shapes (rounded, oval, and irregular), varying from tens of nanometers to 50 micrometres. According to the data of the element distribution maps and the Ca/P ratio obtained from the spectra, the mineral of the dura mater deposits is calcium phosphate of apatite composition. The significant oxygen content in the locations of calcified particles (according to the distribution maps) is explained by the presence of the phosphate group of apatite (PO_4).

Conclusions

1. Macroscopically, the tissue of the dura mater, which was removed from the area of the falx cerebri, was a dense tissue without visible signs of biomineralization. Histologically, the tissue of the dura mater was a dense connective tissue, the inner surface of which was covered with a single-layer flat epithelium. Some samples showed probable signs of biomineralization - small formations of various sizes and irregular shapes.

2. Histochemically, the presence of biominerals was confirmed by the von Koss method (identified calcium phosphate compounds) and alizarin red S staining (differentiated calcium compounds from iron deposits). Histochemical study of the structure of the dura mater by the Van Gieson method and PAS-reaction of groups I and II showed their similar structure (a noticeable number of collagen fibres, single PAS-positive cells around vessels).

3. Immunohistochemical examination of the dura mater with antibodies against osteopontin revealed a significant difference between the studied and control groups ($p<0.001$), which confirms the important role of osteopontin in the process of biomineralization in this tissue.

4. Scanning electron microscopy showed that biominerals in the dura mater are represented by tens to hundreds of formations of various shapes (rounded, oval and irregular), the sizes of which vary from tens of nanometers to 50 micrometres. Their composition was analyzed using maps and spectra of energy-dispersive X-ray spectroscopy and most probably corresponded to calcium hydroxyapatite.

References

[1] Adams, L. C., Böker, S. M., Bender, Y. Y., Fallenberg, E. M., Wagner, M., Buchert, R., … & Makowski, M. R. (2017). Assessment of intracranial meningioma-associated calcifications using susceptibility-weighted MRI. *Journal of Magnetic Resonance Imaging,* 46(4), 1177-1186. doi: 10.1002/jmri.25614

[2] Adeleye, A. O. (2021). Posttraumatic leptomeningeal cyst capsule as a cost-free autograft for its repair: case illustrated technical reports. *Neurosurgical Review,* 44(3), 1775-1778. doi: 10.1007/s10143-020-01364-6

[3] Arikök, A. T., Önder, E., Seçkin, H., Kaçar, A., Fesli, R., Oguz, A. S., & Alper, M. (2014). Osteopontin expressions correlate with WHO grades and predict recurrence in meningiomas. Brain Tumor Pathology, 31(2), 94-100. doi: 10.1007/s10014-013-0152-2

[4] Arima, H., Hasegawa, T., Yamato, Y., Yoshida, G., Banno, T., Oe, S., … & Matsuyama, Y. (2023). Postoperative neurological complications in intradural extramedullary tumors: A 10-year experience of a single center. Neurochirurgie, 69(5), 101476. doi: 10.1016/j.neuchi.2023.101476

[5] Aydin, H. E., Kizmazoglu, C., Kaya, I., Husemoglu, B., Sozer, G., Havitcioglu, H., & Arslantas, A. (2019). Biomechanical properties of the cranial dura mater with puncture defects: An In Vitro study. *Journal of Korean Neurosurgical Society,* 62(4), 382-388. doi: 10.3340/jkns.2018.0130

[6] Balasa, A., Kunert, P., Dziedzic, T., Bielecki, M., Kujawski, S., & Marchel, A. (2021). Comparison of dural grafts and methods of graft fixation in Chiari malformation type I decompression surgery. *Scientific Reports,* 11(1), 14801. doi: 10.1038/s41598-021-94179-4

[7] Calabro, R. S., Spadaro, L., Marra, A., & Bramanti, P. (2014). Fahr's disease presenting with dementia at onset: A case report and literature review. *Behavioural Neurology,* 2014, 750975. doi: 10.1155/2014/750975

[8] Das, D. K. (2009). Psammoma body: A product of dystrophic calcification or of a biologically active process that aims at limiting the growth and spread of tumor? *Diagnostic Cytopathology,* 37(7), 534-541. doi: 10.1002/dc.21081

[9] De Pedro-Cuesta, J., Almazan-Isla, J., Tejedor-Romero, L., Ruiz-Tovar, M., Avellanal, F., Rabano, A., … & Garcia Lopez, F. J. (2021). Human prion disease surveillance in Spain, 1993-2018: an overview. *Prion,* 15(1), 94-106. doi: 10.1080/19336896.2021.1933873

[10] Deng, H., Zheng, W., & Jankovic, J. (2015). Genetics and molecular biology of brain calcification. *Ageing Research Reviews*, 22, 20-38. doi: 10.1016/j.arr.2015.04.004

[11] Ghorbanlou, M., Moradi, F., & Mehdizadeh, M. (2022). Frequency, shape, and estimated volume of intracranial physiologic calcification in different age groups investigated by brain computed tomography scan: a retrospective study. *Anatomy and Cell Biology,* 55(1), 63-71. doi: 10.5115/acb.21.137

[12] Giachelli, C. M. (1999). Ectopic calcification: Gathering hard facts about soft tissue mineralization. *American Journal of Pathology,* 154(3), 671-675. doi: 10.1016/S0002-9440(10)65313-8

[13] Kiyoshi, T., Yoshihiro, M., Kazuya, Y., Kazu, K., Hirokazu, S., Kenichi, K., & Yasuharu, N. (2023). Dural reconstruction following resection of ventral and lateral spinal cord meningiomas: Fenestrated Durotomy with Oversized Graft technique. *Journal of Clinical Neuroscience*, 116, 120-124. doi: 10.1016/j.jocn.2023.09.003

[14] Komori, T. (2022). [The 2021 WHO Classification of Tumors, 5th edition, Central Nervous System Tumors: A Short Review]. *Brain and Nerve = Shinkei Kenkyu No Shinpo,* 74(6), 803-809. doi: 10.11477/mf.1416202124

[15] Lin, C. K., Tsai, W. C., Lin, Y. C., & Hueng, D. Y. (2012). Osteopontin predicts the behaviour of atypical meningioma. *Histopathology,* 60(2), 320-325. doi: 10.1111/j.1365-2559.2011.04085.x

[16] Liu, L., Lu, Y., Peng, W., Geng, D., Wen, J., Xiong, J., … & Yin, B. (2017). Imaging features of intracranial psammomatous meningioma. *Journal of Neuroradiology,* 44(6), 395-399. doi: 10.1016/j.neurad.2017.06.003

[17] Ma, H., Sun, Y., Tang, Y., Shen, Y., Kan, Z., Li, Q., … & Li, Z. (2021). Robust Electrospun Nanofibers from Chemosynthetic Poly(4-hydroxybutyrate) as Artificial Dural Substitute. *Macromolecular Bioscience,* 21(7). doi: 10.1002/mabi.202100134

[18] Nagai Yamaki, V., de Souza Godoy, L. F., Alencar Bandeira, G., Tavares Lucato, L., Correa Lordelo, G., Fontoura Solla, D. J., … & Silva Paiva, W. (2021). Dural-based lesions: is it a meningioma? *Neuroradiology,* 63(8), 1215-1225. doi: 10.1007/s00234-021-02632-y

[19] Nouri, M., Schneider, J. R., Shah, K. A., Katz, J. M., & Dehdashti, A. R. (2020). Sphenoid Wing Meningioma with Surgical Revascularization of an Injured Anterior Temporal Artery. *World Neurosurgery,* 140, 192. doi: 10.1016/j.wneu.2020.04.223

[20] Saade, C., Najem, E., Asmar, K., Salman, R., Achkar, B. El., & Naffaa, L. (2019). Intracranial calcifications on CT: An updated review. *Journal of Radiology Case Reports*, 13(8), 1-18. doi: 10.3941/jrcr.v13i8.3633

[21] Sakai, K., Hamaguchi, T., Sanjo, N., Murai, H., Iwasaki, Y., Hamano, T., … & Yamada, M. (2020). Diffusion-weighted magnetic resonance imaging in dura mater graft-associated Creutzfeldt-Jakob disease. *Journal of the Neurological Sciences,* 418, 117094. doi: 10.1016/j.jns.2020.117094

[22] Steitz, S. A., Speer, M. Y., McKee, M. D., Liaw, L., Almeida, M.,

Yang, H., & Giachelli, C. M. (2002). Osteopontin inhibits mineral deposition and promotes regression of ectopic calcification. *American Journal of Pathology,* 161(6), 2035-2046. doi: 10.1016/S0002-9440(10)64482-3

[23] Wang, Y., Guo, Q., Wang, W., Wang, Y., Fang, K., Wan, Q., … & Wu, T. (2022). Potential use of bioactive nanofibrous dural substitutes with controlled release of IGF-1 for neuroprotection after traumatic brain injury. *Nanoscale,* 14(48), 18217-18230. doi: 10.1039/d2nr06081g

[24] Whitehead, M. T., Oh, C., Raju, A., & Choudhri, A. F. (2015). Physiologic pineal region, choroid plexus, and dural calcifications in the first decade of life. *American Journal of Neuroradiology,* 36(3), 575-580. doi: 10.3174/ajnr.A4153

[25] Yalcin, A., Ceylan, M., Bayraktutan, O. F., Sonkaya, A. R., & Yuce, I. (2016). Age and gender related prevalence of intracranial calcifications in CT imaging; data from 12,000 healthy subjects. *Journal of Chemical Neuroanatomy,* 78, 20-24. doi: 10.1016/j.jchemneu.2016.07.008

КОМПЛЕКСНЕ ДОСЛІДЖЕННЯ БІОМІНЕРАЛІЗАЦІЇ ТВЕРДОЇ МОЗКОВОЇ ОБОЛОНИ: МОРФОЛОГІЧНІ, КРИСТАЛОГРАФІЧНІ ТА ІМУНОГІСТОХІМІЧНІ АСПЕКТИ

Денисенко А. П., Піддубний А. М., Ткаченко І. А., Шубін П. А., Тарабаров С. І., Москаленко Р. А.

Біомінералізація - широко розповсюджений серед живих організмів процес утворення біомінералів. В центральній нервовій системі цей феномен зустрічається як в нормі, так і в патології. В нормі це може бути проявом вікових змін, причому поширеність біомінералів збільшується з віком. В той же час це може бути ознакою патології - пухлинного росту, дистрофії, порушень метаболізму та інше. Метою даною роботи є вивчення морфологічних особливостей твердої мозкової оболони з ознаками біомінералізації. В роботі досліджено 30 зразків твердої мозкової оболони з ознаками біомінералізації (група I) та 30 зразків без даних ознак (група II) отриманих під час розтинів у патологоанатомічному відділенні Сумської обласної клінічної лікарні. Для морфологічної характеристики твердої мозкової оболони застосували гістологічний, гістохімічний та імуногістохімічний методи, а також сканувальну електронну мікроскопію. Статистичну обробку результатів імуногістохімічного дослідження проведено в статистичному пакеті GraphPad Prism 8.0 з використанням параметричних і непараметричних методів дослідження. Для розподілу зразків на групи опирались на гістологічний метод - забарвлення гематоксиліном-еозином. Гістохімічні методи (забарвлення алізариновим червоним, метод фон Косса) підтвердили наявність сполук кальцію в досліджуваній групі. Забарвлення за Ван Гізоном візуалізувало колагенові волокна твердої мозкової оболони, а PAS реакція не виявила наявність глікозаміногліканів в складі мінеральних депозитів. Імуногістохімічне дослідження тканини твердої мозкової оболони антитілами проти остеопонтину виявило значну різницю між досліджуваною та контрольною групою (p<0,001), що підтверджує важливу роль остеопонтину в процесі біомінералізації в даній тканині. За допомогою сканувальної електронної мікроскопії було з'ясовано, що біомінерали в твердій мозковій оболоні представлені десятками-сотнями утворень різної форми (округлої, овальної та неправильної), розміри яких коливаються від десятків нанометрів до 50 мікрометрів. Їх склад був проаналізований за допомогою карт та спектрів енергодисперсійної рентгенівської спектроскопії та найбільш ймовірно відповідав гідроксиапатиту кальцію. Отже, для твердої мозкової оболони характерна біомінералізація, що проявляється утворенням мікроскопічних композитів з гідроксиапатиту кальцію.

Ключові слова: *кальцифікація, тверда мозкова оболона, остеопонтин, кальцію гідроксиапатит, гістологія, гістохімія, сканувальна електронна мікроскопія з енергодисперсійною рентгенівською спектроскопією.*

Author's contribution

Denysenko A. P.: research concept and design, receiving data, analysis and interpretation of data, design of the article.
Piddubnyi A. M.: analysis and interpretation of data, critical review, final approval.
Tkachenko I. A.: analysis and interpretation of data, critical review, final approval.
Shubin P. A.: analysis and interpretation of data, critical review, final approval.
Tarabarov S. I.: receiving data, analysis and interpretation of data, design of the article.
Moskalenko R. A.: research concept and design, analysis and interpretation of data, critical review, final approval.

DOI: 10.31393/morphology-journal-2023-29(4)-08 Reports of Morphology, Vol. 29, №4, Pages 58-63

ISSN 1818-1295 eISSN 2616-6194

REPORTS OF MORPHOLOGY

Official Journal of the Scientific Society of Anatomists, Histologists, Embryologists and Topographic Anatomists of Ukraine

journal homepage: https://morphology-journal.com

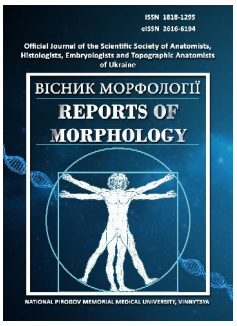

Histological changes in the liver of rats under the influence of Vipera berus berus venom

Turbal L. V.[1], Yaremenko L. M.[1], Maievskyi O. Ye.[2]

[1]Bogomolets National Medical University, Kyiv, Ukraine
[2]Educational and Scientific Center "Institute of Biology and Medicine", Taras Shevchenko National University of Kyiv, Kyiv, Ukraine

ARTICLE INFO
Received: 20 July 2023
Accepted: 6 October 2023

UDC: 61:615.9/616:616-005/616.3

CORRESPONDING AUTHOR
e-mail: ludmilaturbal@gmail.com
Turbal L. V.

CONFLICT OF INTEREST
The authors have no conflicts of interest to declare.

FUNDING
Not applicable.

DATA SHARING
Data are available upon reasonable request to corresponding author.

Animal venoms contain a whole complex of compounds, among which there are peptides, proteins, as well as other organic molecules and salts. Their toxins are able to cause pronounced disturbances in the functioning of physiological systems, leading to the appearance of pathological conditions, complications, or even death. The aim of the research is to study the histological changes in the liver of rats under the influence of Vipera berus berus venom. Experimental studies were carried out on white non-linear male rats. The animals were conditionally divided into two groups - a control and an experimental group of 10 individuals in each. Experimental rats were injected intraperitoneally with a semi-lethal dose (LD50) (1.576 mg/g-1) of Vipera berus berus venom in saline solution. Animals of the control group were injected intraperitoneally with only saline solution. Rats were removed from the experiment 24 hours after exposure to the venom, anesthetized by cervical dislocation. Liver samples of animals of all groups were taken for microscopic examination. Histological preparations of the liver were stained with hematoxylin and eosin. Histological preparations were studied using a SEO SCAN light microscope. To identify the key enzyme of the citric acid cycle - succinate dehydrogenase, histochemical studies were performed according to the Nakhlas method. To study the features of glycogen accumulation in hepatocytes, sections were stained using Schiff's reagent, after pretreatment with iodic acid (PAS reaction) in Shabadash's modification. An immunohistochemical research method was used to detect a subpopulation of CD86+ cells in the liver of experimental animals. Under the influence of Vipera berus berus venom, the development of alterative changes in the liver parenchyma and vascular disorders were microscopically revealed. The appearance of foci of leukocyte infiltration was established, which indicates the development of inflammatory processes. A histochemical study of the content of succinate dehydrogenase in the liver of animals injected with Vipera berus berus venom showed uneven activity of the mitochondrial enzyme in the lobules. A histochemical study of glycogen in hepatocytes of the liver of rats exposed to Vipera berus berus venom showed a decrease in the content of trophic inclusions. An increase in the population of CD86+ cells indicates reactive inflammatory processes observed in the body as a result of the action of components of Vipera berus berus venom.

Keywords: *vipers, liver, succinate dehydrogenase, glycolen, CD86+.*

Introduction

In the processes of evolutionary adaptation, a significant number of both invertebrates and vertebrates have acquired poisonous properties. Their venoms play numerous functions, providing adaptation, protection and necessary for hunting prey and interspecies competition. A combination of environmental, genetic, climatic and biogeographical factors over millions of years has given rise to a fascinating variety of their constituent toxic components, which have become a key feature of these animal species [3, 4, 18]. Animal venoms contain a whole complex of compounds, among which there are peptides, proteins, as well as other organic molecules and salts. Their toxins are able to cause pronounced disturbances in the functioning of physiological systems, leading to the appearance of pathological conditions, complications, or even death [5, 13, 20].

To date, the scientometric databases contain studies regarding the biological activity of certain components of the venom of snakes and vipers, the peculiarities of their tropism to tissues and organs. It has been established that their toxic substances exhibit a wide range of pathological effects in relation to most vital systems, causing damage to the lungs, heart, kidneys, skeletal muscles, etc. [6, 11, 12, 14]. However, the number of experimental works on the influence of the venom of various species of snakes and vipers on the morpho-functional changes of the liver is too limited. The fact that the liver occupies one of the main places in the detoxification processes of exogenous and endogenous toxic compounds is indisputable. In modern conditions of the world existence, the human body is in constant contact with toxicants of various origins, and the ability of the liver to quickly dispose of them determines in a certain way the ability to survive and maintain homeostasis parameters at a relatively constant level. However, during the metabolism of many xenobiotics, including animal venom toxins, irreversible changes in the features of histological organization and the course of biochemical processes in liver cells are possible, which ultimately leads to its dysfunction in general, and in severe cases to the development of toxic necrosis. Scientists assume that this condition arises as a result of the formation of toxic metabolites during detoxification, which have a detrimental effect on the molecular structures of hepatocytes, causing their death [15, 16, 17, 19].

The aim of the research is to study the histological changes in the liver of rats under the influence of Vipera berus berus venom.

Materials and methods

Experimental studies were carried out on white non-linear male rats. For preliminary acclimatization, the animals were kept for 7 days in the animal facility of Taras Shevchenko National University of Kyiv, and and then kept in laboratory conditions at constant temperature (22±3 °C), humidity (60±5 %) and light (12 h light/12 h dark cycle), being fed standard rodent food and water ad libitum [7]. All experiments were conducted in accordance with the National Institutes of Health Guidelines for the Care and Use of Laboratory Animals and the European Council Directive of November 24, 1986 for the Care and Use of Laboratory Animals (86/609/EEC). The research was approved and confirmed by the bioethics commission of the Institute of Biology and Medicine of the Taras Shevchenko National University of Kyiv (protocol № 2 dated August 19, 2021).

Vipera berus berus venom was obtained from the V. N. Karazin Kharkiv National University. The lyophilized crude venom was stored at -20 °C and then dissolved in saline solution immediately before the experiment.

The animals were conditionally divided into two groups - a control and an experimental group of 10 individuals in each. Experimental rats were injected intraperitoneally with a semi-lethal dose (LD50) (1.576 mg/g-1) of Vipera berus berus venom in saline solution. Animals of the control group were injected intraperitoneally with only saline solution. Rats were removed from the experiment 24 hours after exposure to the venom, anesthetized by cervical dislocation.

Liver samples of animals of all groups were taken for microscopic examination. The pieces were fixed in a 10 % formalin solution for 1 day. Next, the pieces were dehydrated in alcohols of increasing concentration and embedded in paraffin blocks. Histological preparations of the liver were stained with hematoxylin and eosin [10]. Histological preparations were studied using a SEO SCAN light microscope and photo-documented using a Vision CCD camera with a system of image output from histological preparations.

To identify the key enzyme of the citric acid cycle - succinate dehydrogenase, histochemical studies were performed according to the Nakhlas method [10]. These studies were carried out on sections made in a cryostat microtome from unfixed tissue using nitro blue tetrazole. The precipitate in the form of blue granules of diformazan testified to the presence and localization of the enzyme.

To study the features of glycogen accumulation in hepatocytes, sections were stained using Schiff's reagent, after pretreatment with iodic acid (PAS reaction) in Shabadash's modification.

An immunohistochemical research method was used to detect a subpopulation of CD86+ cells in the liver of experimental animals. Liver sections (thickness 4 μm) made from paraffin blocks using an AMR-400 rotary microtome (Amos scientific, Australia) were subjected to deparaffinization and rehydrated. Antigen recovery was performed in the KOS histoprocessor (Milestone, Italy). In the immunohistochemical staining protocol, mouse monoclonal primary antibodies Anti-CD86 (BP2-44514-0.1 mg, Novus Biologicals, USA) and the polymer detection system Mouse/Rabbit PolyVue™ HRP/DAB (Diagnostic BioSystems, USA) were used. Sections were counterstained with Mayer's hematoxylin (Biognost, Croatia).

Results

Histological studies of rat liver preparations under the influence of Vipera berus berus viper venom showed the manifestation of reactive alterative changes in the stroma and parenchyma of the organ. Violations of the microcirculatory system are observed, namely, sinusoidal hemocapillaries, the lumens of which are unevenly expanded, full of blood, with erythrocyte stasis, few lymphocytes are noted. Sinusoids with narrowed lumens were also detected (Fig. 1). Leukocyte infiltration is observed in the connective tissue around the triads. Stasis and coagulation of erythrocytes are found in the lumen of blood-filled interlobular veins (Fig. 2).

The location of hepatocytes in the form of plates, which

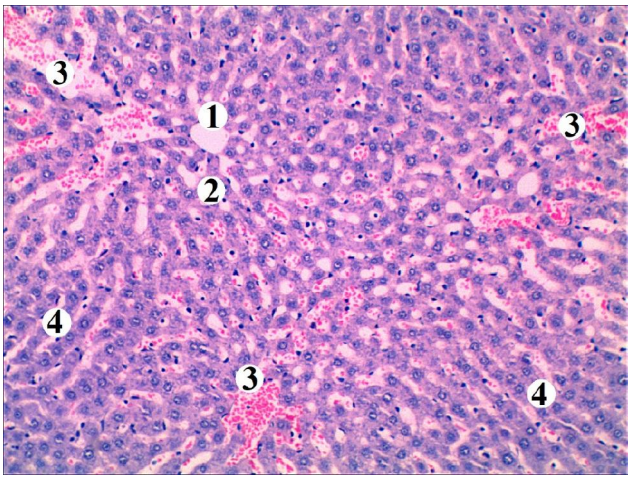

Fig. 1. Microscopic changes in the rat liver under the influence of Vipera berus berus venom: 1 - central vein, 2 - dilated lumens of sinusoidal hemocapillaries, 3 - erythrocyte stasis, 4 - hepatocyte plate. Staining with hematoxylin and eosin. Magnification: x100.

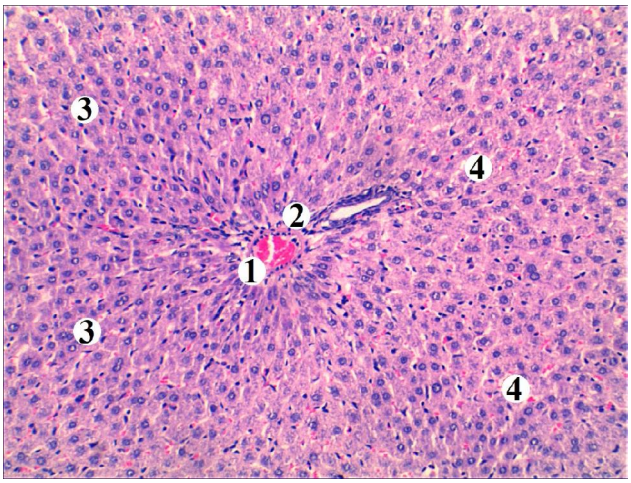

Fig. 2. Microscopic changes in the rat liver under the influence of Vipera berus berus venom: 1 - blood-filled interlobular vein with coagulation of erythrocytes in the lumen, 2 - lymphohistiocytic infiltration of the portal tract, 3 - hepatocyte plates, 4 - unevenly expanded spaces of sinusoidal hemocapillaries. Staining with hematoxylin and eosin. Magnification: x100.

diverge radially, is mostly preserved. Hepatocytes with hyperchromic nuclei are found in the periportal and centrilobular areas of classic liver lobes. Individual cells with pyknotic nuclei and intensely basophilic cytoplasm were observed, especially in the periportal areas. Many nuclei in the cells are normochromic. Binucleated hepatocytes with light euchromatin nuclei were found in the centrolobular parts of the lobule (Fig. 3). An increase in the population of Kupffer cells was noted in the space of Disse.

A histochemical study of the content of succinate dehydrogenase in the liver of animals injected with Vipera berus berus venom showed uneven activity of the mitochondrial enzyme in the lobules. Hepatocytes with moderate enzyme activity are intensely stained, characterized by large granules of diformazan and a powdery-amorphous sediment and are located mainly in the peripheral areas of the lobule (Fig. 4). In the centrolobular zone, hepatocytes with a low degree of staining are observed, which indicates a decrease in succinate dehydrogenase in the cytoplasm of cells. The average value of the activity coefficient of succinate dehydrogenase in hepatocytes of the liver of experimental rats is 3.652±0.171 nmol succinate/(min/mg protein), which is significantly ($p<0.001$) 0.76 times lower than the similar parameter of the intact group of animals.

A histochemical study of glycogen in hepatocytes of the liver of rats exposed to Vipera berus berus venom showed a decrease in the content of trophic inclusions. In most hepatocytes, there is an accumulation of pink-red glycogen granules peripherally, while part of the cytoplasm is freed from its contents and has an oxyphilic color (Fig. 5). There are individual cells with the typical localization of this trophic

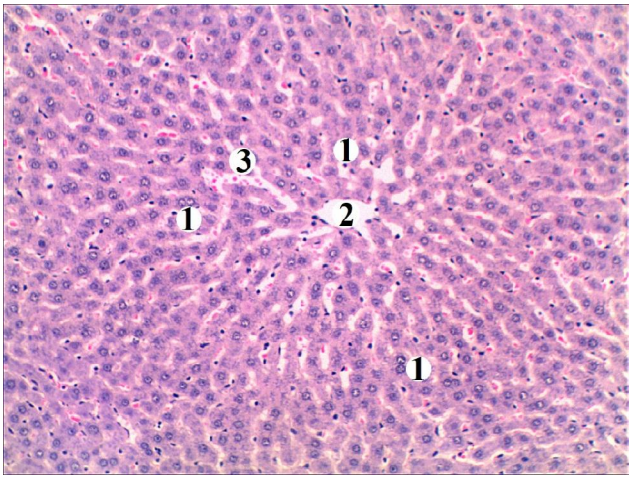

Fig. 3. Microscopic changes in the rat liver under the influence of Vipera berus berus venom: 1 - binucleated hepatocytes, 2 - central vein, 3 - expanded sinusoidal hemocapillaries with formal elements in the lumen. Hematoxylin and eosin staining. Magnification: x100.

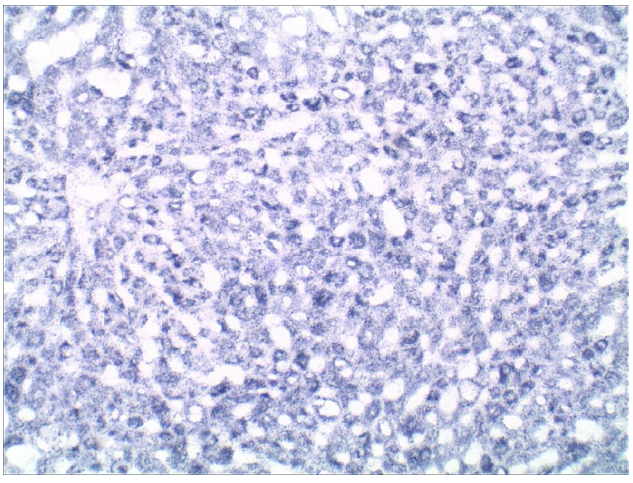

Fig. 4. Succinate dehydrogenase activity in rat liver hepatocytes under the influence of Vipera berus berus venom. Cells with low and high enzyme activity. The Nakhlas method. Magnification: x200.

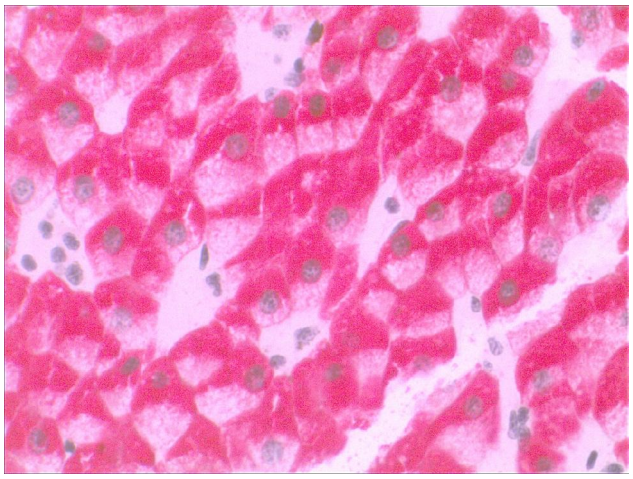

Fig. 5. The presence of glycogen in the liver of rats exposed to Vipera berus berus venom. Low content of trophic inclusions in the cytoplasm of hepatocytes. Shabadash method. Magnification: x400.

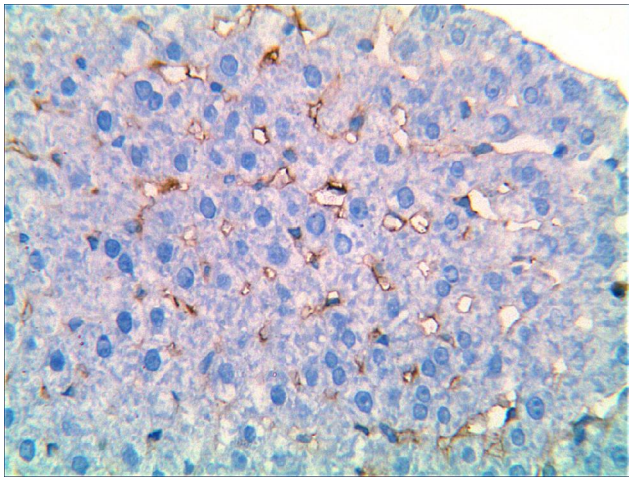

Fig. 6. Expression of CD86+ cells of the rat liver lobule under the influence of Vipera berus berus venom. Immunohistochemical reaction of CD86+ antibody. Staining with Mayer's hematoxylin. Magnification: x400.

compound. The average value of the cytochemical indicator is 3.413±0.160 nmol succinate/(min/mg protein) and decreases significantly ($p<0.001$) by 0.69 times compared to the indicator of the intact group of animals.

Immunohistochemical examination of the liver of animals injected with Vipera berus berus venom showed that populations of CD86+ cells are found in different areas of the liver lobe. Most of them have light brown or brown cytoplasm with numerous processes that lie along the lumen of the sinusoid, sometimes found in the perisinusoidal spaces (Fig. 6). The degree of expression of CD86 transmembrane glycoprotein is low (+--), but more intense compared to the intact group of animals. An increase in the population of CD86+ cells indicates reactive inflammatory processes observed in the organ due to the action of components of the Vipera berus berus venom.

Discussion

Envenomation as a result of snake and viper bites is accompanied by morphological and biochemical changes in the victim's body. A. K. Asmari et al. [2] investigated serological markers of acute hepatotoxicity caused by Echys pyramidum snake venom in rats. After 3-6 hours of intraperitoneal venom injection, pronounced changes in the functional activity of the organ were detected in experimental animals. In particular, an increase in serum levels of ALT, alkaline phosphatase, gammaglutamyl transpeptidase (GGT) and bilirubin were recorded. Liver damage was accompanied by a significant and dose-dependent decrease in the activity of antioxidant defense enzymes, namely superoxide dismutase (SOD) and catalase (CAT) in liver tissue. The authors reported on the activation of lipid peroxidation (LP) as a result of the generation of a significant amount of reactive oxygen species (ROS), which led to hepatocyte apoptosis. In addition, an increase in markers of oxidative stress (OS), the activity of cytoplasmic, lysosomal and extracellular matrix-degrading enzymes, and levels of pro-inflammatory mediators were characteristic.

According to certain studies, the toxins of Crotalus durissus terrificus vipers cause the development of acute liver damage. Its administration to rats at a dose of 100 mg/kg caused an increase in the activity of AST, ALT, alkaline phosphatase, and GGT after 3 hours of the experiment. Histological studies of the liver tissue under these conditions at different times (from 3 to 12 hours) demonstrated the presence of disorganization of the structural components of the organ, swelling of hepatocytes, and sometimes their necrosis. Histioleukocyte infiltration, congestion in vessels and a significant increase in the functional activity of Kupffer cells were also detected [8].

The results of research by Ghosh R. and co-authors [9] on the hepatotoxicity of Vipera russelli viper venom confirmed the development of destructive and dystrophic changes in the structure of the liver under the conditions of its administration to experimental animals. During histological examination of organ samples, signs of karyopyknosis, karyorrhexis of hepatocytes, their vacuolar and fatty dystrophy were observed. Sometimes characteristic manifestations of necrosis of liver cells, pronounced dilatation of sinusoidal capillaries, stagnation of central veins were noted. Leukocyte infiltration of liver tissue was characteristic. An increase in ALT and AST activity was recorded in the blood plasma of experimental rats.

S. Al-Quraishy et al. [1], studying the effect of Naja haje snake venom on the structural and functional parameters of the liver of laboratory rats, proved its hepatotoxic effect and ability to cause the development of OS. The levels of AST, ALT, GGT, and bilirubin increased in the blood serum of animals. The activation of LP and the increase of NO in liver homogenates were characteristic. At the same time, the content of glutathione in blood plasma and organ tissue and the activity of such enzymes as glutathione reductase

(GR), glutathione-S-transferase (GST), CAT decreased significantly. At the same time, high levels of SOD and glutathione peroxidase (GPx) were detected. The authors note that under these conditions, the functioning of the respiratory chain complexes of hepatocyte mitochondria, in particular II, III and V, was disturbed. Histological studies revealed leukocyte infiltration of liver tissue around the central veins, expansion of sinusoidal capillaries, vacuolization of hepatocyte cytoplasm, and increased activity of Kupffer cells. Severe necrosis or apoptosis of liver cells was observed in some places. Immunohistochemical studies established the pronounced activity of caspase-3 in hepatocytes, which demonstrates their high readiness for apoptosis.

Conclusions

1. Under the influence of Vipera berus berus venom, the development of alterative changes in the liver parenchyma and vascular disorders were microscopically revealed. The appearance of foci of leukocyte infiltration was established, which indicates the development of inflammatory processes, many binucleated hepatocytes are found in the lobules as an adaptive and compensatory reaction of the organ, unevenly and locally sharply expanded sinusoidal hemocapillaries with a sludge effect of erythrocytes are also noted.

2. A histochemical study of the content of succinate dehydrogenase in the liver of animals injected with Vipera berus berus venom showed uneven activity of the mitochondrial enzyme in the lobules.

3. A histochemical study of glycogen in hepatocytes of the liver of rats exposed to Vipera berus berus venom showed a decrease in the content of trophic inclusions.

4. An increase in the population of CD86+ cells indicates reactive inflammatory processes observed in the body as a result of the action of components of Vipera berus berus venom.

References

[1] Al-Quraishy, S., Dkhil, M. A., & Abdel Moneim, A. E. (2014). Hepatotoxicity and oxidative stress induced by Naja haje crude venom. *J Venom Anim Toxins Incl Trop Dis*, 20 (1). doi: 10.1186/1678-9199-20-42

[2] Asmari, A. K., Khan, H. A., Banah, F. A., Buraidi, A. A., & Manthiri, R. A. (2015). Serum biomarkers for acute hepatotoxicity of Echis pyramidum snake venom in rats. *Int J Clin Exp Med,* 8(1), 1376-1380. PMID: 25785140

[3] Balija, T., Leonardi, A., Brgles, M., Sviben, D., Kurtovic, T., Halassy, B., … & Krizaj, I. (2020). Biological activities and proteomic profile of the venom of Vipera ursinii ssp., a very rare Karst Viper from Croatia. *Toxins* (Basel), 12(3), 187. doi: 10.3390/toxins12030187

[4] Bennett, J. M., Sunday, J., Calosi, P., Villalobos, F., Martinez, B., Molina-Venegas, R., … & Olalla-Tarraga, M. A. (2021). The evolution of critical thermal limits of life on Earth. *Nat Commun,* 12(1), 1198. doi: 10.1038/s41467-021-21263-

[5] Casewell, N. R., Jackson, T. N. W., Laustsen, A. H., & Sunagar, K. (2020). Causes and consequences of snake venom variation. *Trends Pharmacol Sci*, 41(8), 570-581. doi: 10.1016/j.tips.2020.05.006

[6] Chaiyabutr, N., Chanhome, L., Vasaruchapong, T., Laoungbua, P., Khow, O., Rungsipipat, A., … & Sitprija, V. (2020). The pathophysiological effects of Russell's viper (Daboia siamensis) venom and its fractions in the isolated perfused rabbit kidney model: A potential role for platelet activating factor. *Toxicon X,* (7), 100046. doi: 10.1016/j.toxcx.2020.100046

[7] Dobrelia, N. V., Boitsova, L. V. & Danova, I. V. (2015). Правова база для проведення етичної експертизи доклінічних досліджень лікарських засобів з використанням лабораторних тварин [Legal basis for ethical examination of preclinical studies of drugs using laboratory animals]. *Фармакологія та лікарська токсикологія - Pharmacology and drug toxicology,* (2), 95-100.

[8] França, R. F., Vieira, R. P., Ferrari, E. F., Souza, R. A., Osorio, R. A. L., Prianti-Jr, A. C. G., … & Ribeiro, W. (2009). Acute hepatotoxicity of Crotalus durissus terrificus (South American rattlesnake) venom in rats. *J Venom Anim Toxins Incl Trop Dis,* 15(1), 61-78. doi: 10.1590/S1678-91992009000100007

[9] Ghosh, R., Mana, K., & Sarkhel, S. (2018). Ameliorating effect of Alstonia scholaris L. bark extract on histopathological changes following viper envenomation in animal models. *Toxicol Rep,* 5, 988-993. doi: 10.1016/j.toxrep.2018.10.004.

[10] Horalskyi, L. P., Khomych, V. T., & Kononskyi, O. I. (2011). *Основи гістологічної техніки і морфофункціональні методи досліджень у нормі та при патології [Fundamentals of histological technique and morphofunctional research methods in normal and pathology].* Житомир, Полісся - Zhytomyr: Polissya.

[11] Karabuva, S., Lukšić, B., Brizić, I., Latinović, Z., Leonardi, A., & Križaj, I. (2017). Ammodytin L is the main cardiotoxic component of the Vipera ammodytes ammodytes venom. *Toxicon,* 139, 94-100. doi: 10.1016/j.toxicon.2017.10.003

[12] Makarova, Y. V., Kryukova, E. V., Shelukhina, I. V., Lebedev, D. S., Andreeva, T. V., Ryazantsev, D. Y., … & Utkin, Y. N. (2018). The First recombinant viper three-finger toxins: Inhibition of muscle and neuronal nicotinic acetylcholine receptors. Dokl Biochem Biophys, 479(1), 127-130. doi: 10.1134/S1607672918020205

[13] Malina, T., Krecsak, L., Westerström, A., Szeman-Nagy, G., Gyemant, G., M-Hamvas, M., … & Vasas, G. (2017). Individual variability of venom from the European adder (Vipera berus berus) from one locality in Eastern Hungary. *Toxicon,* 135, 59-70. doi: 10.1016/j.toxicon.2017.06.004

[14] Marinho, A. D., Silveira, J. A. M., Chaves Filho, A. J. M., Jorge, A. R. C., Nogueira Junior, F. A., Pereira, V. B. M., … & Monteiro, H. S. A. (2021). Bothrops pauloensis snake venom-derived Asp-49 and Lys-49 phospholipases A2 mediates acute kidney injury by oxidative stress and release of inflammatory cytokines. *Toxicon,* 190, 31-38. doi: 10.1016/j.toxicon.2020.12.004

[15] Mohi-Ud-Din, R., Mir, R. H., Sawhney, G., Dar, M. A., & Bhat, Z. A. (2019). Possible pathways of hepatotoxicity caused by chemical agents. *Curr Drug Metab*, 20(11), 867-879. doi: 10.2174/1389200220666191105121653

[16] Razok, A., Shams, A., & Yousaf, Z. (2020). Cerastes cerastes snakebite complicated by coagulopathy and cardiotoxicity with electrocardiographic changes. *Toxicon,* 188, 1-4. doi: 10.1016/j.toxicon.2020.10.003

[17] Silva, A., Kuruppu, S., Othman, I., Goode, R. J., Hodgson, W. C., & Isbister, G. K. (2017). Neurotoxicity in Sri Lankan Russell's viper (Daboia russelii) envenoming is primarily due to U1-

viperitoxin-Dr1a, a pre-synaptic neurotoxin. *Neurotox Res,* 31(1), 11-19. doi: 10.1007/s12640-016-9650-4

[18] Siqueira-Silva, T., Lima, L., Chaves-Silveira, J., Amado, T., Naipauer, J., Riul, P., … & Martinez, P. (2021). Ecological and biogeographic processes drive the proteome evolution of snake venom. *Global Ecology and Biogeography,* 30(10), 1978-1989. doi: 10.1111/geb.13359

[19] Tohamy, A. A., Mohamed, A. F., Abdel Moneim, A. E., & Diab, M. S. M. (2014). Biological effects of Naja haje crude venom on the hepatic and renal tissues of mice. *J King Saud Univ Sci,* 26(3), 205-212. doi: 10.1016/j.jksus.2014.01.003

[20] Wang, S. Z., & Qin, Z. H. (2018). Anti-Inflammatory and immune regulatory actions of Naja naja atra venom. *Toxins* (Basel), 10(3), 100. doi: 10.3390/toxins10030100

ГІСТОЛОГІЧНІ ЗМІНИ ПЕЧІНКИ ЩУРІВ ЗА УМОВ ВПЛИВУ ОТРУТИ ГАДЮК VIPERA BERUS BERUS

Турбал Л.В., Яременко Л.М., Маєвський О.Є.

Отрути тварин містять цілий комплекс сполук, серед яких пептиди, білки, а також інші органічні молекули та солі. Їх токсини здатні викликати виражені порушення у функціонуванні фізіологічних систем, що призводить до виникнення патологічних станів, ускладнень і навіть смерті. Метою дослідження є вивчення гістологічних змін в печінці щурів під впливом отрути гадюки Vipera berus berus. Експериментальні дослідження проводили на білих нелінійних щурах-самцях. Тварин умовно розділили на дві групи - контрольну та дослідну, по 10 особин у кожній. Піддослідним щурам внутрішньоочеревинно вводили напівлетальну дозу (LD50) (1,576 мг/г-1) отрути Vipera berus berus на фізіологічному розчині. Тваринам контрольної групи вводили внутрішньоочеревинно тільки фізіологічний розчин. Щурів виводили з експерименту через 24 години після впливу отрути, знеживлюючи шляхом цервікальної дислокації. Відбирали зразки печінки тварин усіх груп для мікроскопічного дослідження. Гістологічні препарати печінки забарвлювали гематоксиліном та еозином. Гістологічні препарати досліджували за допомогою світлового мікроскопа SEO SCAN. Для ідентифікації ключового ферменту циклу лимонної кислоти - сукцинатдегідрогенази, проводили гістохімічні дослідження за методом Нахласа. Для вивчення особливостей накопичення глікогену в гепатоцитах зрізи фарбували реактивом Шиффа після попередньої обробки йодною кислотою (PAS-реакція) у модифікації Шабадаша. Імуногістохімічним методом виявлено субпопуляцію клітин CD86+ у печінці експериментальних тварин. Під впливом отрути гадюки Vipera berus berus мікроскопічно виявлено розвиток альтеративних змін паренхіми печінки та судинних розладів. Встановлено появу вогнищ лейкоцитарної інфільтрації, що свідчить про розвиток запальних процесів. Гістохімічне дослідження вмісту сукцинатдегідрогенази в печінці тварин, яким вводили отруту Vipera berus berus, показало нерівномірність активності мітохондріального ферменту в часточках. При гістохімічному дослідженні глікогену в гепатоцитах печінки щурів, які зазнали дії отрути Vipera berus berus, виявлено зниження вмісту трофічних включень. Збільшення популяції клітин CD86+ свідчить про реактивні запальні процеси, що спостерігаються в організмі внаслідок дії компонентів отрути гадюки.

Ключові слова: *гадюки, печінка, сукцинатдегідрогеназа, глікоген, CD86+.*

Author's contribution

Turbal L. V.: analysis of scientific literature, development of the main theoretical and practical provisions of the study, conducting the study, analysis of the obtained results.

Yaremenko L. M.: development of the study's main theoretical and practical provisions, formulation of conclusions.

Maievskyi O. Ye.: development of the study's main theoretical and practical provisions, formulation of conclusions.

DOI: 10.31393/morphology-journal-2023-29(4)-09 Reports of Morphology, Vol. 29, №4, Pages 64-69

ISSN 1818-1295 eISSN 2616-6194

REPORTS OF MORPHOLOGY

Official Journal of the Scientific Society of Anatomists, Histologists, Embryologists and Topographic Anatomists of Ukraine

journal homepage: https://morphology-journal.com

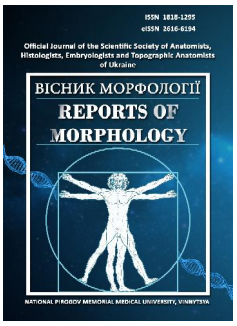

Electron microscopic changes in interstitial endocrinocytes of rats testicles during administration of triptorellin for 365 days

Stetsuk Ye. V., Shepitko V. I., Boruta N. V., Vilkhova O. V., Skotarenko T. A., Rud M. V.
Poltava State Medical University, Poltava, Ukraine

ARTICLE INFO
Received: 28 July 2023
Accepted: 11 October 2023

UDC: 616.679:615.35:599.365.3

CORRESPONDING AUTHOR
e-mail: stetsuk78@gmail.com
Stetsuk Y. V.

CONFLICT OF INTEREST
The authors have no conflicts of interest to declare.

FUNDING
Not applicable.

DATA SHARING
Data are available upon reasonable request to corresponding author.

Triptorelin is a gonadotropin-releasing hormone agonist that is a potent inhibitor of testosterone (in men) and estrogen (in women) synthesis and is used to treat advanced prostate cancer. Studies of the mechanisms of regulation and synthesis of testosterone formation in testicular interstitial cells demonstrate multiple endogenous targets that can increase testosterone biosynthesis, which may moderate the effects of testosterone depletion. Triptorelin, a synthetic analog of the neurohormone gonadoliberin, suppresses the expression of the GnRH receptor in the pituitary gland, but does not change the functioning of the pituitary-testicular complex. The purpose of the work is to study the electron microscopic changes in the interstitial endocrinocytes of the testes of rats after the administration of triptorelin for 365 days.The experiment was conducted on 35 sexually mature male white rats. The rats were divided into 2 groups: the control group (I) was injected with a physiological solution, the II group with central deprivation of the synthesis of luteinizing hormone was injected subcutaneously with triptorelin at a dose of 0.3 mg of the active substance per kg of the rat's body weight. The study of the interstitial space in the testicles of white rats showed that long-term administration of triptorelin causes hormonal dysregulation of the hypothalamus-pituitary-testis system, which leads to quantitative and qualitative changes in the endocrine cells of the interstitial space of the testis, which is confirmed by electron microscopic changes in subcellular structures. The maximum effect of triptorelin is determined from the 180th day of observation, which is characterized by an increase in degenerative changes in endocrinocytes, and the detection of Reinke crystals in the cytoplasm of interstitial endocrinocytes from the 270th day of observation.

Keywords: *testes, electron microscopy, rats, interstitial endocrinocytes, luteinizing hormone, triptorelin.*

Introduction

As is known [1, 2, 7, 8], interstitial endocrinocytes maintain a high level of androgen (testosterone or androstenedione), necessary for the differentiation of male genital organs and masculinization of the brain. Androgen production declines with the loss of these cells, reaching its lowest point in the postpartum period. Testosterone levels then gradually increase to high levels with the development of testicular interstitial endocrinocytes from stem cells. In adults, luteinizing hormone (LH), binding to LH receptors of interstitial endocrinocytes, stimulates the production of cAMP, increasing the rate of cholesterol translocation into mitochondria. LH is a gonadotropic peptide hormone of the anterior lobe of the pituitary gland, which stimulates the secretion of sex hormones by the pituitary gland, both in women and in men [4, 6, 13]. In its turn, LH is the central regulator that controls the production of the male sex hormone - testosterone, through the "pituitary - testis" system with the activation of interstitial endocrinocytes to produce testosterone, which in turn stimulates the growth and development of testicular cells and tissues. The increase in testosterone concentration under the influence of LH is due to LH-stimulated proliferation of interstitial endocrinocytes [12]. In conditions of deficiency or complete absence of LH caused by the administration of chemotherapy drugs in oncological pathologies, the death of cells of the seminiferous tubules occurs due to the activation of apoptosis and stress of the endoplasmic reticulum of cells of the spermatogenic series and supporting sustentocytes [15, 18].

Triptorelin, a synthetic analogue of the neurohormone

gonadoliberin (gonadotropin-releasing hormone, GnRH) [7, 11], suppresses the expression of the GnRH receptor in the pituitary gland, but did not change the functioning of the pituitary-testicular complex. Physical changes during puberty require the concerted efforts of many organs; these changes are initiated by activation of the hypothalamic-pituitary-gonadal axis. The first hormonal change during puberty is the pulsatile release of GnRH, caused by disinhibition of the hypothalamic-pituitary-gonadal axis [8, 16]. Although the cause of this disinhibition is largely unknown, the subsequent release of GnRH then stimulates pulsatile LH release.

The purpose of the work is to study the electron microscopic changes in the interstitial endocrinocytes of the testes of rats after the administration of triptorelin for 365 days.

Materials and methods

The study was conducted on 35 sexually mature white male rats. Animals were randomly divided into 2 groups: control (10 animals) and experimental (25 animals). Rats from the control group received injection of physiological saline. Experiment lasted 365 days. The animals of the experimental group were injected with a solution of triptorelin acetate at the rate of 0.3 mg of the active substance per kg of animal weight to simulate central deprivation of luteinizing hormone synthesis [5]. Animals were removed from the experiment on the 30th, 90th, 180th, 270th, and 365th days by overdose with ether anesthesia. Animals were kept in standard vivarium conditions of the Poltava State Medical University.

The study is a fragment of the research project "Experimental morphological study of cryopreserved placenta transplants action diphereline, ethanol and 1 % methacrylic acid on the morphofunctional status in a number of internal organs", state registration № 0119U102925.

Experimental animals were sacrificed in strict compliance with the provisions of the "European Convention for the Protection of Vertebrate Animals Used for Experimental and Other Scientific Purposes"; (Strasbourg, 1986), as well as with the "General Ethical Principles of Animal Experiments" adopted by the First National Congress on Bioethics (Kyiv, 2001). The research was approved and confirmed by the bioethics commission of the Poltava State Medical University (protocol № 195 - 06.24.2021).

For electron microscopic studies [3], fragments of the organ were fixed in a 2.5% solution of glutaraldehyde, fixed in a 1% solution of osmium tetroxide in a phosphate buffer (pH 7.2-7.4), dehydrated in alcohol and propylene oxide, and poured into a mixture of epoxy resins with araldite. Ultrathin sections were prepared on a ZKB-3 ultramicrotome (Sweden) and grids were made. Sections were contrasted first in a 1 % solution of uranyl acetate in methanol, and then with lead citrate according to Reynolds. The preparations were studied on an electron microscope PEM-125 K (serial number 38-76, TU 25-07-871-70), accelerating voltage 50-75 KW.

Results

One of the features of the endocrinocyte population of the control group of animals was the variety of cell shapes from round, oval to polygonal; in a small amount, there were also cells of a processive and spindle-shaped form. The round cells had a diameter of 14-18 μm. The first three cell forms were characterized by medium and large nuclei and well-developed cytoplasm. In the nuclei, euchromatin is distributed evenly over the entire area, the content of parietal heterochromatin varies. The described morphological characteristics are characteristic of mature, functionally active cells. The analysis of the distribution by groups of cells with different sizes of nuclei showed that in the population of testicular endocrinocytes cells with average sizes of nuclei predominate, there are more than 60% of them. The differentiated cells had a moderately developed smooth endoplasmic reticulum, which often formed large vacuolar expansions. Mitochondria are numerous, the mitochondrial matrix is quite dense, and tubular and mixed cristae are not always visible in it. On the surface of individual cells, there are protrusions of the cytolemma of various shapes. Contacts of cell processes with blood and lymphatic capillaries are often found. In the areas of contact between cells and capillaries in the surface layer of endocrinocyte cytoplasm, there were many exocytotic vesicles. Lipid droplets were large in size, but occurred rarely and not in every cell. The content of lysosomes in the cytoplasm of endocrinocytes is low. The cytoplasmic membrane corresponded structurally to the elementary membrane. Cells are interconnected by desmosomes and gap junctions.

When studying electrograms of an experimental group of animals on the 30th day of observation, we established that interstitial endocrinocytes were located near blood vessels or peritubularly, in groups or singly. They had rounded cores with 1-2 nucleoli. A well-developed smooth endoplasmic reticulum was found in the cytoplasm, which was represented by numerous branching tubules filled with a thin fibrous substance, on the membranes of which numerous ribosomes were present (Fig. 1).

Mitochondria of medium size, with an osmiophilic matrix and a small number of crystals. A characteristic feature was the presence in the cytoplasm of secretory granules of different sizes and electron density, localized in the well-developed lamellar apparatus of the cytoplasmic Golgi complex. Their characteristic feature is the presence of lipid inclusions and small, electron-dense hormonal granules in the cytoplasm. The latter are observed near the well-developed Golgi complex or in peripheral areas of the cytoplasm near the hemocapillary.

The presence of numerous mitochondria, the cristae of which are immersed in a matrix of moderate electron density, is characteristic of the cells of this observation group. The large volume of the cell cytoplasm that belongs to the mitochondria is connected with the fact that the synthesis of steroid hormones started on the endoplasmic reticulum is still being completed in these organelles. A typical picture for

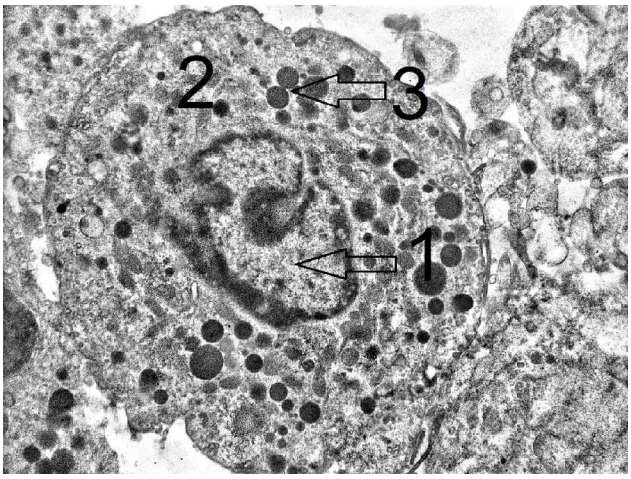

Fig. 1. Endocrinocyte of the stroma of the testis on the 30th day of observation. 1 - endocrinocyte nucleus, 2 - endocrinocyte cytoplasm, 3 - inclusions. x9 000.

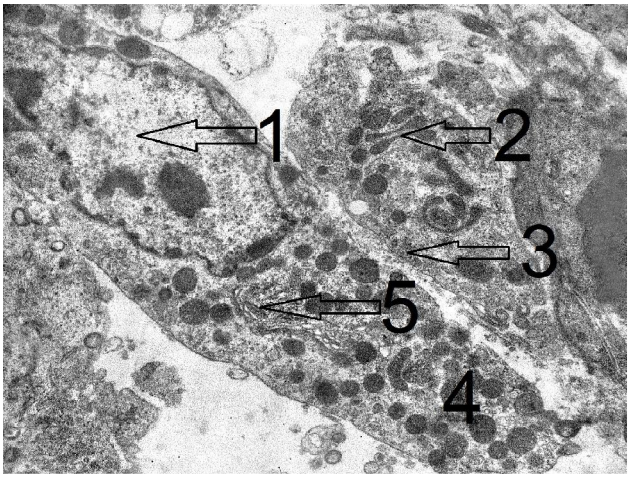

Fig. 2. Endocrinocyte of the stroma of the testis on the 90th day of observation. 1 - endocrinocyte nucleus, 2 - Golgi complex, 3 - mitochondria, 4 - inclusion, 5 - endoplasmic reticulum. x9 000.

cells is the close contact of mitochondria with elements of the endoplasmic smooth reticulum.

In the experimental group of animals, on the 90th day of observation, it was established that in the Leydig cells, minor destructive disturbances in the ultrastructural organization of the lamellar cytoplasmic Golgi complex were detected. In some cells, the smooth membranes of the Golgi complex were randomly oriented and surrounded by single large electron-transparent vacuoles, lipid inclusions, and secretory granules. The cytoplasmic membrane of glandulocytes was loose, thickened, and had a high electron density. A small number of cells had fragmented smooth endoplasmic reticulum. Hyaloplasm of glandulocytes was significantly brightened and contained very few free ribosomes and polysomes, in comparison with the control group of animals and with the previous term. In the cytoplasm, there are few mitochondria, they are single, but different in size and shape, the matrix of which is not detected, single cristae are found (Fig. 2).

The 180th day of observation was characterized by a significant decrease in the number of endocrinocytes in the interstitial lumen of convoluted tubules. A small number of cells with signs of destruction of the nucleus and cytoplasm are found in the interstitial tissue. The cells contain many pinocytotic vesicles, and the cytolemma forms pinocytotic intussusceptions, especially on the vascular surface. Neighboring endocrinocytes may have been disconnected from each other. The cells are characterized by the presence of a large cytoplasm, in which the smooth endoplasmic reticulum is well developed, which evenly fills the entire cytoplasm, and the rough endoplasmic reticulum is represented by separate short, widely anastomosing with each other. The share of agranular endoplasmic reticulum in the cells of a number of cells can reach 50 % or more. Nucleoli are not found in the nuclei of cells. Centrioles are rarely detected in cells, in those cells where they are detected, they are usually adjacent to the Golgi complex. Lipid inclusions and a low number of lysosomes are also found in endocrinocytes. The above-described

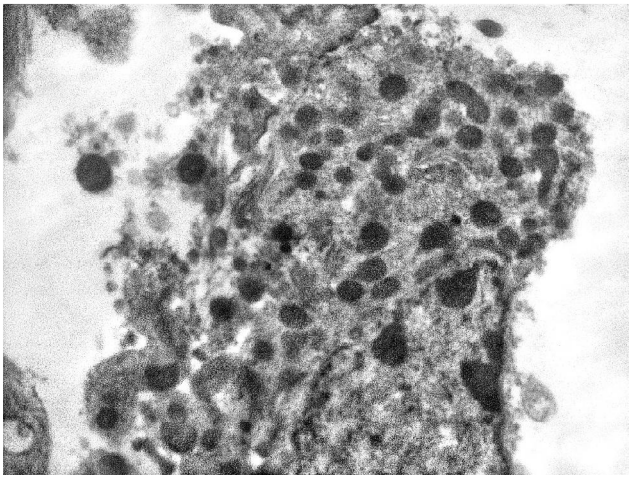

Fig. 3. Lipid inclusions of the endocrinocyte of the testis stroma on the 180th day of observation. x12 000.

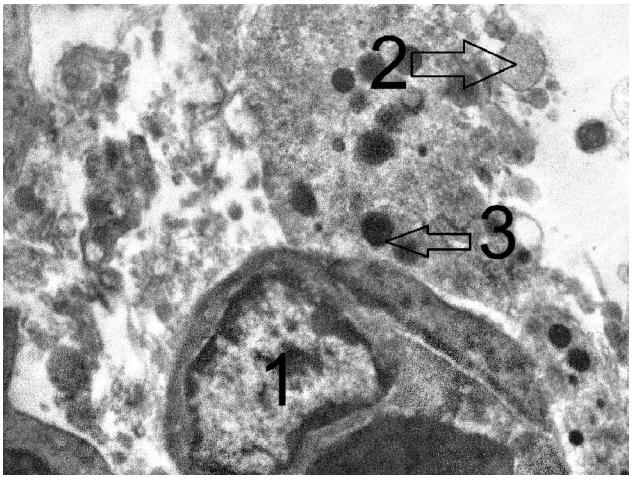

Fig. 4. Endocrinocyte of the stroma of the testis on the 270th day of observation. 1 - endocrinocyte nucleus, 2 - Reinke crystals, 3 - lipid inclusions. x12 000.

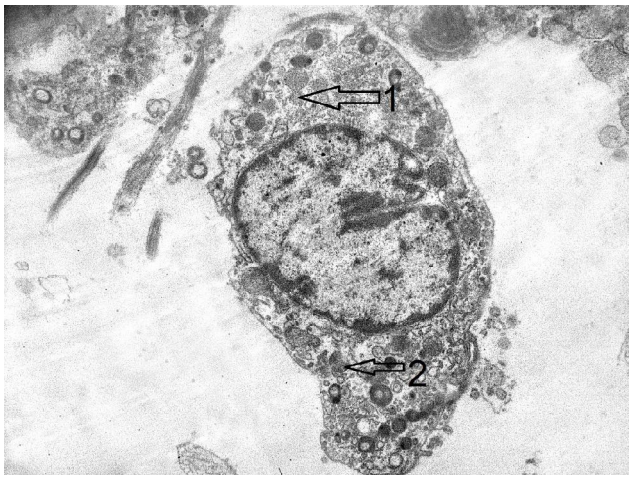

Fig. 5. Endocrinocyte of the stroma of the testis on the 365th day of observation. 1 - intracellular Reinke crystals, 2 - mitochondria. x9 000.

state of interstitial endocrinocytes was observed in opposition to active spermatogenesis in convoluted seminiferous tubules (Fig. 3).

The 270th day of observation was characterized by a decrease in the number of endocrinocytes, single cells near blood capillaries. A large number of cells (endocrinocytes, fibroblasts, macrophages) with signs of destruction are found in the interstitial tissue. These cells are relatively small, flat or polygonal in shape, with acidophilic cytoplasm, vacuolated on the periphery, smooth endoplasmic reticulum is not detected, single mitochondria of rounded shape. In the cytoplasm of endocrinocytes, the hexon-shaped prisms, with well-defined edges and corners, formations in the form of a "wasp's nest" - Reinke crystals (which are layering resulting from the disintegration of the membranes of the smooth endoplasmic reticulum) are sometimes determined (Fig. 4).

In the studied animals, on the 365th day, fibrosis of the interstitial connective tissue of convoluted tubules was detected. The number of vessels is increased. Endocrinocytes are small in size, single. In the cytoplasm of which single lipid granules, endoplasmic reticulum and Golgi complex are poorly developed. Core of normal size, light-optical. Nucleoli are absent. Mitochondria are round, single. We found the presence of Reinke crystals in the cytoplasm of interstitial endocrinocytes and outside the borders of the cells themselves (Fig. 5).

Discussion

The differences we identified in the morphological parameters of endocrinocytes at different observation periods when triptorelin was administered obviously indicate that triptorelin causes increasing destructive disturbances in the ultrastructural organization of these cells, which are manifested by different pathological stages and the degree of their functional activity of the internal components of the cell. The analysis of the structure of the population of interstitial endocrinocytes showed that the basis of the population of these testicular cells is rounded, oval or polygonal cells of medium size with a well-developed cytoplasm, medium, sometimes large nuclei. These are mature differentiated cells that, as a result of determination and differentiation, have acquired clearly expressed specialization, the ability to synthesize androgens. These cells have a well-developed smooth endoplasmic reticulum, numerous mitochondria, and lipid droplets can be detected in the cytoplasm. Small, spindle-shaped cells, similar in some structural features to fibroblasts, are the youngest and least differentiated cells. They are probably the source of maintaining the constancy of cell composition in this population. It is known that no mitotic activity was detected in the pubertal population of endocrinocytes, as evidenced by our results and literature data [1, 2, 6, 9]. Therefore, stability in the population is ensured by a dynamic balance between the processes of differentiation of endocrinocytes from their poorly differentiated precursors and the processes of their death. The rat endocrinocyte population belongs to cell populations of a stable type. This is evidenced by the fact that no mitoses were detected among the interstitial endocrinocytes of the testes in any of the sexually mature rats studied by us. The great diversity in the content of lipid inclusions in the cytoplasm of interstitial endocrinocytes of different mammals is caused by several factors. For example, according to other data [20], animals in which seasonality in reproductive activity is not expressed, as a rule, have few liposomes in the cytoplasm of interstitial endocrinocytes, lipid droplets of different (both low and high) electron density are found in the cytoplasm, and in the content of lipid inclusions in these animals varies little depending on sexual activity. Animals that do not exhibit seasonality in reproduction usually contain few lipid inclusions in the cytoplasm of endocrinocytes. On the contrary, in animals with a seasonal nature of reproduction, many lipid droplets of different electron density, surrounded by a membrane, are almost always found in the cytoplasm of such cells. Our data on this issue confirm the information available in the literature [14, 19]. It should be noted that the number of secretory inclusions is no longer an indicator that clearly indicates a low or high level of steroidogenesis in cells. A large amount of a secretory product in a cell can be: a) an indicator of a delay in the secretory process at the stage of secretion removal; b) an indicator of high functional activity. The latter is observed if the agranular endoplasmic reticulum in the cells is well developed, mitochondria are numerous, frequent contacts of mitochondria with smooth endoplasmic reticulum vesicles and lipid droplets. An important role in the analysis of morphological equivalents of steroidogenesis can be played by counting the number of mitochondria, but also by taking into account the peculiarities of the structure of mitochondrial structures. Thus, tubulovesicular cristae in mitochondria are characteristic of steroid-producing cells. Therefore, the

presence of a large number of mitochondria with tubulovesicular cristae is one of the indicators of active steroidogenesis. Interstitial endocrinocytes of testes may contain pigment inclusions in the cytoplasm. Among the rats we studied, the highest content of pigment inclusions in the cytoplasm of interstitial endocrinocytes was not noted. The frequency of finding Reinke's crystals, their number and volume of the crystal in relation to the volume of the cell correlates with age, increasing in the older age group [1, 17], as is known from the literature. Correlation with the level of testosterone was not found in the literature, which allows to mark Reinke crystals as a product of degenerative processes in the cell [10], which can also be indirectly evidenced by an increase, as well as their number in testicular biopsies from subjects with cryptorchidism [2, 12]. Therefore, the presence of these crystals in our experiment with the introduction of triptorelin in the interstitial cells and in the pericellular space indicates the cessation of androgen synthesis in them and intrinsic degenerative changes in the cells.

The results obtained by us are a theoretical justification for the development of methods for correcting violations of the generative and endocrine function of the testicles in the case of pathological effects on the body, with damage to endo- and paracrine regulations. Data on the functional morphology of the testes at the stages of adaptation to changes in the endocrine and immune function of the testes expand the existing understanding of the causes of spermatogenesis disorders and its regulation.

Conclusions

1. Long-term administration of triptorelin causes hormonal dysregulation in the hypothalamus-pituitary-testis system, which leads to quantitative and qualitative changes in the population of endocrine cells in the interstitial space of the testis, which is confirmed by electron microscopic changes in subcellular structures.

2. The maximum effect of triptorelin is determined from the 180th day of observation, which is characterized by an increase in degenerative changes in endocrinocytes, and the detection of Reinke crystals in the cytoplasm of interstitial endocrinocytes from the 270th day of observation.

References

[1] Almeida, S., Rato, L., Sousa, M., Alves, M. G., & Oliveira, P. F. (2017). Fertility and sperm quality in the aging male. *Current pharmaceutical design,* 23(30), 4429-4437. doi: 10.2174/1381612823666170503150313

[2] Atallah, A., Mhaouty-Kodja, S., & Grange-Messent, V. (2017). Chronic depletion of gonadal testosterone leads to blood-brain barrier dysfunction and inflammation in male mice. *Journal of Cerebral Blood Flow & Metabolism,* 37(9), 3161-3175. doi: 10.1177/0271678 X16683961

[3] Bahriy, M. M., Dibrova, V. A., Popadynets, O. H., & Hryshchuk, M. I. (2016). *Методики морфологічних досліджень: монографія [Methods of morphological research: monograph].* Вінниця: Нова книга - Vinnytsya: Nova knyha.

[4] Belanger, J., Tremblay, C., Davis, A., & Arnocky, S. (2019). Luteinizing hormone. *Encyclopedia of Evolutionary Psychological Science*, 1-8. doi: 10.1007/978-3-319-16999-6_1812-1

[5] Botte, M. C., Lerrant, Y., Lozach, A., Berault, A., Counis, R., & Kottler, M. L. (1999). LH down-regulates gonadotropin-releasing hormone (GnRH) receptor, but not GnRH, mRNA levels in the rat testis. *Journal of Endocrinology,* 162(3), 409-415. doi: 10.1677/joe.0.1620409

[6] Chung, J. Y., Brown, S., Chen, H., Liu, J., Papadopoulos, V., & Zirkin, B. (2020). Effects of pharmacologically induced Leydig cell testosterone production on intratesticular testosterone and spermatogenesis. *Biology of reproduction,* 102(2), 489-498. doi: 10.1093/biolre/ioz174

[7] Garza, S., & Papadopoulos, V. (2023). Testosterone recovery therapy targeting dysfunctional Leydig cells. *Andrology,* 11(5), 816-825. doi: 10.1111/andr.13304

[8] Garza, S., Chen, L., Galano, M., Cheung, G., Sottas, C., Li, L., ... & Papadopoulos, V. (2022). Mitochondrial dynamics, Leydig cell function, and age-related testosterone deficiency. *The FASEB Journal,* 36(12), e22637. doi: 10.1096/fj.202201026R

[9] Han, S., Luo, J., Xu, S., Zhao, L., Yao, C., Xu, J., ... & Li, P. (2022). Low-Intensity Pulsed Ultrasound Alleviates Human Testicular Leydig Cell Senescence In Vitro. *International Journal of Molecular Sciences*, 24(1), 418. doi: 10.3390/ijms24010418

[10] Hotta, Y., Kataoka, T., & Kimura, K. (2019). Testosterone deficiency and endothelial dysfunction: nitric oxide, asymmetric dimethylarginine, and endothelial progenitor cells. *Sexual medicine reviews,* 7(4), 661-668. doi: 10.1016/j.sxmr.2019.02.005

[11] Liu, F. H., Yang, D. Z., Wang, Y. F., Liang, X. P., Peng, W. M., Cao, C. A., ... & Guo, Z. M. (2007). Making of the animal model with sterilized testes. *Zhonghua nan ke xue= National Journal of Andrology*, 13(2), 125-129. PMID: 17345767

[12] Merseburger, A. S., & Hupe, M. C. (2016). An update on triptorelin: current thinking on androgen deprivation therapy for prostate cancer. *Advances in therapy,* 33, 1072-1093. doi: 10.1007/s12325-016-0351-4

[13] Mossadegh-Keller, N., & Sieweke, M. H. (2018). Testicular macrophages: Guardians of fertility. *Cellular Immunology,* 330, 120-125. doi: 10.1016/j.cellimm.2018.03.009

[14] Rawla, P. (2019). Epidemiology of prostate cancer. *World journal of oncology,* 10(2), 63-89. doi: 10.14740/wjon1191

[15] Rice, M. A., Malhotra, S. V., & Stoyanova, T. (2019). Second-generation antiandrogens: from discovery to standard of care in castration resistant prostate cancer. *Frontiers in oncology,* 9, 801. doi: 10.3389/fonc.2019.00801

[16] Scovell, J. M., & Khera, M. (2018). Testosterone replacement therapy versus clomiphene citrate in the young hypogonadal male. *European urology focus,* 4(3), 321-323. doi: 10.1016/j.euf.2018.07.033

[17] Swelum, A. A. A., Saadeldin, I. M., Zaher, H. A., Alsharifi, S. A., & Alowaimer, A. N. (2017). Effect of sexual excitation on testosterone and nitric oxide levels of water buffalo bulls (Bubalus bubalis) with different categories of sexual behavior and their correlation with each other. *Animal reproduction science,* 181, 151-158. doi: 10.1016/j.anireprosci.2017.04.003

[18] Wang, M., Yang, Y., Cansever, D., Wang, Y., Kantores, C., Messiaen, S., ... & Bhushan, S. (2021). Two populations of self-maintaining monocyte-independent macrophages exist in

adult epididymis and testis. *Proceedings of the National Academy of Sciences*, 118(1), e2013686117. doi: 10.1073/pnas.2013686117

[19] Zhao, Y., Liu, X., Qu, Y., Wang, L., Geng, D., Chen, W., ... & Lv, P. (2019). The roles of p38 MAPK® COX2 and NF-kB® COX2 signal pathways in age-related testosterone reduction. *Scientific Reports,* 9(1), 10556. doi: 10.1038/s41598-019-46794-5

[20] Zirkin, B. R., & Papadopoulos, V. (2018). Leydig cells: formation, function, and regulation. *Biology of reproduction,* 99(1), 101-111. doi: 10.1093/biolre/ioy059

ЕЛЕКТРОННОМІКРОСКОПІЧНІ ЗМІНИ В ІНТЕРСТИЦІЙНИХ ЕНДОКРИНОЦИТАХ СІМ'ЯНИКІВ ЩУРІВ ПРИ ВВЕДЕННІ ТРИПТОРЕЛІНУ ПРОТЯГОМ 365 ДІБ

Стецук Є. В., Шепитько В. І., Борута Н. В., Вільхова О. В., Скотаренко Т. А., Рудь М. В.

Трипторелін є агоністом гонадотропін-рилізинг-гормону, який є потужним інгібітором синтезу тестостерону (у чоловіків) та естрогену (у жінок) і використовується для лікування прогресуючого раку простати. Дослідження механізмів регуляції та синтезу утворення тестостерону в тестикулярних інтерстиційних клітинах демонструють численні ендогенні мішені, які можуть збільшити біосинтез тестостерону, що може пом'якшити ефекти зниження тестостерону. Трипторелін, синтетичний аналог нейрогормону гонадоліберину, пригнічує експресію рецептора GnRH в гіпофізі, але не змінює функціонування гіпофізарно-тестикулярного комплексу. Мета дослідження - вивчити електронномікроскопічні зміни інтерстиціальних ендокриноцитів сім'яників щурів після введення трипторелінy протягом 365 діб. Експеримент проведено на 35 статевозрілих самцях білих щурів. Щури були поділені на 2 групи: контрольна група (I) - вводили фізіологічний розчин, II група з центральною депривацією синтезу лютеїнізуючого гормону - підшкірно вводили трипторелін у дозі 0,3 мг діючої речовини на кг маси тіла щура. Проведене дослідження інтерстиційного простору в сім'яниках білих щурів показало, що довготривале введення трипторелінy викликає гормональну дисрегуляцію за системою гіпоталамус-гіпофіз-яєчко, що призводить до кількісних та якісних змін в ендокринних клітинах інтерстиційного простору яєчка, яке підтверджується електронномікроскопічними змінами субклітинних структур. Максимальний вплив трипторелінy визначається з 180-ї доби спостереження, що характеризується підвищенням дегенеративних змін в ендокриноцитах та виявленням з 270-ї доби спостереження кристалів Рейнке в цитоплазмі інтерстиційних ендокриноцитів.

Ключові слова: *сім'яники, електронна мікроскопія, щури, інтерстиційні ендокриноцити, лютеїнізуючий гормон, трипторелін.*

Author's contribution

Stetsuk Ye. V.: work concept and design, data collection and analysis, responsibility for statistical analysis, writing the article.
Shepytko V. I.: final approval of the article.
Boruta N. V.: responsibility for statistical analysis.
Vilkhova O. V.: work concept and design.
Skotarenko T. A.: writing the article.
Rud M. V.: writing the article.

DOI: 10.31393/morphology-journal-2023-29(4)-10 Reports of Morphology, Vol. 29, №4, Pages 70-78

ISSN 1818-1295 eISSN 2616-6194

REPORTS OF MORPHOLOGY

Official Journal of the Scientific Society of Anatomists, Histologists, Embryologists and Topographic Anatomists of Ukraine

journal homepage: https://morphology-journal.com

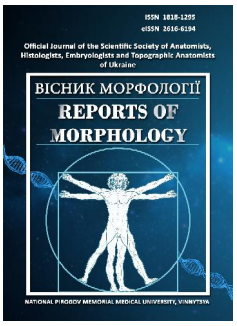

Neuroprotective effect of 2-ethyl-6-methyl-3-hydroxypyridine succinate on the sciatic nerve and its segmental centers in experimental paclitaxel-induced peripheral neuropathy

Herashchenko S. B., Ostrovskyi M. M., Kulynych H. B., Markiv I. M.
Ivano-Frankivsk National Medical University, Ivano-Frankivsk, Ukraine

ARTICLE INFO
Received: 8 August 2023
Accepted: 20 October 2023

UDC: 616-009+616-009.6+611.08

CORRESPONDING AUTHOR
e-mail: gera271261@gmail.com
Herashchenko S. B.

CONFLICT OF INTEREST
The authors have no conflicts of interest to declare.

FUNDING
Not applicable.

DATA SHARING
Data are available upon reasonable request to corresponding author.

Up to 60 % of patients suffer from the neurotoxicity of the chemotherapy drug Paclitaxel, namely paclitaxel-induced peripheral neuropathy (PIPN), during the treatment of breast cancer, ovarian cancer, and non-small cell lung cancer. Of these, up to 25 % of patients require modification of the paclitaxel treatment regimen, including dose reduction, delay, or discontinuation of therapy. Previous attempts to use neuroprotective agents in humans and in animal models have not shown sufficient efficacy in preventing or significantly reducing the manifestations of PIPN. The aim of our study was to study the effect of the neuroprotective agent 2-ethyl-6-methyl-3-hydroxypyridine succinate (HS) on the morpho-functional parameters of the sciatic nerve and its segmental centers in experimental PIPN. In the experiment, 56 white rats were used, which were injected intraperitoneally with Paclitaxel at a dose of 2 mg/kg of body weight 4 times after one day, after which the animals were divided into an experimental group - 24 animals that were injected with HS and a control group (24 animals, injection of water for injections). The method of studying mechanical allodynia was von Frey monofilaments, thermal hyperalgesia was studied by the hot plate test, and the electron microscopic examination was carried out according to generally accepted methods and studied with the help of a PEM-125 K electron microscope. The results of the hot plate test and the use of von Frey monofilaments showed that the use of HS reliably reduces manifestations of PIPN on the 7th, 14th and 28th days of the experiment. In rats treated with HS, destructive-dystrophic phenomena in the myelin nerve fibers of the sciatic nerve are less pronounced, and in individual fibers in the axon, phenomena of incomplete splitting of mitochondria with the formation of vacuoles filled with medium electron density contents are observed, and small young mitochondria are also visualized. During the first 28 days, we noted less pronounced destructive-dystrophic changes in the neurons of the spinal cord nodes, namely: chromatolysis of light and dark neurons and swelling of their cytoplasm, phenomena of neuronophagy in gliocytes, hypertrophy of certain areas of the myelin sheath. The results of the electron microscopic study are fully consistent with the data of neurophysiological studies and indicate the possibility of using HS as an effective neuroprotector in PIPN.

Keywords: *Paclitaxel, chemotherapy, neuropathy, central nervous system, peripheral nervous system.*

Introduction

Up to 60 % of patients suffer from the neurotoxicity of the chemotherapy drug Paclitaxel, namely paclitaxel-induced peripheral neuropathy (PIPN), during the treatment of breast cancer, ovarian cancer, and non-small cell lung cancer [16, 20]. The main symptoms of such neuropathy are burning pain and numbness in the hands and feet, loss of fine motor skills are so pronounced that up to 25 % of patients require modification of the paclitaxel treatment regimen, including dose reduction, treatment postponement, or even discontinuation of therapy [2, 9, 20].

In vitro models using rat spinal cord neuron cell lines, human induced pluripotent stem cells, and in vivo models in rodents have identified a number of molecular pathways affected by Paclitaxel. The influence is not limited to axons of sensory neurons, but is present in other types of cells,

such as peripheral neuroglia, soma of segmental motor centers, cells of the immune system. These studies showed that Paclitaxel induces altered calcium signaling, the release of neuropeptides and growth factors, mitochondrial damage and the formation of reactive oxygen species, and has a direct effect on the disruption of microtubule transport [13, 21]. However, today there is still no sufficient neuromorphological data on the patterns of pathomorphogenesis of peripheral neuropathies caused by Paclitaxel. Previous attempts to use various neuroprotective agents in humans and in animal models have not shown sufficient effectiveness in preventing or significantly reducing the intensity of PIPN manifestations. The method of electroacupuncture, the action of magnetic fields, the use of cryotherapy and chylotherapy, the use of vitamin E, B vitamins, omega-3 fatty acids, glutathione, acetyl-L-carnitine, amitriptyline, progesterone, minoxidil and a number of other means have been tested, but this did not bring the desired result [6, 8, 11, 15, 19]. Therefore, it is very important to study and develop potential effective approaches during Paclitaxel chemotherapy to prevent and correct this complication. One of the possible ways to prevent damage to the nervous system during chemotherapy could be the use of metabolic drugs that have antioxidant, antihypoxic, and membrane-stabilizing properties. One of them is 2-ethyl-6-methyl-3-hydroxypyridine succinate (HS), which is quite widely used in endocrinology, neurology, and cardiology [4]. In particular, it was established that the use of HS in patients with diabetic neuropathy leads to a significant improvement in objective indicators and is accompanied by a reduction in its symptoms [17, 18].

The purpose of the study is to study the effect of the neuroprotective agent 2-ethyl-6-methyl-3-hydroxypyridine succinate on the morpho-functional parameters of the sciatic nerve and its segmental centers in experimental paclitaxel-induced peripheral neuropathy.

Materials and methods

The study was conducted on the basis of the Department of Histology, Cytology and Embryology of the Ivano-Frankivsk National Medical University. In the experiment, 56 white rats weighing 150-200 g were used. The animals were kept in vivarium conditions at a temperature of 21-24 °, under a normal light regime (day-night) and on a diet with access to food and water ad libitum. The experiment was conducted in accordance with the recommendations of ARRIVE and EU Directive 2010/63/EU on the protection of animals used for scientific purposes, in accordance with the provisions of the "European Convention for the Protection of Vertebrate Animals Used for Experiments and Other Scientific Purposes" (Strasbourg, 2005), Law of Ukraine "On the Protection of Animals from Cruelty" (2006, Article 26), "General Ethical Principles of Animal Experiments", approved by the Fifth National Congress on Bioethics (Kyiv, 2013). The research was approved and confirmed by the bioethics commission of the Ivano-Frankivsk National Medical University (protocol № 122/21 - 09.06.2021).

Animals were injected intraperitoneally with Paclitaxel (Actavis, Romania) at a dose of 2 mg/kg of body weight after one day 4 times before reaching a total dose of 8 mg/kg according to the method of Polomano R. S. [14]. After that, the animals were divided into an experimental group - 24 animals, which were injected with 2-ethyl-6-methyl-3-hydroxypyridine succinate (the drug "Armadine", manufactured by Scientific and Production Firm "Microkhim" LLC), and a control group (24 animals, injection of water for injections). Neurophysiological indicators and electron microscopic picture of the norm were determined on 8 intact animals.

Neurophysiological studies were performed at 3-hour intervals on the 1st, 7th, 14th, and 28th days after the last administration of the HS drug. The hallmark of PIPN, mechanical allodynia, was determined as withdrawal of the hind paw of rats in response to stimulation with von Frey monofilaments using the "up-down" method [3, 24]. The main method of studying thermal hyperalgesia is the hot plate test. During its execution, rats were alternately placed on a metal plate heated to 55±1 ?. A stopwatch was used to measure the time from the moment the animal was placed on the plate to the end point of the test - licking the pads of the front and/or hind paws or jumping up. This time was the time of latent pain reaction. The maximum time the animals stay on the plate - 35 seconds [1, 10].

On the same day, the animals were removed from the experiment by applying ether anesthesia. The material for research (sciatic nerves, spinal nodes and the IX plate of the gray matter of the lumbosacral spinal cord (L2-S1)) was taken on the 1st, 7th, 14th and 28th (6 animals for each period research) days after the last administration of HS. Electron microscopic research was carried out according to generally accepted methods and studied with the help of a PEM-125 K electron microscope, the image was photographed at a magnification of 4000-12000 times.

Results

Neurophysiological studies. Administration of Paclitaxel caused signs of peripheral neuropathy in the form of thermal hyperalgesia and mechanical allodynia in experimental animals.

When performing the von Frey test in intact animals, the mechanical pain threshold was 55.34±7.58 g. In animals of the control group, on the 1st day of the experiment, the mechanical pain threshold decreased to 26.08±3.39 g ($p<0.05$), and on the 7th day it dropped to minimum values and was caused by monofilaments with a pressure force of 18.12±2.03 g ($p<0.001$). From the next term of the experiment, we observed positive dynamics of the development of mechanical allodynia: on the 14th day, the pain threshold increased to 23.24±1.81 g ($p<0.001$), and on the 28th day it was caused by monofilaments with a

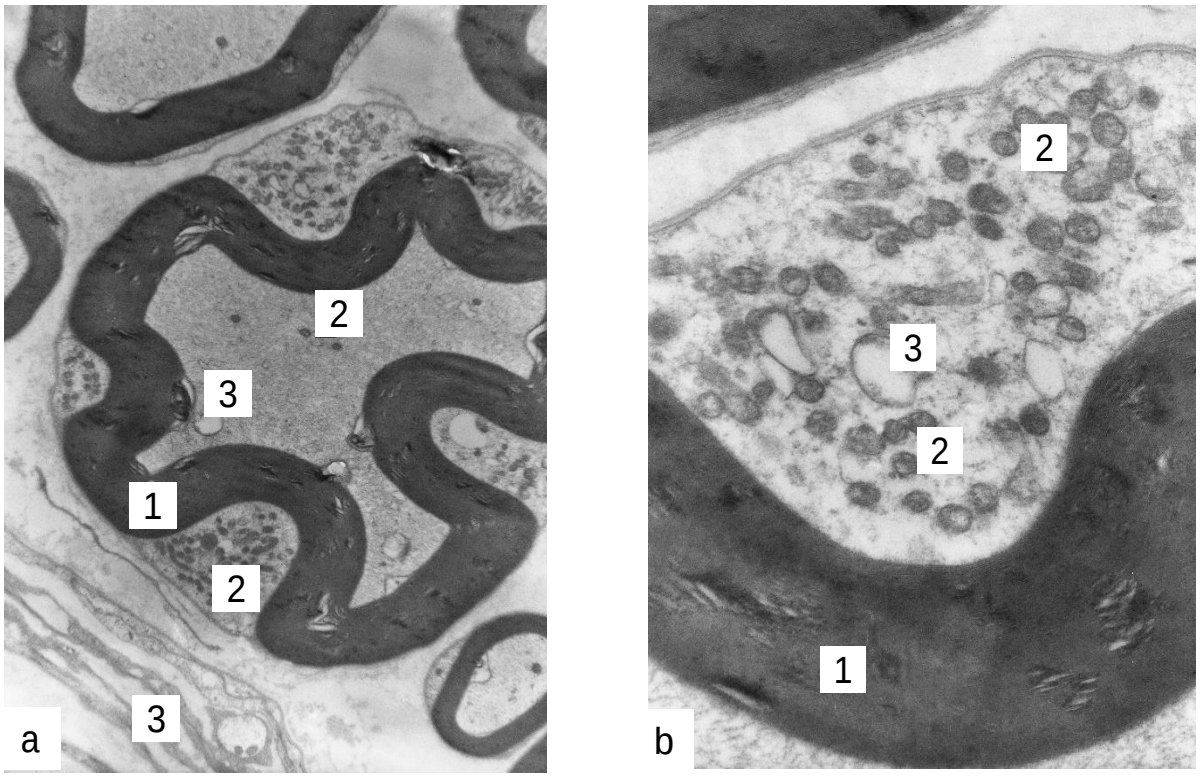

Fig. 1. Pronounced deformation of myelin nerve fibers, vacuolization of mitochondria in the axon, focal splitting of the myelin sheath, proliferation of Schwann cell mitochondria in animals of the control group on the 1st day of the experiment. Electron micrographs. a) x4800, b) x10000. Designation: 1 - myelin sheath, 2 - mitochondria, 3 - vacuoles.

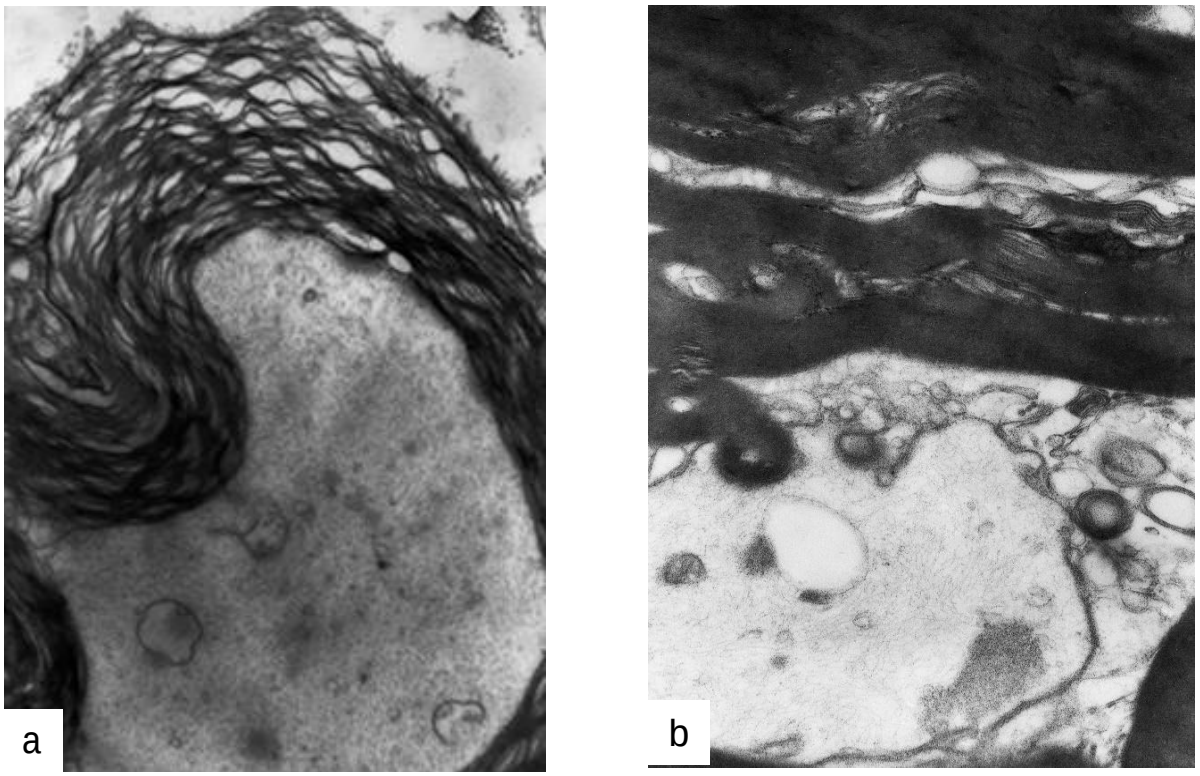

Fig. 2. Layering of lamellae in the myelin sheath (a), disruption of the organization of the myelin sheath in the form of subaxonal inclusions (b) in the control group of animals on the 28th day of the experiment. Electron micrographs. a) x8000, b) x12000.

pressure force of 27.72±5.74 g (p<0.01). In the animals of the experimental group, which underwent HS correction, on the 1st day, the indicator was at the level of 35.43± 4.28 g. On the 7th day, the lowest point was reached - the mechanical pain threshold was 28.32±3.65 g (p<0.05), which is 56.43 % better than the control group. Starting from the 14th day, we observed positive dynamics, which significantly exceeded the recovery indicators in animals of the control group. The threshold of pain sensitivity on the 14th day reached the level of 33.86±3.15 g (p<0.05) - 45.56 % higher compared to the control group, and on the 28th day it was 54.94±8.29 g (p<0.05), which differs by 98.17 % from the similar indicator in the control group of animals.

The duration of stay of intact animals on the "Hot Plate" was 17.20±0.93 s Animals of the control group on the 1st day after the last injection of the drug showed signs of thermal hyperalgesia: the indicator decreased to 12.44±1.25 s (p<0.01). On the 7th day, the lowest level of latent time of pain sensitivity was observed - 9.882±0.711 s (p<0.001). From the next term of the experiment, the indicator shows the dynamics of recovery to the original: on the 14th day, it was 10.28±1.01 s (p<0.001), and on the 28th day - 13.02±0.97 s (p<0.01). Thermal hyperalgesia was significantly less pronounced in animals of the experimental group: on the 1st day, the indicator was 14.13±1.31 s and on the 7th day - 13.82±0.72 s (p<0.001), which is 39.61 % better compared to the control group. Already on the 14th day, we observed the indicator approaching the initial level - 16.88±1.62 s (p<0.01), which is 63.95 % higher compared to the similar indicator of animals of the control group. On the 28th day, the time spent on the "Hot Plat" plate remained close to the initial level - 17.14±1.00 s (p<0.01).

Morphological characteristic. During the electron microscopic examination of preparations of the sciatic nerves of the control group of rats, it was established that on the 1st to 7th day of the experiment, the following are characteristic: deformation of myelin nerve fibers and their myelin sheath, disruption of its lamellae organization, mainly focal defibrillation of the myelin layers, swelling of the peri-axon space (Fig. 1a). We observe axon deformation, vacuolated mitochondria occur in the axoplasm (see Fig. 1b).

In numerous myelinated nerve fibers, we observe deformation of the myelin sheath and axon and an increase in the density of axoplasm. On the 14th-28th day of the experiment, the phenomena of destruction in myelin nerve fibers increase in animals of the control group. In most myelinated nerve fibers, the myelin sheath is thickened due to swelling of Schwann cells and intra-lamellae vacuolation (Fig. 2a). Quite often we observe myelinated nerve fibers with almost complete axon degeneration and severe swelling of the myelin sheath.

Manifestations of vacuolar transformation of membrane

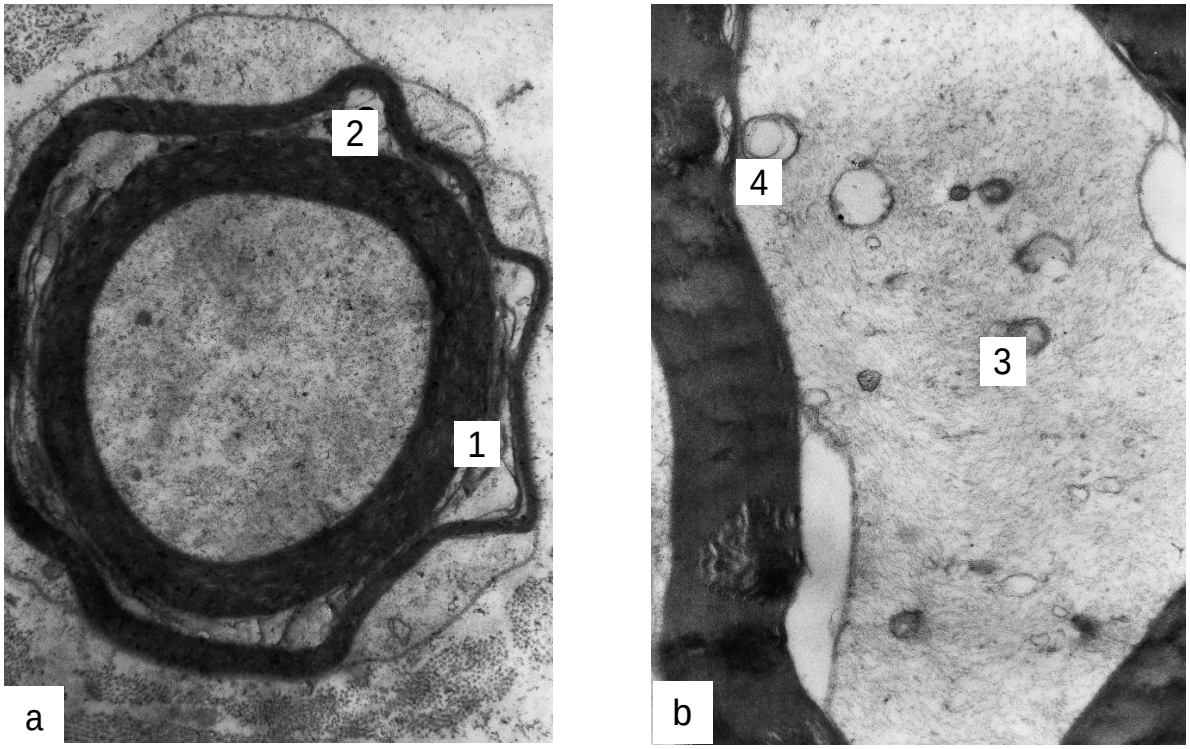

Fig. 3. Defibrillation of the myelin sheath (a), disorganization of neurotubules and neurofilaments (b) in the myelin nerve fibers of the sciatic nerves of animals on the 14th day after the last administration of HS on the background of PIPN. Electron micrographs. a) x6400, b) x96000. Designation: 1 - defibrillation of the myelin sheath, 2 - intra-lamellae vacuoles, 3 - vacuolar transformation of mitochondria, 4 - periaxonal vacuole.

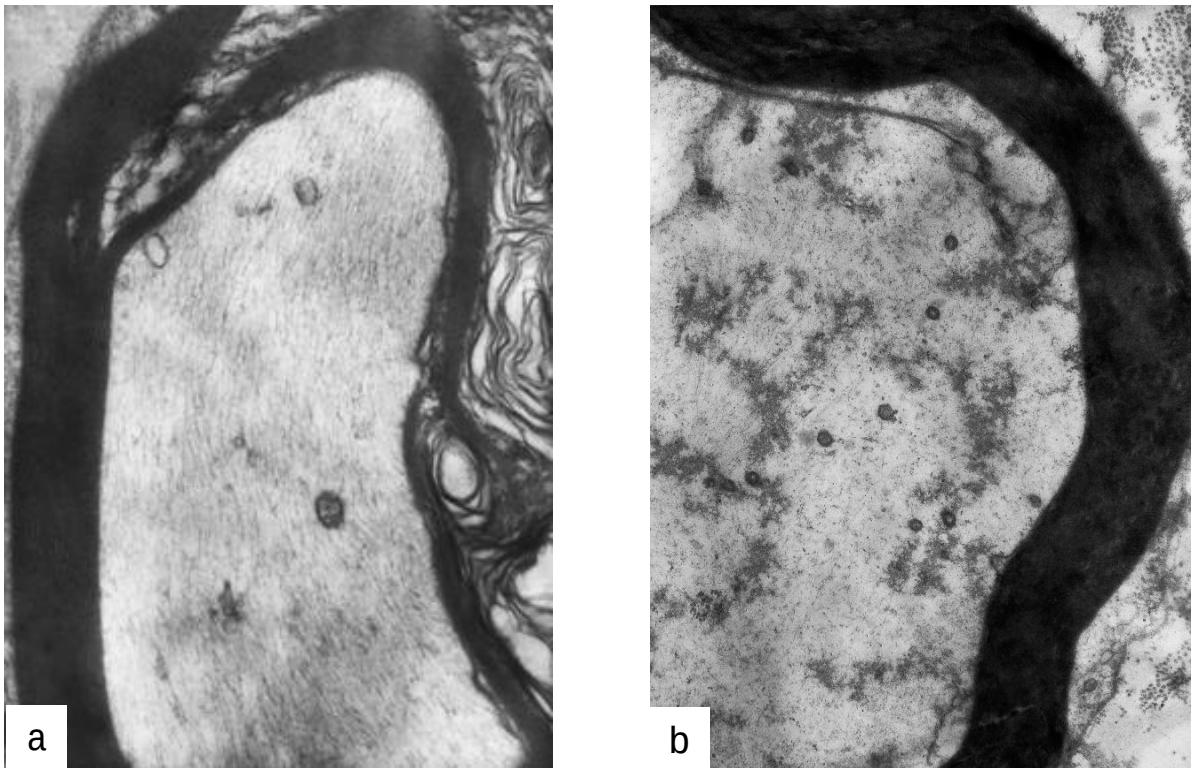

Fig. 4. Intra-lamellae vacuoles (a) and multiple flake-like inclusions against the background of swelling of the axon neuroplasm (b) of myelin nerve fibers of the sciatic nerves of animals of the experimental group on the 28th day of the experiment. Electron micrographs. a) x9600, b) x9600.

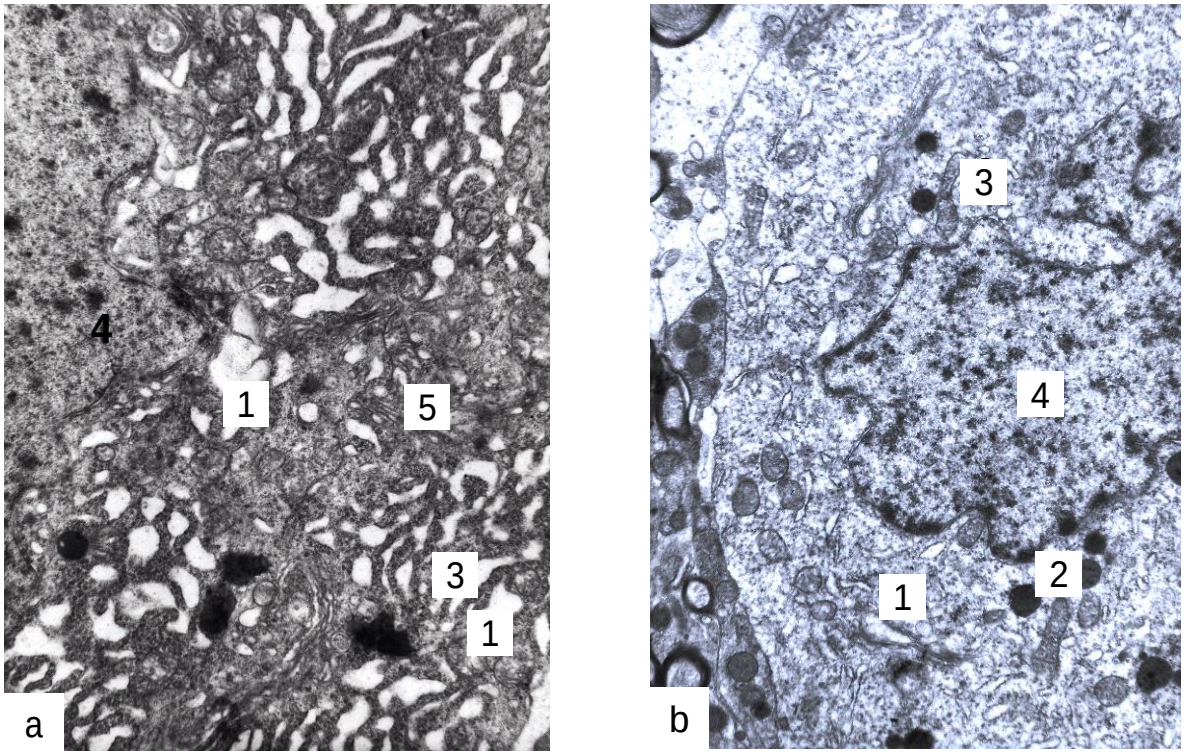

Fig. 5. Increased activity of the granular endoplasmic reticulum, hypertrophy of the Golgi complex in neurons of the anterior horn of the spinal cord. The term of the experiment is 7 days. Electron micrograph. a) x6400, b) x6400. Designation: 1 - autophagosome, 2 - lysosome, 3 - granular endoplasmic reticulum, 4 - nucleus, 5 - Golgi complex.

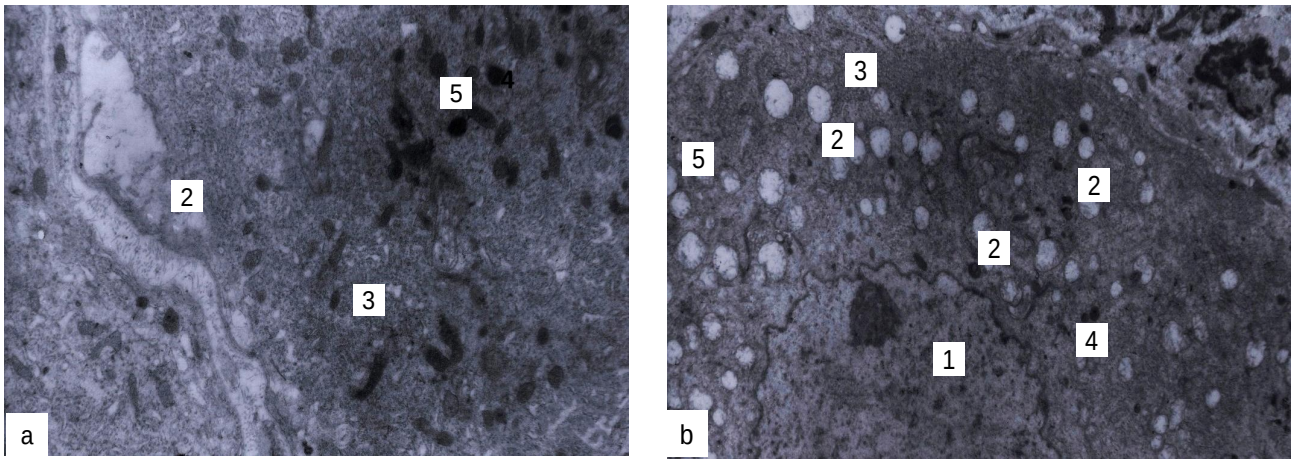

Fig. 6. Peripheral chromatolysis in the neuron of the spinal cord of the experimental group (a) and vacuolar dystrophy in the neuron of the spinal cord of the control group of animals. The term of the experiment is 1 day. Electron micrographs. a) x6400, b) x4800. Designation: 1 - dark neuron nucleus, 2 - vacuoles, 3 - granular endoplasmic reticulum, 4 - lysosomes, 5 - mitochondria.

organelles are increasing. The vast majority of mitochondria are enlarged, with the phenomena of destruction of cristae, lightening of the matrix. On the 28th day of the experiment, pronounced disturbances in the structure of their axons were observed in individual myelinated nerve fibers, smaller and larger vacuoles, including periaxonal vacuoles, were found in the axoplasm (see Fig. 2b). At the same time, the axoplasm of individual axons contains polymorphic vacuoles, a moderate number of neurofilaments and neurotubules. The phenomena of myelinophagy of Schwann cells are frequent, remnants of axial cylinders are determined in their cytoplasm. In the specified terms, significant changes occur, which are manifested by a violation of axon transport systems, in particular, we see conglomerates of neurotubules and neurofilaments and accumulation of synaptic vesicles.

In animals of the research group that received correction, changes in myelin nerve fibers on the 7-28th day are less pronounced. In the sciatic nerves, we observed a polymorphic morphological pattern with the presence of both myelinated nerve fibers of a normal structure and with varying degrees of destruction and signs of structural restoration. In damaged myelinated nerve fibers, the myelin sheath also undergoes changes; it is unevenly thickened, in places of fiberization, but without gross violations of the lamellae structure. Axons contain expanded cisterns of agranular endoplasmic reticulum, vacuolated mitochondria. A distinctive feature of individual myelinated nerve fibers is the manifestation of distorted regeneration, namely the phenomenon of hypertrophy and disorganization of the myelin sheath. Intramyelin vacuoles, slight defibrillation of myelin plates are found in some of the nerve fibers (Fig. 3). Cytoplasmic vacuolation was observed in Schwann cells of myelinated nerve fibers, moderate edema was observed in the endoneurium. In some myelinated nerve fibers with preserved ultrastructure of the myelin sheath, phenomena of axonopathy were found, in particular, the presence of multiple fine-grained inclusions, accumulation of cisterns of agranular endoplasmic reticulum, uneven electron density of hyaloplasm (Fig. 4). Along with the destructively changed myelin nerve fibers, we also observed nerve fibers with pronounced signs of regeneration and the preserved ultrastructure of the myelin sheath.

In neurons of the spinal cord, a 10-day course of HS administration has a positive effect on the morphological state of mitochondria and activates synthetic processes in neurons. On the 7th-28th day after HS correction, an increase in the activity of the granular endoplasmic reticulum (Fig. 5a) can be observed in neurons, and the number of ribosomes attached to its cisternae increases. This ensures the biosynthesis of proteins to restore the protein microstructures of the neuron. Numerous ribosomes and polyribosomes are observed in the neuroplasm. At the same time, the hypertrophy of the Golgi complex, the presence of a sufficient number of lysosomes and autophagosomes in the neuroplasm, which creates the prerequisites for cleaning neurons from toxic and harmful products in order to accelerate their full regeneration (see Fig. 5b).

In the electron microscopic picture of the spinal cord of animals of the control group within 1-28 days after the last administration of HS, mostly neurons with light hyaloplasm (light neurons) are observed. The nuclei of such neurons are located in the center of the cell, their karyolemma contains a peripheral cluster of heterochromatin and clumps of heterochromatin in the karyoplasm against a background of euchromatin. In the cytoplasm of a sensitive pseudounipolar neuron, we observe signs of swelling, few mitochondria, some of which are vacuolated. Dissociated granular endoplasmic reticulum is located perinuclearly as a result of local central chromatolysis of Nissl bodies, and on the periphery of neurons we can see phenomena of chromatolysis and large transparent vacuoles (Fig. 6a).

In the cytoplasm of dark neurons, we see mitochondria of normal structure, Nissl bodies, a small number of smooth endoplasmic reticulum cisternae, ribosomes and polyribosomes.

On the other hand, in the spinal cords of animals with PIPN without HS correction, the majority of dark neurons had signs of pronounced vacuolar dystrophy (see Fig. 6b). Enlightenment of the matrix of mitochondria, disorganization and destruction of their cristae was noted. At the same time, in the soma, we observed an expansion of the cisterns of the granular endoplasmic reticulum and a decrease in the number of fixed ribosomes. Peripheral chromatolysis phenomena were observed in individual bright neurons. These changes occurred against the background of microcirculation disturbances in the spinal nodes: microclasmatosis phenomena were present in the lumen of capillaries, and an increase in the number of micropinocytotic vesicles was observed in the cytoplasm of endotheliocytes, which indicates an increase in transcapillary exchange.

Discussion

Our study was focused on testing 2-ethyl-6-methyl-3-hydroxypyridine succinate as a potential neuroprotector in experimental paclitaxel-induced peripheral neuropathy based on a complex morpho-functional analysis. The morphological changes of the sciatic nerve that we discovered from the beginning to the 28th day of the experiment in the control group of rats coincide with the processes described by other researchers in experimental PIPN, namely: focal destruction and swelling of myelin nerve fibers, pronounced changes in the lamellae of the structure of the myelin sheath, disturbances processes of division in Schwann cells with subsequent involvement in the pathological process of axons and accumulation of neurofilaments and neurotubules [12, 23]. In HS-treated rats, the destructive-dystrophic phenomena in the myelin nerve fibers of the sciatic nerves are less pronounced: edema and intralaminar vacuoles in the myelin sheath are visualized in the myelin nerve fibers. In individual fibers in the axon, phenomena of incomplete splitting of mitochondria with the formation of vacuoles filled with medium electron density contents are observed, and small young mitochondria with a matrix of increased electron density are also visualized.

Examining the motoneurons of the anterior horns of the spinal cord during the first 28 days after the use of HS for the correction of PIPN, we found pronounced regenerative and restorative processes, confirmed by the stable state of mitochondria and the appearance of their young forms in the neuroplasm, hypertrophy of the Golgi complex, and hyperplasia of the granular endoplasmic reticulum. Along with this, light neurons with signs of vacuolar dystrophy are observed. These changes occur against the background of restoration of the ultrastructural organization of the blood-neural barrier. Our data are consistent with the results of other researchers who proved the toxic effect of Paclitaxel on efferent neurons, in particular on axons and soma [5, 22]. The use of HS for the correction of paclitaxel-induced changes in neurons of the spinal cord showed a positive effect. During the first 14-28 days, we noted less pronounced destructive-dystrophic changes in the neurons of the spinal cord nodes, namely: central and peripheral chromatolysis of light and dark neurons and swelling of their cytoplasm, neurophagy phenomena in gliocytes, hypertrophy of certain areas of the myelin sheath, with delamination and separation of myelin plates in the myelin nerve fibers of the posterior root of the spinal cord against the background of HS correction.

Therefore, the pathophysiological mechanisms of neurotoxicity when using Paclitaxel are: degeneration and demyelination of axons, impaired axonal transport, oxidative stress, mitochondrial dysfunction and immune-mediated reactions [7, 8]. The use of HS neutralizes these processes and leads to regenerative and restorative changes in the segmental centers of the sciatic nerves.

The results of the electron microscopic study obtained by us are fully consistent with our data of neurophysiological studies and indicate the possibility of using HS as an effective neuroprotector in PIPN.

Conclusions

1. After the correction of paclitaxel-induced peripheral neuropathy by 2-ethyl-6-methyl-3-hydroxypyridine succinate, the electron microscopic picture of the sciatic nerve, neurons of the anterior horns of the spinal cord, and most of the neurons of the spinal cord nodes showed marked regeneration processes within 1-28 days.

2. The use of 2-ethyl-6-methyl-3-hydroxypyridine succinate at a dose of 10 mg/kg of body weight within 10 days after the last administration of Paclitaxel significantly reduces the manifestations of peripheral neuropathy caused by the latter on the 7th, 14th and 28th that day of the experiment. The disappearance of manifestations of thermal hyperalgesia when using 2-ethyl-6-methyl-3-hydroxypyridine succinate is observed already on the 28th day of the experiment.

References

[1] Bannon, A. W. (1998). Models of Pain: Hot-Plate and Formalin Test in Rodents. *Current Protocols in Pharmacology,* (1), 5-7. doi: 10.1002/0471141755.ph0507s00

[2] Cavaletti, G., & Marmiroli, P. (2015). Chemotherapy-induced peripheral neurotoxicity. *Current opinion in neurology,* 28(5), 500-507. doi: 10.1097/WCO.0000000000000234

[3] Dmitriev, D. V. (2015). Використання аналгезії поперечного площинного блоку (TAP-transversus abdominis plane block) зменшує рівень тол-подібних рецепторів (TLR4) у плазмі маркера гіпералгезії в ранньому післяопераційному періоді [The use of transversus abdominis plane block (TAR-

transversus abdominis plane block) analgesia reduces the level of toll-like receptors (TLR4) in the plasma marker of hyperalgesia in the early postoperative period]. *Медицина неотложных состояний=Emergency Medicine*, (8), 50-54.

[4] Dronov, S. N. (2015). Фармакология мексидола и его применение в психоневрологической практике [Pharmacology of Mexidol and its use in psychoneurological practice]. *Актуальні проблеми сучасної медицини: Вісник української медичної стоматологічної академії=Actual problems of modern medicine: Bulletin of the Ukrainian Medical Stomatological Academy*, 15(3-1 (51)), 328-335.

[5] Ewertz, M., Qvortrup, C., & Eckhoff, L. (2015). Chemotherapy-induced peripheral neuropathy in patients treated with taxanes and platinum derivatives. *Acta oncologica,* 54(5), 587-591. doi: 10.3109/0284186X.2014.995775

[6] Gewandter, J. S., Mohile, S. G., Heckler, C. E., Ryan, J. L., Kirshner, J. J., Flynn, P. J., ... & Morrow, G. R. (2014). A phase III randomized, placebo-controlled study of topical amitriptyline and ketamine for chemotherapy-induced peripheral neuropathy (CIPN): a University of Rochester CCOP study of 462 cancer survivors. *Supportive Care in Cancer,* 22, 1807-1814. doi: 10.1007/s00520-014-2158-7

[7] Gornstein, E. L., & Schwarz, T. L. (2017). Neurotoxic mechanisms of paclitaxel are local to the distal axon and independent of transport defects. *Experimental neurology,* 288, 153-166. doi: 10.1016/j.expneurol.2016.11.015

[8] Hershman, D. L., Lacchetti, C., Dworkin, R. H., Lavoie Smith, E. M., Bleeker, J., Cavaletti, G., ... & Loprinzi, C. L. (2014). Prevention and management of chemotherapy-induced peripheral neuropathy in survivors of adult cancers: American Society of Clinical Oncology clinical practice guideline. *J Clin Oncol,* 32(18), 1941-1967. doi: 10.1200/JCO.2013.54.0914

[9] Hertz, D. L., Childs, D. S., Park, S. B., Faithfull, S., Ke, Y., Ali, N. T., ... & Lustberg, M. (2021). Patient-centric decision framework for treatment alterations in patients with Chemotherapy-induced Peripheral Neuropathy (CIPN). *Cancer treatment reviews,* 99, 102241. PMID: 34174668

[10] Hestehave, S., Munro, G., Pedersen, T. B., & Abelson, K. S. (2017). Antinociceptive effects of voluntarily ingested buprenorphine in the hot-plate test in laboratory rats. *Laboratory Animals,* 51(3), 264-272. doi: 10.1177/0023677216668553

[11] Huang, H., He, M., Liu, L., & Huang, L. (2016). Vitamin E does not decrease the incidence of chemotherapy-induced peripheral neuropathy: a meta-analysis. *Contemporary Oncology/Wspolczesna Onkologia*, 20(3), 237-241. doi: 10.5114/wo.2016.61567

[12] Magdy, T., Burmeister, B. T., & Burridge, P. W. (2016). Validating the pharmacogenomics of chemotherapy-induced cardiotoxicity: What is missing?. *Pharmacology & therapeutics,* 168, 113-125. doi: 10.1016/j.pharmthera.2016.09.009

[13] Nehate, C., Jain, S., Saneja, A., Khare, V., Alam, N., Dhar Dubey, R., & N Gupta, P. (2014). Paclitaxel formulations: challenges and novel delivery options. *Current drug delivery,* 11(6), 666-686. doi: 10.2174/1567201811666140609154949

[14] Polomano, R. C., Mannes, A. J., Clark, U. S., & Bennett, G. J. (2001). A painful peripheral neuropathy in the rat produced by the chemotherapeutic drug, paclitaxel. *Pain,* 94(3), 293-304. doi: 10.1016/S0304-3959(01)00363-3

[15] Schloss, J. M., Colosimo, M., Airey, C., Masci, P., Linnane, A. W., & Vitetta, L. (2017). A randomised, placebo-controlled trial assessing the efficacy of an oral B group vitamin in preventing the development of chemotherapy-induced peripheral neuropathy (CIPN). *Supportive care in cancer,* 25, 195-204. doi: 10.1007/s00520-016-3404-y

[16] Seretny, M., Currie, G. L., Sena, E. S., Ramnarine, S., Grant, R., MacLeod, M. R., ... & Fallon, M. (2014). Incidence, prevalence, and predictors of chemotherapy-induced peripheral neuropathy: a systematic review and meta-analysis. *Pain*®, 155(12), 2461-2470. doi: 10.1016/j.pain.2014.09.020

[17] Skopin, P. I., Zorkina, A. V., Kulaev, M. T., & Peshev, A. A. (2011). Изучение влияния препаратов антиоксидантного действия на физиологические реакции животных, получающих противоопухолевую химиотерапию [Studying the effect of antioxidant drugs on the physiological reactions of animals receiving antitumor chemotherapy]. *Биомедицина=Biomedicine*, (3), 70-75.

[18] Skopin, P. I., Zorkina, A. V., & Skopina, Y. A. (2013). Этилметилгидроксипиридина сукцинат ограничивает эндотоксикоз на поздних сроках роста опухоли и снижает токсичность паллиативной химиотерапии в эксперименте [Ethylmethylhydroxypyridine succinate limits endotoxicosis in late stages of tumor growth and reduces the toxicity of palliative chemotherapy in an experiment]. *Фундаментальные исследования=Fundamental research*, (2 Part 1), 167-171.

[19] Stillman, M., & Cata, J. P. (2006). Management of chemotherapy-induced peripheral neuropathy. *Current pain and headache reports*, 10, 279-287. doi: 10.1007/s11916-006-0033-z

[20] Tufano, A. M., Teplinsky, E., & Landry, C. A. (2021). Updates in neoadjuvant therapy for triple negative breast cancer. *Clinical Breast Cancer,* 21(1), 1-9. doi: 10.1016/j.clbc.2020.07.001

[21] Wani, M. C., & Horwitz, S. B. (2014). Nature as a Remarkable Chemist: A personal story of the discovery and development of Taxol®. *Anti-cancer drugs*, 25(5), 482-487. doi: 10.1097/CAD.0000000000000063

[22] Weaver, B. A. (2014). How Taxol/paclitaxel kills cancer cells. *Molecular biology of the cell,* 25(18), 2677-2681. doi: 10.1091/mbc.E14-04-0916

[23] Wei, Y., Pu, X., & Zhao, L. (2017). Preclinical studies for the combination of paclitaxel and curcumin in cancer therapy. *Oncology reports,* 37(6), 3159-3166. doi: 10.3892/or.2017.5593

[24] Zhang, Z., Hu, Y., Zhao, Y., Chen, C., Guo, Q., & Sun, Z. (2009). Behavioral and ultrastructural changes of intrathecal administered ropivacaine in spinal cord of rats. Zhong nan da xue xue bao. Yi xue ban=Journal of Central South University. *Medical Sciences,* 34(4), 362-368. PMID: 19411757

НЕЙРОПРОТЕКТОРНИЙ ВПЛИВ 2-ЕТИЛ-6-МЕТИЛ-3-ГІДРОКСИПІРИДИНУ СУКЦИНАТУ НА СІДНИЧИЙ НЕРВ ТА ЙОГО СЕГМЕНТАРНІ ЦЕНТРИ ПРИ ЕКСПЕРИМЕНТАЛЬНІЙ ПАКЛІТАКСЕЛ-ІНДУКОВАНІЙ ПЕРИФЕРІЙНІЙ НЕЙРОПАТІЇ

Геращенко С. Б., Островський М. М., Кулинич Г. Б., Марків І. М.

До 60 % пацієнтів страждають від нейротоксичності хіміопрепарату Паклітаксел, а саме паклітаксел-індукованої периферійної нейропатії (ПІПН), у процесі лікування раку молочної залози, раку яєчників, недрібноклітинного раку легень. З них до 25 % пацієнтів потребують модифікації схеми лікування паклітакселом, включаючи зниження дози, відкладення чи припинення терапії. Попередні спроби застосування нейропротекторних середників у людей і на тваринних моделях не показали достатньої ефективності щодо запобігання або суттєвого зниження проявів ПІПН. Метою нашого дослідження

стало вивчення впливу нейропротекторного середника 2-етил-6-метил-3-гідроксипіридину сукцинату (ГС) на морфо-функціональні параметри сідничого нерва та його сегментарних центрів при експриментальній ПІПН. В експерименті використали 56 білих щурів, яким вводили внутрішньоочеревинно Паклітаксел у дозі 2 мг/кг маси тіла через одну добу 4 рази, після цього тварин поділили на дослідну групу - 24 тварини, яким вводили ГС і контрольну (24 тварини, введення води для ін'єкцій) групи. Методом вивчення механічної алодинії були монофіламенти фон Фрея, термічну гіпералгезію вивчали тестом "гаряча пластинка", а електронномікроскопічне дослідження здійснювали згідно загальноприйнятих методів і вивчали за допомогою електронного мікроскопа ПЕМ-125 К. Результати тестів "гаряча пластинка" та використання монофіламентів фон Фрея показали, що застосування ГС достовірно знижує прояви ПІПН на 7-у, 14-у та 28-ту доби експерименту. У щурів, що отримували лікування ГС, деструктивно-дистрофічні явища в мієлінових нервових волокнах сідничого нерва є менш вираженими, а у окремих волокнах в осьових циліндрах спостерігаються явища незавершеного відщеплення мітохондрій з утворенням заповнених вмістом середньої електронної щільності вакуолей, а також візуалізуються дрібні молоді мітохондрії. Упродовж перших 28 діб у нейронах спинномозкових вузлів ми відмічали менш виражені деструктивно-дистрофічні зміни, а саме: хроматоліз світлих та темних нейронів та набряк їхньої цитоплазми, явища нейронофагії у гліоцитах, гіпертрофія окремих ділянок мієлінової оболонки. Результати електронномікроскопічного дослідження повністю узгоджуються з даними нейрофізіологічних досліджень і вказують на можливість використання ГС як ефективного нейропротектора при ПІПН.

Ключові слова: *паклітаксел, хіміотерапія, нейропатія, центральна нервова система, периферійна нервова система.*

Author's contribution

Herashchenko S. B.: methodology and original project writing, project administration, software, supervision, data visualization.
Ostrovskyi M. M.: conceptualization, research implementation, data visualization, formal analysis and validation.
Kulynych H. B.: research, statistical processing, review writing and editing.
Markiv I. M.: research, statistical processing, review writing and editing.

REQUIREMENTS FOR ARTICLES

For publication, scientific articles are accepted only in English only with translation on Ukrainian, which contain the following necessary elements: UDC code; title of the article (in English and Ukrainian); surname, name and patronymic of the authors (in English and Ukrainian); the official name of the organization (institution) (in English and Ukrainian); city, country (in English and Ukrainian); structured annotations (in English and Ukrainian); keywords (in English and Ukrainian); introduction; purpose; materials and methods of research; research results; discussion; conclusions; bibliographic references.

The title of the article briefly reflects its contents and contains no more than 15 words.

Abstract. The volume of the annotation is 1800-2500 characters without spaces. The text of an annotation in one paragraph should not contain general phrases, display the main content of the article and be structured. The abstract should contain an introductory sentence reflecting the relevance of the study, the purpose of the study, a brief description of the methods of conducting research (2-3 sentences with the mandatory provision of the applied statistical methods), a description of the main results (50-70% of the volume of the abstract) and a concise conclusion (1 sentence). The abstract should be clear without familiarizing the main content of the article. Use the following expressions: "Detected ...", "Installed ...", "Fixed ...", "Impact assessed ...", "Characterized by regularities ...", etc. In an annotation, use an active rather than passive state.

Keywords: 4-6 words (or phrases).

"Introduction"

The introduction reflects the state of research and the relevance of the problem according to the world scientific literature (at least 15 references to English articles in international journals over the past 5 years). At the end of the entry, the purpose of the article is formulated (contains no more than 2-3 sentences, in which the problem or hypothesis is addressed, which is solved by the author).

"Materials and methods"

The section should allow other researchers to perform similar studies and check the results obtained by the author. If necessary, this section may be divided into subdivisions. Depending on the research objects, the ethical principles of the European Convention for the protection of vertebrate animals must be observed; Helsinki Declaration; informed consent of the surveyed, etc. (for more details, see "Public Ethics and its Conflict"). At the end of this section, a "statistical processing of results" section is required, which specifies the program and methods for processing the results obtained by the automobile.

"Results"

Requirements for writing this section are general, as well as for all international scientific publications. The data is presented clearly, in the form of short descriptions, and must be illustrated by color graphics (no more than 4) or drawings (no more than 8) and tables (no more than 4), the information is not duplicated.

"Discussion"

In the discussion, it is necessary to summarize and analyze the results, as possible, compare them with the data of other researchers. It is necessary to highlight the novelty and possible theoretical or practical significance of the results of the research. You should not repeat the information already listed in the "Introduction" section. At the end of the discussion, a separate paragraph should reflect the prospects for using the results obtained by the author.

"Conclusion"

5-10 sentences that summarize the work done (in the form of paragraphs or solid text).

"Acknowlegements"

Submitted after conclusion before bibliographic references.

"References"

References in the text are indicated by Arabic numerals in square brackets according to the numerology in the list of references. The list of references (made without abbreviations) sorted by alphabet, in accordance with the requirements of APA Style (American Psychological Association Style): with the obligatory referencing of all authors, work titles, journal names, or books (with obligatory publication by the publishing house, and editors when they are available), therefore, numbers or releases and pages. In the Cyrillic alphabets references, give the author's surnames and initials in English (Cyrillic alphabet in brackets), the title of the article or book, and the name of the magazine or the publisher first to be submitted in the original language of the article, and then in square brackets in English. If available, doi indexes must be provided on www.crossref.org (at least 80% of the bibliographic references must have their own doi indexes). Links to online publications, abstracts and dissertations are not welcome.

After the list of references, it is necessary to provide information about all authors (in English, Ukrainian and Russian): last name, first name and patronymic of the author, degree, place of work and position, **ORCID number** (each of the authors of the ORCID personal number if absence - free creation on the official website http://www.orcid.org) to facilitate the readers of this article to refer to your publications in other scientific publications.

The last page of the text should include the surname, name and patronymic of the author, degree, postal address, telephone number and e-mail of the author, with which the editors will maintain contact.

Concluding remarks

The manuscript should be executed in such a way that the number of refinements and revisions during the editorial of the article was minimal.

When submitting the article, please observe the following requirements. The volume of the article - not less than 15 and not more than 25 pages, Times New Roman, 14 pt, line spacing - one and a half, fields - 2 cm, sheet A4. Text materials should be prepared in the MS Word editor (* .docx), without indentations. Math formulas and equations to prepare in the embedded editor; graphics - in MS Excel. Use the units of the International Measurement System. Tables and drawings must contain the name, be numbered, and references to them in the text should be presented as follows: (fig. 1), or (table 1). The drawings should be in the format "jpg" or "tif"; when scanned, the resolution should be at least 800 dpi; when scanning half-tone and color images, the resolution should be at least 300 dpi. All figures must be represented in the CMYK palette. The statistical and other details are given below the table in the notes. Table materials and drawings place at the end of the text of the manuscript. All elements of the text in images (charts, diagrams, diagrams) must have the Times New Roman headset.

Articles are sent to the editorial board only in electronic form (one file) at the e-mail address nila@vnmu.edu.ua

Responsible editor - Gunas Igor Valeryovich (phone number: + 38-067-121-00-05; e-mail: igor.v.gunas@gmail.com).

Signed for print 15.12.2023
Format 60x84/8. Printing offset. Order № 1798. Circulation 100.
Vinnytsia. Printing house “TVORY”, Nemyrivske shose St., 62a,
Vinnytsya, 21034
Phone: 0 (800) 33-00-90, (096) 97-30-934, (093) 89-13-852,
(098) 46-98-043
e-mail: tvory2009@gmail.com
http://www.tvoru.com.ua